

AD_____

AWARD NUMBER: W81XWH-08-1-0510

TITLE: Viroreplicative Gene Therapy Targeted to Prostate Cancer

PRINCIPAL INVESTIGATOR: Noriyuki Kasahara, M.D., Ph.D.

CONTRACTING ORGANIZATION: University of California, Los Angeles
Los Angeles, CA 90095

REPORT DATE: August 2010

TYPE OF REPORT: Final

PREPARED FOR: U.S. Army Medical Research and Materiel Command
Fort Detrick, Maryland 21702-5012

DISTRIBUTION STATEMENT: Approved for Public Release;
Distribution Unlimited

The views, opinions and/or findings contained in this report are those of the author(s) and should not be construed as an official Department of the Army position, policy or decision unless so designated by other documentation.

REPORT DOCUMENTATION PAGE			<i>Form Approved</i> <i>OMB No. 0704-0188</i>		
Public reporting burden for this collection of information is estimated to average 1 hour per response, including the time for reviewing instructions, searching existing data sources, gathering and maintaining the data needed, and completing and reviewing this collection of information. Send comments regarding this burden estimate or any other aspect of this collection of information, including suggestions for reducing this burden to Department of Defense, Washington Headquarters Services, Directorate for Information Operations and Reports (0704-0188), 1215 Jefferson Davis Highway, Suite 1204, Arlington, VA 22202-4302. Respondents should be aware that notwithstanding any other provision of law, no person shall be subject to any penalty for failing to comply with a collection of information if it does not display a currently valid OMB control number. PLEASE DO NOT RETURN YOUR FORM TO THE ABOVE ADDRESS.					
1. REPORT DATE 1 August 2010		2. REPORT TYPE Final		3. DATES COVERED 1 Aug 2008 – 31 Jul 2010	
4. TITLE AND SUBTITLE Viroreplicative Gene Therapy Targeted to Prostate Cancer			5a. CONTRACT NUMBER		
			5b. GRANT NUMBER W81XWH-08-1-0510		
			5c. PROGRAM ELEMENT NUMBER		
6. AUTHOR(S) Noriyuki Kasahara, M.D., Ph.D. E-Mail: nkasahara@mednet.ucla.edu			5d. PROJECT NUMBER		
			5e. TASK NUMBER		
			5f. WORK UNIT NUMBER		
7. PERFORMING ORGANIZATION NAME(S) AND ADDRESS(ES) University of California, Los Angeles Los Angeles, CA 90095			8. PERFORMING ORGANIZATION REPORT NUMBER		
9. SPONSORING / MONITORING AGENCY NAME(S) AND ADDRESS(ES) U.S. Army Medical Research and Materiel Command Fort Detrick, Maryland 21702-5012			10. SPONSOR/MONITOR'S ACRONYM(S)		
			11. SPONSOR/MONITOR'S REPORT NUMBER(S)		
12. DISTRIBUTION / AVAILABILITY STATEMENT Approved for Public Release; Distribution Unlimited					
13. SUPPLEMENTARY NOTES					
14. ABSTRACT Replication-competent retrovirus (RCR) vectors can propagate specifically within actively dividing cancer cells and achieve highly efficient and tumor-selective gene delivery. To improve their tumor-specificity and safety profile, we have developed RCR vectors regulated by two different tissue-specific promoters. The first is regulated by a synthetic variant of the probasin promoter (ARR2PB), exhibits high specificity for androgen receptor (AR)-positive prostate cancer cells. The second incorporates a newly developed androgen-independent synthetic regulatory element (PSES) which is highly active in PSA-/PSMA-positive prostate cancer cells, both in the presence and absence of androgen. The wild type promoter in the retrovirus long-terminal repeat (LTR) sequence was replaced with ARR2PB and PSES promoter sequences, and the efficiency and specificity of transduction and replication by the resultant RCR vectors was examined in vitro and in vivo. We have also developed prostate-targeted RCR vectors carrying the yeast cytosine deaminase (yCD) gene, which converts the nontoxic prodrug 5-fluorocytosine (5FC) into the chemotoxin 5-fluorouracil, and the potency and selectivity of the cytotoxic effect mediated by these vectors was examined.					
15. SUBJECT TERMS None provided.					
16. SECURITY CLASSIFICATION OF:			17. LIMITATION OF ABSTRACT	18. NUMBER OF PAGES	19a. NAME OF RESPONSIBLE PERSON
a. REPORT U	b. ABSTRACT U	c. THIS PAGE U			USAMRMC
			UU	55	19b. TELEPHONE NUMBER (include area code)

Table of Contents

	<u>Page</u>
Introduction.....	1
Body.....	1 - 24
Key Research Accomplishments.....	25
Reportable Outcomes.....	26 - 27
Conclusion.....	28
References.....	29 - 31
Final Report Bibliography / Personnel List	32 - 33
Appendices.....	33 - 52

Final Report**November 19, 2010****I. INTRODUCTION**

The use of replication-competent viruses represents an emerging technology with the potential to achieve highly efficient gene transfer to tumors, as each successfully transduced tumor cell itself becomes a virus-producer cell, sustaining further transduction events even after initial administration. In contrast to various other replicating viruses now in development as naturally oncolytic agents, murine leukemia virus (MLV)-based replication-competent retroviruses (RCR) can replicate without immediate lysis of host cells and can spread via direct cell-to-cell budding, and may be less likely to elicit robust immune responses that prematurely terminate virus propagation. Yet, until now, use of RCR vectors has rarely been considered due to the potential risks of uncontrolled virus spread.

Recently, we have demonstrated that RCR vectors are capable of highly efficient gene delivery associated with viral replicative spread throughout solid tumors *in vivo*, resulting in significant therapeutic benefit when used for suicide gene therapy. Furthermore, due to the intrinsic inability of MLV to infect quiescent normal cells, RCR-mediated gene transfer was, in fact, highly selective for rapidly dividing cancer cells. However in view of the known potential for retroviral integration-mediated genotoxicity, additional mechanisms to target the virus specifically to cancer cells should be pursued.

We have established proof-of-concept for cell type-specific transcriptional control of RCR vectors by incorporation of two different prostate-specific regulatory sequences into the viral promoter: (1) ARR2PB, a modified version of the androgen-dependent probasin promoter, which confers stringent control of virus replication and transgene expression restricted to actively-dividing, androgen receptor-positive prostate cancer cells, and (2) PSES, a newly developed androgen-independent synthetic regulatory element, which transcriptionally targets RCR vectors to late-stage, PSA / PSMA-positive, androgen receptor-negative prostate tumors. We have characterized the specificity, efficiency, therapeutic efficacy, and safety of ARR2PB-targeted vs. PSES-targeted RCR vectors in a step-wise progression, first using vectors carrying marker genes to follow viral replication and spread *in vitro* and *in vivo*, followed by development and testing of vectors carrying suicide genes. These prostate-targeted vectors have been compared against wild type untargeted RCR vectors in both immunodeficient and immunocompetent rodent models, including LNCaP human prostate cancer xenograft model in athymic nude mice as well as a unique *Pten* knockout model of spontaneous murine prostate cancer.

II. BODY

During the period from 1st August 2008 – 31st August 2010, we have substantially accomplished the Tasks listed in the approved Statement of Work, shown below.

Statement of Work:

- Task 1.* Construction of RCR vectors targeted to human prostate cancer cells (Months 1–6)
- Task 2.* Testing the cell type-specificity of prostate-targeted RCR vectors in culture (Months 6–12)
- Task 3.* Testing the replicative specificity of prostate-targeted RCR vectors *in vivo* (Months 8–18)
- Task 4.* Testing the therapeutic efficacy of prostate-targeted RCR vectors *in vivo* (Months 12–24)

RESEARCH ACCOMPLISHMENTS:**Task 1. Construction of RCR vectors targeted to human prostate cancer cells (Months 1–6)**

Here we have developed replication-competent retrovirus (RCR) vectors that have been transcriptionally targeted to specific cell types via promoter modification, for application to gene therapy of prostate cancer. Our hypothesis is that transcriptional targeting of RCR vectors specifically to prostate cancer cells provides an effective mechanism to limit the spread of virus to normal tissues, while enabling more selective transduction of tumor tissue.

RESULTS:

Construction of ARR2PB-MLV and PSES-MLV hybrid long terminal repeat (LTR) sequences

Transcriptional activity of retrovirus vectors can be regulated through the replacement of sequences in the viral long terminal repeat (LTR) with cell-specific promoter elements. The LTR consists of 3 distinct regions, designated U3, R, and U5, which are repeated at each end of the provirus genome. Promoter elements that control transcription of the RNA genome, and therefore replication of the virus, reside in the U3 region. The R region contains the start site of transcription, and therefore the upstream U3 promoter sequences are not included in the genomic RNA transcript. However, the transcript reads through to the U3 sequence in the 3' LTR, which is subsequently re-duplicated at the terminus of the newly formed 5' LTR during viral reverse transcription. Thus, modifications of the LTR promoter must be incorporated into the 3' LTR U3 region to be retained over serial replication cycles. The size of any inserted sequences can theoretically be of any size, but ideally, should be approximately the same size range as that of the natural viral promoter/enhancer sequences in the U3 region, i.e., about 500 bp.

Fortunately, highly prostate-specific promoter elements of reasonable size are available and have been well characterized, and can be used for this type of transcriptional targeting strategy:

ARR2PB, an improved version of the probasin promoter: One of the most well-characterized proteins uniquely produced by the prostate gland is the rat probasin protein. The probasin promoter from -426 to +28 in the 5' untranslated region contains androgen responsive elements and has been shown to stringently direct prostate-specific gene expression in vitro [1] and in transgenic mice [2], particularly for targeted overexpression of SV40 T antigen, resulting in the establishment of transgenic models of prostate cancer (TRAMP mice) [3].

More recently, a synthetic probasin promoter, ARR2PB, with tandem duplication of the androgen responsive regions, has been demonstrated to confer a high level of transgene expression specifically in the prostatic luminal epithelium and is strongly regulated by androgens [4,5]. The ARR2PB promoter has been successfully used to drive androgen-dependent, prostate cell-specific expression of transgenes in vitro and in vivo [5,6], particularly in transgenic mice [4,7-9] as well as from adenoviral vectors [10-12]. As noted above, gene expression from RCR vectors can be stringently controlled by the ARR2PB promoter, thereby transcriptionally targeting RCR vector replication to prostate cancer cells with functionally intact androgen receptors in the presence of DHT [13].

PSES, a newly developed prostate-specific promoter: Kao, Gardner, et al. recently developed an artificial chimeric promoter (PSES), containing modified regulatory elements derived from PSA and PSMA genes [14]. This novel promoter was silent in PSA-/PSMA-negative prostate cancer cell lines and non-prostate cells, but was highly active in PSA-/PSMA-positive prostate cancer cells, both in the presence and absence of androgen [14]. PSES-driven luciferase activity from an adenovirus vector, Ad-PSES-luc, was reported to be up to 1000-fold higher in these prostate cancer cell lines than in non-prostate cell lines [14]. *In vivo*, luciferase activity after systemic injection of Ad-PSES-luc in mice was reported to be low in all major organs, but high luciferase activity was found upon injection into prostate, and more recently, this promoter has been used to drive prostate-specific replication of an oncolytic adenovirus [15]. Hence the PSES promoter may be particularly useful for prostate-specific gene expression in late stage, androgen-independent disease.

Hybrid promoter design strategy: In previous studies, we found that some of the original MLV-LTR sequences need to be retained for the virus to replicate successfully. For example, the very 5' end of the U3 region is recognized by viral integrase protein, and so this sequence needs to be retained for virus integration into the target cell genome. Furthermore, as the LTRs are duplicated at both 5' and 3' ends of the viral genome, these repeat sequences must provide both promoter and polyadenylation functions, and in fact, the TATA box sequence in the MLV-LTR promoter actually overlaps with a polyadenylation signal. Thus, specific sequences inherent in the original MLV-LTR are important for its dual functions and hence for optimal replication of the virus.

Therefore, prostate cell-specific MLV-LTR constructs were generated by overlap extension PCR to precisely replace MLV U3 sequences from just downstream of the LTR 5' end, to just upstream of the TATA box. This interval was replaced with the corresponding (i.e., just upstream of the TATA box) regulatory sequences from either the ARR2PB promoter or the PSES promoter (**Fig. 1**). Based on this design, transcription should be initiated at the 5' border of the R region, as occurs in wild type MLV.

Construction of ARR2PB- and PSES- hybrid LTR-driven RCR vectors

Next, these hybrid LTR constructs were engineered into the amphotropic (4070A) RCR vector genome, which contains a viral envelope gene that exhibits broad species tropism, including human as well as mouse cells. The hybrid LTR sequence was initially placed downstream to replace the retroviral 3' LTR. Due to its downstream location, this modified 3' LTR U3 region will not function as a promoter (and will function instead as a polyadenylation signal) upon transfection of the provirus construct into 293 cells, and so initial production of the vector transcript will proceed normally, directed by 5' LTR which is still the wild type sequence. However, after a single round of reverse transcription and viral replication, the ARR2PB or PSES sequence will be re-duplicated in the U3 region of the 5' LTR (**Fig. 2**), and thereafter should specify prostate cell-specific replication of the virus.

It should be noted in this context that, although insertions of non-essential transgenes in the U3 region are prone to deletion, the prostate-specific promoter elements in this case will completely replace the wild type promoter elements in the viral LTR, therefore deletions of the prostate-specific promoter would simply result in a virus that is unable to replicate, and we hypothesized that there would be selection pressure against such deletions.

We first constructed such ARR2PB- and PSES-targeted RCR vectors containing the GFP marker gene. Subsequently, prostate-targeted RCR vectors carrying the yeast cytosine deaminase (yCD) suicide gene were also constructed similarly (see below).

Figure 1: Structure of replication-competent MLV vectors containing hybrid LTRs.

Each vector contains the *gag*, *pol*, and amphotropic (4070A strain-derived) *env* structural genes of MLV, as well as an internal ribosome entry site (IRES)-green fluorescent protein (GFP) cassette inserted immediately downstream of the *env* gene. The natural MLV-LTR comprises U3, R, and U5 regions. The transcriptional control sequences of MLV are located primarily in the U3 region, which also contains CAAT and TATA box sequences. In all vectors, the U3 region in the 5' LTR was replaced by the CMV immediate-early promoter for improved transcription of the viral genome in 293T producer cells during the initial round of vector production. As the 5' LTR's U3 region is used as the viral promoter, the CMV sequence is not transcribed and is not present in the viral genomic mRNA. The 3' LTR is then used as the template for reduplication of the 5' LTR during reverse transcription of the RNA virus to DNA in the process of viral replication. We therefore replaced the 3' LTR of the RCR vector with the hybrid LTRs. The U3 sequence in each of the hybrid LTRs, from just downstream of the 5' border to the TATA box just upstream of the 3' border, was replaced with the corresponding ARR2PB or PSES regulatory sequences.

pACE-emd (wild type)



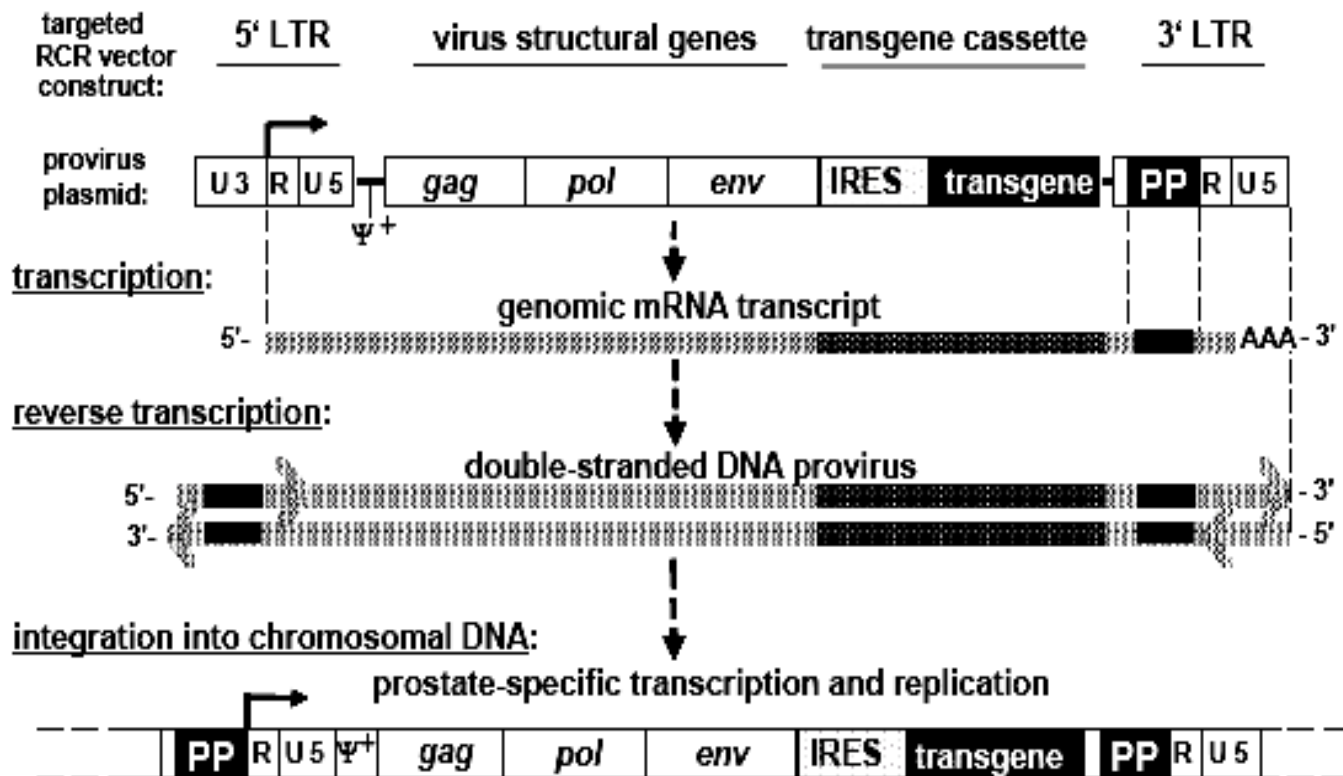
pACE-At-emd (targeted ARR2PB promoter)



pACE-PSES-emd (targeted PSES promoter)



Figure 2: Replication of RCR vectors targeted to prostate cancer cells.
(PP: prostate-specific promoter, LTR: long terminal repeat, Ψ: packaging signal)



Construction of prostate-targeted RCR vectors expressing suicide genes

As suicide genes, we initially proposed to test three different prodrug-activating enzymes: 1) Yeast cytosine deaminase (yCD), 2) E. coli purine nucleoside phosphorylase (PNP), and 3) Herpes simplex thymidine kinase (HSV-tk). Of these, we have found that PNP is potent, but its prodrug Fludara causes significant toxicity, and HSV-tk is unstable in the RCR vector (data not shown). Accordingly, we have devoted a considerable amount of effort to optimizing the yCD suicide gene RCR vector, in order to enhance its genomic stability over serial replication cycles, as well as its potency.

We first focused on improving the yCD suicide gene, which encodes a prodrug activator enzyme that converts the inactive antifungal prodrug 5-fluorocytosine (5-FC) to the highly potent anticancer drug 5-fluorouracil (5FU), as RCR vectors using this suicide gene have moved forward to Phase I clinical trials for the treatment of patients suffering from glioblastoma multiforme (grade IV glioma). The original RCR-yCD vector had two potential weaknesses for clinical use. First, although genomic stability of the virus is enough to show impressive efficacy in rodent models, the extent of viral replication required to infect and probably reinfect larger human tumors is greater, and could require better stability of the vector genome. Second, the native yCD protein is not very efficient at 37°C [16] and the use of yeast codons, rather than human, could limit protein synthesis rates. In order to address these issues before proceeding to human clinical trials, we have modified the original vector back bone of Logg et al. [13], and inserted various forms of the cytosine deaminase gene into the vector. Therapeutic candidates have been tested for: stability over multiple rounds of replication; cytosine deaminase expression and activity in vitro; cell killing with 5-FC in tissue culture. Through these efforts, we have now successfully developed a highly optimized RCR vector expressing the yCD suicide gene.

The back-bone of the pACE-GFP plasmid and the pACE-CD (T5.0000) plasmids [13,17] was modified in the GFP plasmid to remove unnecessary repeat and potentially destabilizing sequences, and facilitate transgene insertion. The resultant plasmid was designated pAC3-GFP / T5.0006 (**Table 1, Fig. 3**) and this plasmid was used as a basis for the vectors encoding cytosine deaminase and variants. We first codon-optimized the yeast CD gene for preferred human codon usage (designated yCD1), and inserted it into the AC3 backbone to generate pAC3-yCD1 / T5.0001, (**Table 1, Fig. 3**). The yeast enzyme is known to be optimally active at around 26°C, but has previously been shown to be stabilized in bacteria at 37°C by alteration of 3 amino acids [16]. Therefore we asked if incorporation of these mutations into the humanized yeast gene (designated yCD2) would show a similar stabilization in human and mammalian cells, and constructed pAC3-yCD2 / T5.0002 (**Table 1, Fig. 3**). It has also been reported that the fusion of the yeast gene encoding uracil phosphoribosyl transferase (UPRT; EC 2.4.2.9) to the yCD gene leads to increased sensitivity to 5-FC in cells expressing the hybrid enzyme compared to cells expressing yCD alone [18,19]. The mechanism of this increased activity appears to be a hybrid effect of stabilization of the yeast CD gene and enhanced conversion of 5-FU to FUMP. One of the attractions of the yCD/5-FC system is that the 5-FU metabolite is diffusible resulting in a bystander effect (killing of adjacent cells without the gene) so the value of adding a pyrimidine salvage gene such as UPRT was uncertain. Nevertheless, we synthesized and tested three vectors containing the hybrid salvage genes, and inserted them into the improved AC3 backbone (**Table 1, Fig. 3**). The first, yCD2-U is a conventional fusion of the CD2 gene with the yeast UPRT gene, with the CD stop and the UPRT start codons removed and used to generate pAC3-yCD2-U / T5.0003). The second, yCD-O used the human orotic acid phosphoribosyl transferase (OPRT; orotidine-5'-phosphate:pyrophosphate phosphoribosyltransferase; EC 2.4.2.10) gene, fused in the same way to the CD2 gene to generate pAC3-yCD2-O / T5.0004. The human OPRT is normally a domain of a multifunctional protein, UMP synthase [20] that also carries a domain encoding activity for orotidine-5'-monophosphate decarboxylase (EC 4.1.1.23), the next enzyme in the anabolic nucleotide synthesis pathway in humans leading to production of UMP, or 5F-UMP after 5-FU or 5-FC administration. OPRT normally converts 5-FU to FUMP in chemotherapy and down-regulation of the endogenous enzyme can cause 5-FU resistance in tumor cells [21]. Another CD-OPRT hybrid gene was also constructed, with a linker (SGGGASGGGASGGGASGGGA) between CD and OPRT to generate pAC3-yCD2-LO / T5.0005. Table 1 summarizes the descriptions of the various CD genes that were synthesized and inserted into the pAC3 plasmid back bone, and **Fig. 3** shows the configurations of the respective RCR vectors.

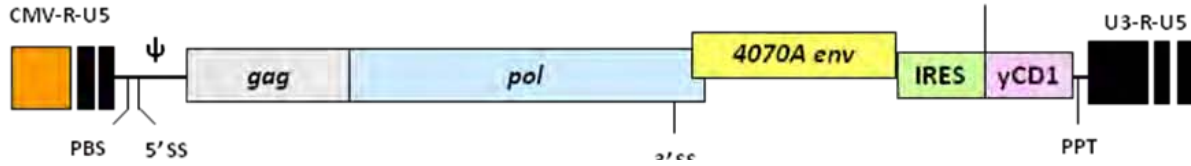
Table 1: Improved RCR vectors containing cytosine deaminase (CD) variants

Vector Code	Reference name	Transgene	Transgene Size (bp)	Notes
NA	pACE-GFP	Emerald GFP	717	Unmodified vector, Ref [13,17]
T5.0000	pACE-yCD	Wt yeast CD	477	Unmodified vector - used by Tai et al. [22]
T5.0001	pAC3-yCD1	modified CD (CD1)	477	Modified vector &IRES, humanized codons
T5.0002	pAC3-yCD2	modified CD (CD2)	477	Modified vector &IRES, humanized codons+3pt mutations
T5.0003	pAC3-yCD2-U	CD2-UPRT	1227	Modified vector &IRES, (humanized codons+3pt mutations)- UPRT fusion
T5.0004	pAC3-yCD2-O	CD2-OPRT	1200	Modified vector &IRES, (humanized codons+3pt mutations) -OPRT fusion
T5.0005	pAC3-yCD2-LO	CD2-L-OPRT	1260	Modified vector &IRES, (humanized codon+3pt mutations)-LINK-OPRT fusion
T5.0006	pAC3-GFP	Emerald GFP	717	Emerald GFP, modified vector, unmodified IRES
T5.0007	pAC3-yCD	Wt yeast CD	477	Modified vector backbone, unmodified IRES

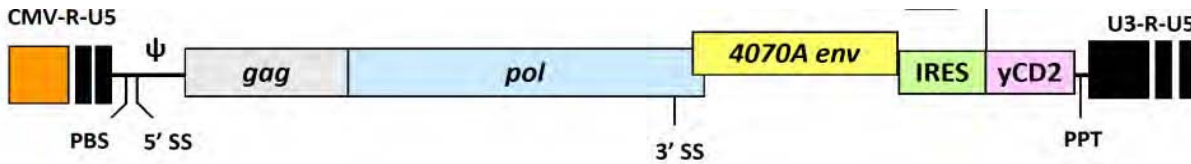
The most promising suicide gene candidate, based on results from Task 2 studies (below), was then used to replace the GFP gene in the ARR2PB- and PSES-targeted RCR vectors.

Figure 3: Structure of RCR vectors with wild type and optimized or hybrid yCD transgene cassettes.

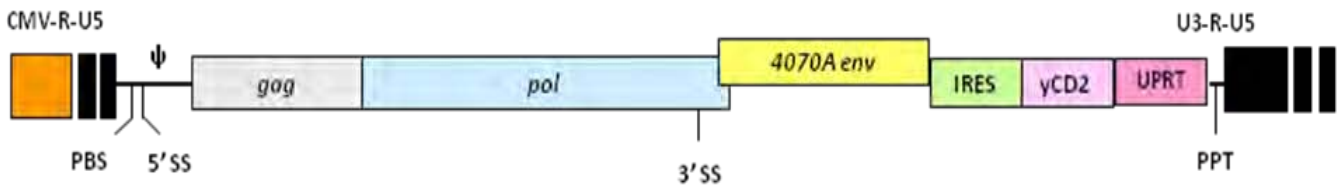
pAC3-yCD1 (T5.0001)



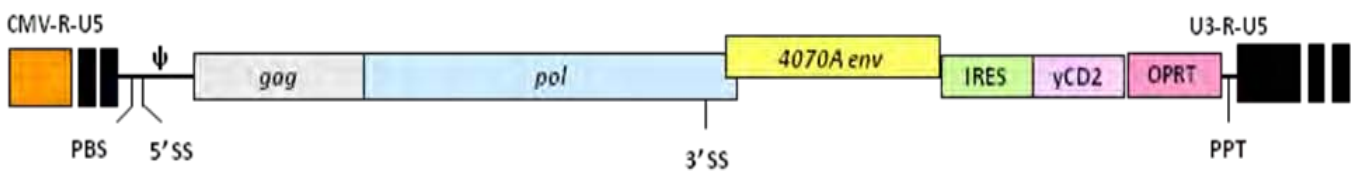
pAC3-yCD2 (T5.0002)



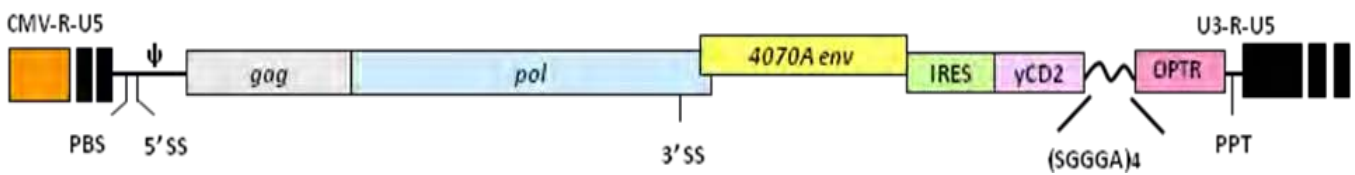
pAC3-yCD2-U (T5.0003)



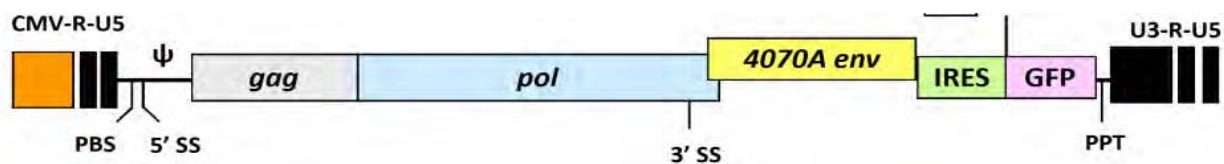
pAC3-yCD2-O (T5.0004)



pAC3-yCD2-LO (T5.0005)



pAC3-GFP (T5.0006)



pAC3-yCD (T5.0007)



Task 2. Testing cell type-specificity of prostate-targeted RCR vectors in culture (Months 6–12)

The cell-type specificity of vector replication and transgene expression by ARR2PB- or PSES-LTR hybrid promoter-driven RCR constructs was confirmed by infection and serial passage in a variety of prostate cancer cell lines versus non-prostatic control cells (Table 2). Please note that, as shown in **Table 2**, most of the prostate cancer cell lines used (except for PC3) are positive for androgen receptor (AR) as well as PSA and PSMA, and were therefore expected to be permissive for both ARR2PB- as well as PSES-driven RCR vector replication and transgene expression.

Table 2: Human prostate cancer cell lines and non-prostatic control cells used in this study.

Abbreviations used are as indicated below the table.

Prostate cancer cell lines

	endogenous genes			predicted promoter activity	
	AR	PSA	PSMA	ARR2PB	PSES
LNCaP	+	+	+	+	+
MDA PCa 2b	+	+	+	+	+
C4-2	+	+	+	+	+
CWR22rv1	+	+	+	+	+
PC-3	–	–	–	–	–

Non-prostate cancer (control) cell line

293T (human embryonic kidney cell)

AR: androgen receptor

PSA: prostate-specific antigen

PSMA: prostate-specific membrane antigen

RESULTS:**Selectivity and androgen-dependence of ARR2PB- and PSES-targeted RCR vector replication**

Replication of ARR2PB-targeted RCR vector (ACE-At-GFP) and PSES-targeted RCR vector (ACE-PSES-GFP) was tested in both prostate cancer cells as well as non-prostatic cell lines as shown above in **Table 2**, using fluorescence-activated cell sorter (FACS) analysis to monitor spread of the GFP transgene.

In LNCaP and MDA-PCa-2b prostate cancer cells cultured under normal serum conditions starting at a 1% infection rate (i.e., virus:cell ratio at inoculation, also called ‘multiplicity of infection (MOI)’ = 0.01), the ARR2PB-driven RCR vector replicated with kinetics only moderately slower than the untargeted wild type LTR promoter-driven RCR vector (**Fig. 4**), as indicated by the progressively increasing number of GFP-positive cells in both groups. Notably, the PSES-driven RCR vector replicated with kinetics that were even more efficient, and comparable to that of the wild type vector.

Furthermore, as expected, GFP expression in 293T non-prostatic control cells, as well as in PC3 prostate cancer cells which are negative for AR as well as PSA and PSMA, remained restricted to a very low number of cells infected by the initial inoculum, with no evidence of further RCR spread even upon continued culture (**Fig. 4**).

The ARR2PB-driven RCR vector was also tested in LNCaP cells cultured in media with charcoal-stripped serum to remove endogenous steroids, with or without addition of 1 nM dihydrotestosterone (DHT). In the absence of DHT, LNCaP cells inoculated with ACE-At-GFP vector showed no increase in GFP over time. In contrast, the percentage of GFP-positive LNCaP cells increased with addition of DHT, confirming that the ARR2PB-driven RCR vector is active only upon androgen induction (**Fig. 5**).

In contrast, LNCaP cells inoculated with RCR vector ACE-PSES-GFP showed progressive increases in GFP-positive cells over time in both the presence and absence of DHT, indicating that PSES-driven RCR vector replication and transgene expression was androgen-independent (**Fig. 5**).

Figure 4: Targeted RCR vectors show robust replication in LNCaP and MDA-PCa-2b cells. Each curve shows spread of GFP expression in the indicated cell lines, as demonstrated by flow cytometric analysis at each time point after inoculation with wild type control vector ACE-GFP, or prostate-targeted vectors ACE-At-GFP and ACE-PSES-GFP.

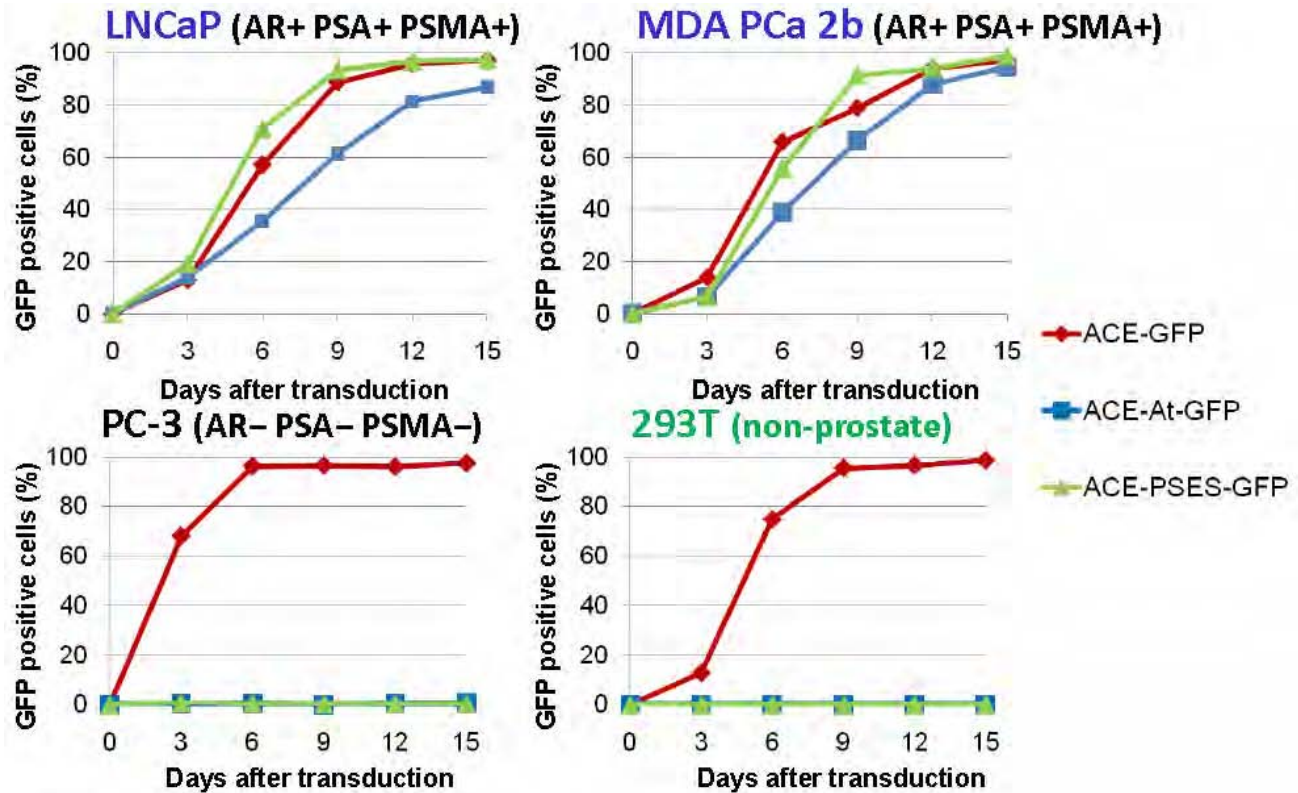
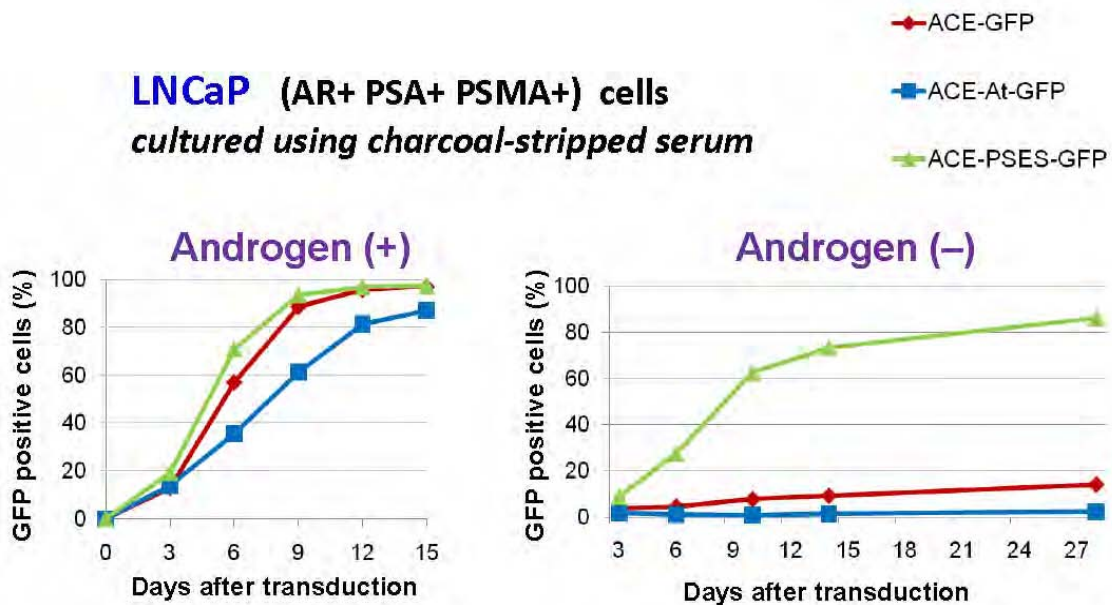


Figure 5: Androgen-dependence of targeted RCR vector replication in LNCaP cells. Each curve shows spread of GFP expression in LNCaP cells in the presence and absence of androgen, as demonstrated by FACS analysis at each time point after inoculation with the indicated vector.

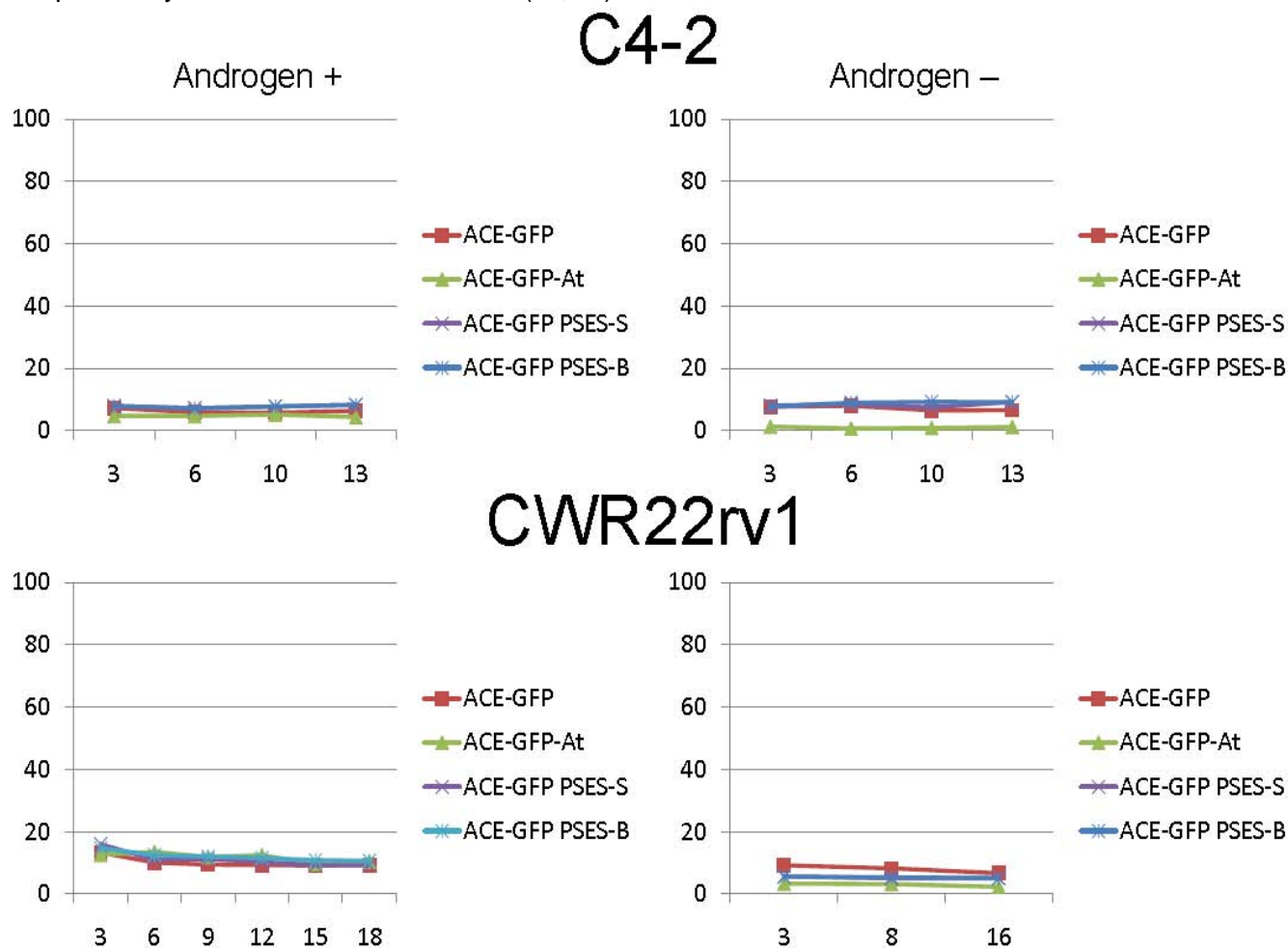


Unpublished Data

However, neither ARR2PB- or PSES-driven RCR vector appeared to be capable of replication in C4-2 or CWR22rv1 cells (**Fig. 6**). This was unexpected, as both cell lines are reported to be AR-positive as well as PSA- and PSMA-positive. In fact, C4-2 cells were initially isolated as a subline of LNCaP, and although these cells have been reported to have lost androgen-responsiveness, they do express low steady state levels of androgen-receptor [23], and have been used to test PSA promoter-driven transgenes in adenovirus vectors [24] as well as PSES-driven adenovirus vectors [14,15]. Similarly, CWR22rv1 cells express androgen receptor as well as PSA and PSMA, and these cells were also among the prostate cancer cell lines originally used to validate the transcriptional activity and selectivity of the PSES regulatory element [14,15].

Figure 6: CWR22rv1 and C4-2 cells are refractory to targeted RCR vector replication.

Each curve shows spread of GFP expression in these cells in the presence and absence of androgen, as demonstrated by FACS analysis at each time point after inoculation with the indicated vector. Two independently constructed PSES vectors (-S, -B) were tested in these cells to confirm results.



Notably, both cell lines were also resistant to wild type RCR vector ACE-GFP infection. Hence, the lack of vector replication in these cells cannot be solely attributed to lack of prostate-specific ARR2PB or PSES promoter activity. In this regard, it has recently come to light that CWR22rv1 cells are primarily composed of a single clonal cell line marked by at least 10 integrated copies of the newly discovered human retrovirus XMRV (xenotropic murine leukemia virus-related virus) [25]. These endogenous XMRV sequences do appear to direct the expression of viral proteins and production of high titer retrovirus from these cells. Although the xenotropic receptor utilized by XMRV differs from the amphotropic receptor utilized by our RCR vectors, it is likely that endogenous XMRV retrovirus expression has activated innate anti-viral defense mechanisms in these cells (e.g., interferon, TRIM-5 α , APOBEC-3G, Tetherin, etc.) that also block replication of the exogenously added RCR vector.

Unpublished Data

Similarly, it is also possible that C4-2 cells, which were derived by repeated xenotransplantation of LNCaP cells co-inoculated with MS bone stromal cells in castrated nude mice, may have acquired a similar xenotropic endogenous murine retrovirus during the process of derivation, although this has not yet been evaluated in the literature. Notably, however, we have observed that murine cell lines such as B16 melanoma and MBT-2 bladder cancer cells, which have been reported to show activation of endogenous retroviruses, are also the only cells we have tested to date that are highly refractory to RCR vector infection and replication. Thus, it is likely that a more fundamental block to retrovirus infection exists in these particular cell lines.

Replication of wild type and prostate-targeted RCR vectors in murine prostate cancer cell lines

We also tested replication of ARR2PB-targeted RCR vector (ACE-At-GFP) and PSES-targeted RCR vector (ACE-PSES-GFP) in *Pten*-deleted, AR-positive murine prostate adenocarcinoma cell lines derived from the *Pten*-knockout transgenic mouse model of prostate cancer [26,27]. The *Pten* ('phosphatase and tensin homolog deleted on chromosome 10') tumor suppressor gene encodes a phosphatase that antagonizes phosphatidylinositol-3-kinase (PI3-K) / protein kinase B (Akt) signaling [28], and is frequently disrupted in a variety of tumors, including prostate cancer [29]. In this recently developed transgenic knockout model, deletion of loxP-flanked sequences in the *Pten* tumor suppressor gene is achieved by probasin-driven expression of Cre recombinase. The resultant animals exhibit spontaneous development of hyperplasia and metaplasia of the prostatic epithelium, followed by PIN lesions and progression to invasive adenocarcinoma, and subsequent micrometastasis [27].

Three different cell lines derived from this model were used: PTEN-P8, PTEN-CaP8, and E4. The PTEN-P8 cell line was isolated directly from true adenocarcinoma arising spontaneously in this prostate cancer model, generated by mating mice with bi-allelic floxed PTEN loci with mice expressing Cre recombinase under the control of a prostate-specific promoter [27]. Notably, PTEN-P8 cells are deleted in only one PTEN allele, are only weakly tumorigenic *in vivo*, and no longer express the recombinase [26]. Subsequently, PTEN-CaP8 cells were derived from PTEN-P8 by introduction of a retroviral vector constitutively expressing Cre, resulting in deletions in both PTEN alleles, and exhibit much more robust tumorigenicity *in vivo* [26]. The E4 cell line is also an AR-positive, androgen-dependent cell line independently derived from a *Pten*-knockout prostate tumor, and shows markers associated with epithelial-mesenchymal transition [30]. Notably, when re-implanted *in vivo*, this cell line formed sarcomatoid carcinoma in both male and female mice, characterized by spindle-shaped cells co-expressing both epithelial and mesenchymal markers.

PTEN-P8 cells were permissive for both wild type and ARR2PB-targeted RCR vector replication, as indicated by progressive spread of GFP over time (**Fig. 7**). However, both PTEN-CaP8 and E4 prostate cancer cells derived from the same type of *Pten*-knockout model were refractory to both ARR2PB- and PSES-targeted RCR vector replication, regardless of the initial MOI used (**Fig. 8 & 9**). In contrast, wild type RCR vector ACE-GFP showed robust transmission of the GFP transgene associated with viral replication over time, indicating that there was no intrinsic block to retrovirus replication, and instead suggesting that ARR2PB and PSES promoters were not functional in these cell lines. Notably, it has been shown that probasin expression is lost in late-stage tumors in both TRAMP and *Pten*-KO prostate cancer models, and there is no murine equivalent of human PSA, which may account for these results.

Figure 7: PTEN-P8 cells are permissive for wild type and targeted RCR vector replication.

Each curve shows spread of GFP expression, as measured by FACS analysis at each time point after inoculation of 10e5 target cells were with the indicated vector at MOI = 0.05 on day 0.

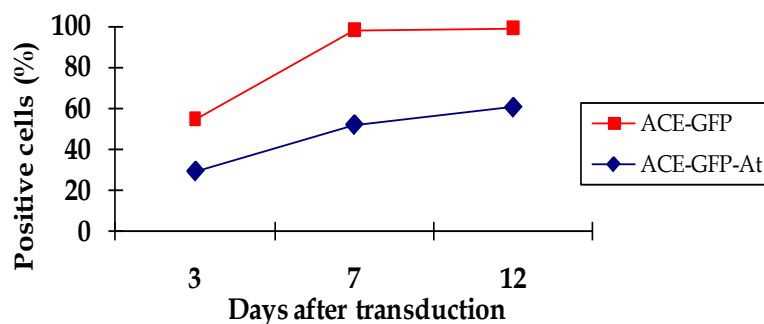


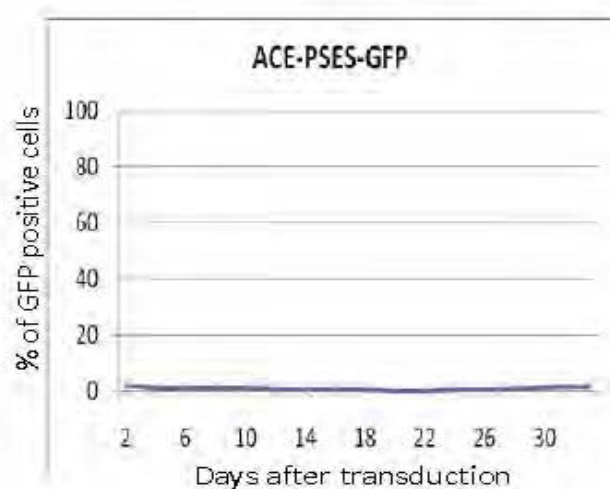
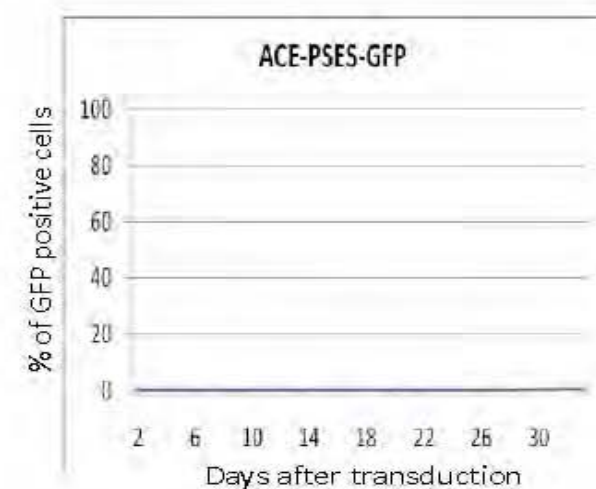
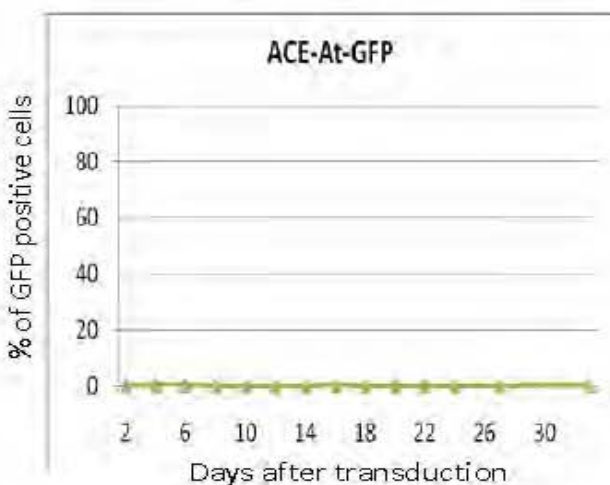
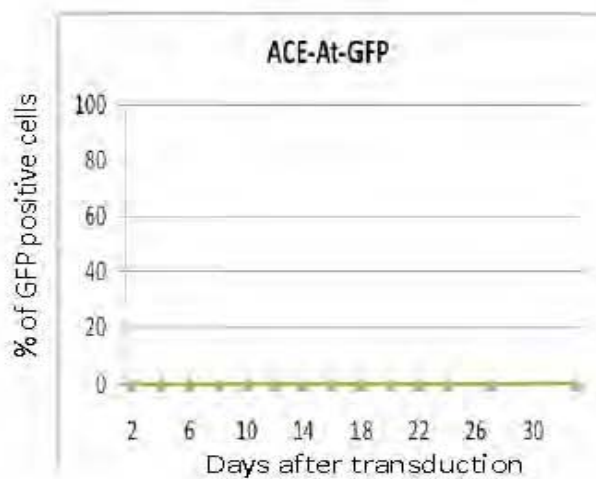
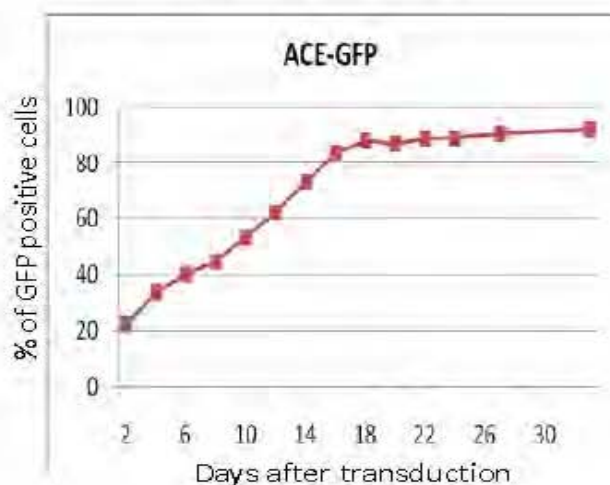
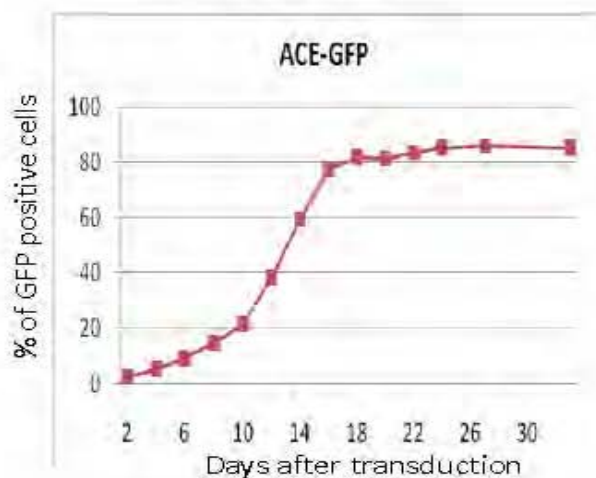
Figure 8: PTEN-CaP8 cells are not permissive for targeted RCR vector replication.

Each curve shows spread of GFP expression, as measured by FACS analysis at each time point after inoculation of 10e5 target cells were with the indicated vector at MOI = 0.01 and 0.1 on day 0.

CaP8 cells

Initial MOI=0.01

Initial MOI=0.1

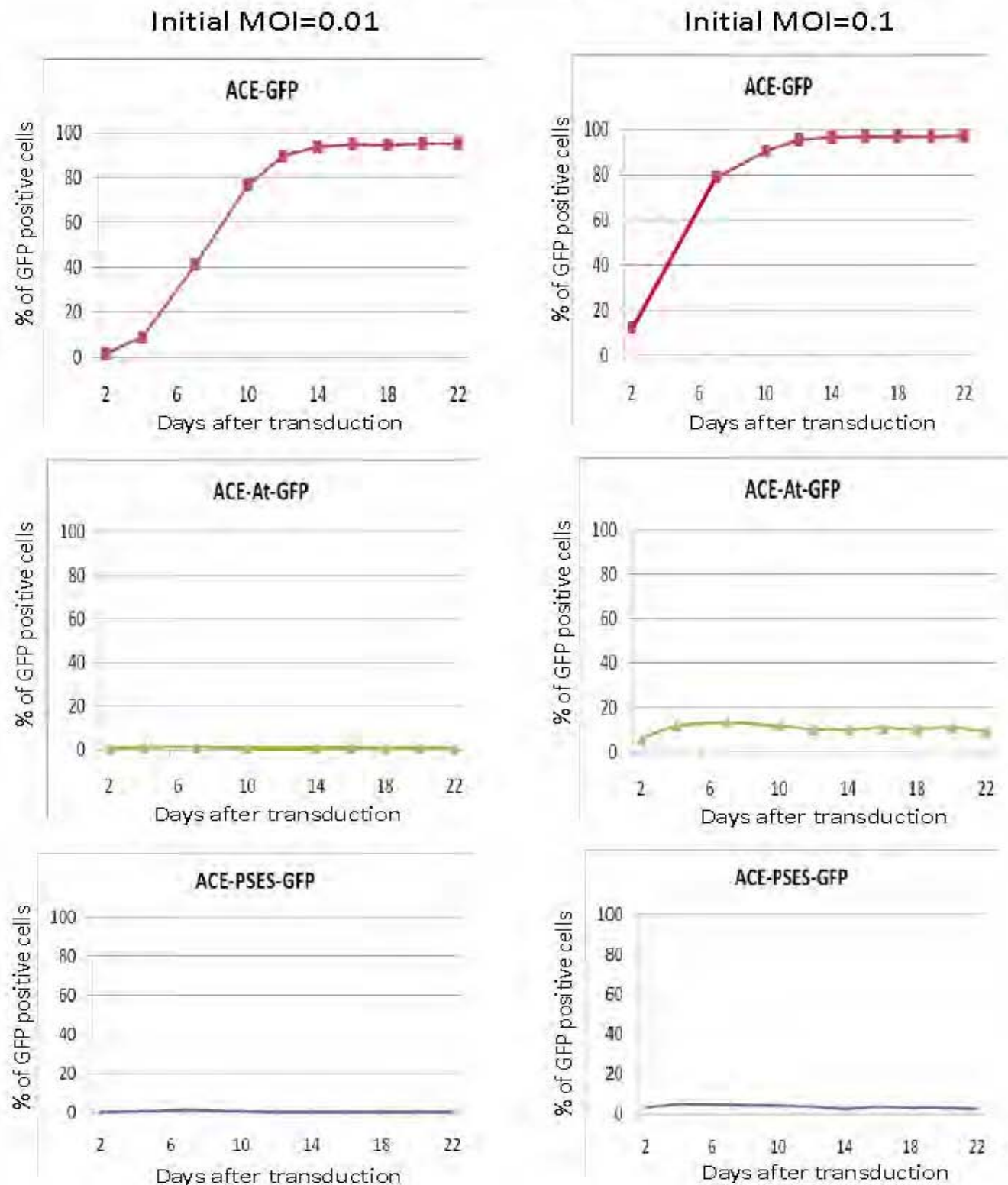


Unpublished Data

Figure 9: E4 cells are not permissive for targeted RCR vector replication.

Each curve shows spread of GFP expression, as measured by FACS analysis at each time point after inoculation of 10e5 target cells were with the indicated vector at MOI = 0.01 and 0.1 on day 0.

E4 cells



Unpublished Data

Enhanced genomic stability of improved RCR vectors with codon-optimized suicide genes

A key consideration in choice of vector is the stability of the genome over multiple cycles of replication. To test this genomic stability, each RCR vector was used to infect 10^6 target cells at an initial multiplicity of infection (MOI) of 0.01. At seven days post-infection, another 100-fold dilution of supernatant was passed onto another 10^6 naïve cells, grown for 7 days, then re-passaged onto fresh cells in the same manner, and so on for up to 12 passages over a 3-month period (P1 - P12, **Fig. 10**). At the end of each passage, genomic DNA was isolated from the fully infected cells, and PCR was performed using primers spanning the IRES-transgene cassette in the provirus, and the amplification products were run on a gel to assess the genomic integrity of the vector.

Representative results are shown in **Fig. 10**. The original vector pACE-yCD (T5.0000) was observed to be stable until about passage 5 - 6. This is the virus that was previously shown to have significant therapeutic benefit in various human xenograft and murine syngeneic tumor models. T5.0007 (pAC3-yCD) which has the same transgene (yCD) but an altered viral backbone is stable up to P7 - 8, revealing that the alterations to the vector backbone did improve the genetic stability of the virus. It should be noted that, even up to passage 7, if every aliquot of 100-fold diluted virus supernatant spreading to 10^6 cells at every passage were utilized, the total number of cells that could be transduced by these vectors is equivalent to $10^6 \times (100)^7 = 10^{20}$ target cells.

Interestingly, T5.0001 (pAC3-yCD1), which contains a codon-optimized version of yCD, was markedly more stable than T5.0000 and T5.0007, and shows stability to passage 11 with a slightly lower band appearance at passage 12. This indicates that altering the coding sequence of CD while maintaining the same amino acid sequence had resulted in further stabilization of the virus genome. This further suggests that other unstable gene inserts may be stabilized by varying the coding sequence.

T5.0002 (pAC3-yCD2), which also contains a codon-optimized version of yCD along with 3 additional point mutations that heat-stabilize the enzyme at 37 °C, was found to be equally stable. In fact, in repeat experiments, T5.0002 proved to be the most stable vector among all of those tested.

The yCD-UPRT and yCD-OPRT fusion gene inserts proved to be less stable; T5.0004 and T5.0005 (yCD-OPRT hybrids) appeared about as stable as T5.0000 (the original therapeutic construct). However, T5.0003 (CD-UPRT) was considerably less stable than T5.0000, and was not used further.

These serial passage experiments were repeated 2 additional times. Repeat experiments showed that genomic instability appeared around the same passage number each time. However, the band pattern of these repeats were usually not the same as on preceding stability experiments (data not shown) suggesting that the instability is a stochastic process, in agreement with previous data showing that the instabilities can arise from repeats of as small as 4 base pairs in length [31].

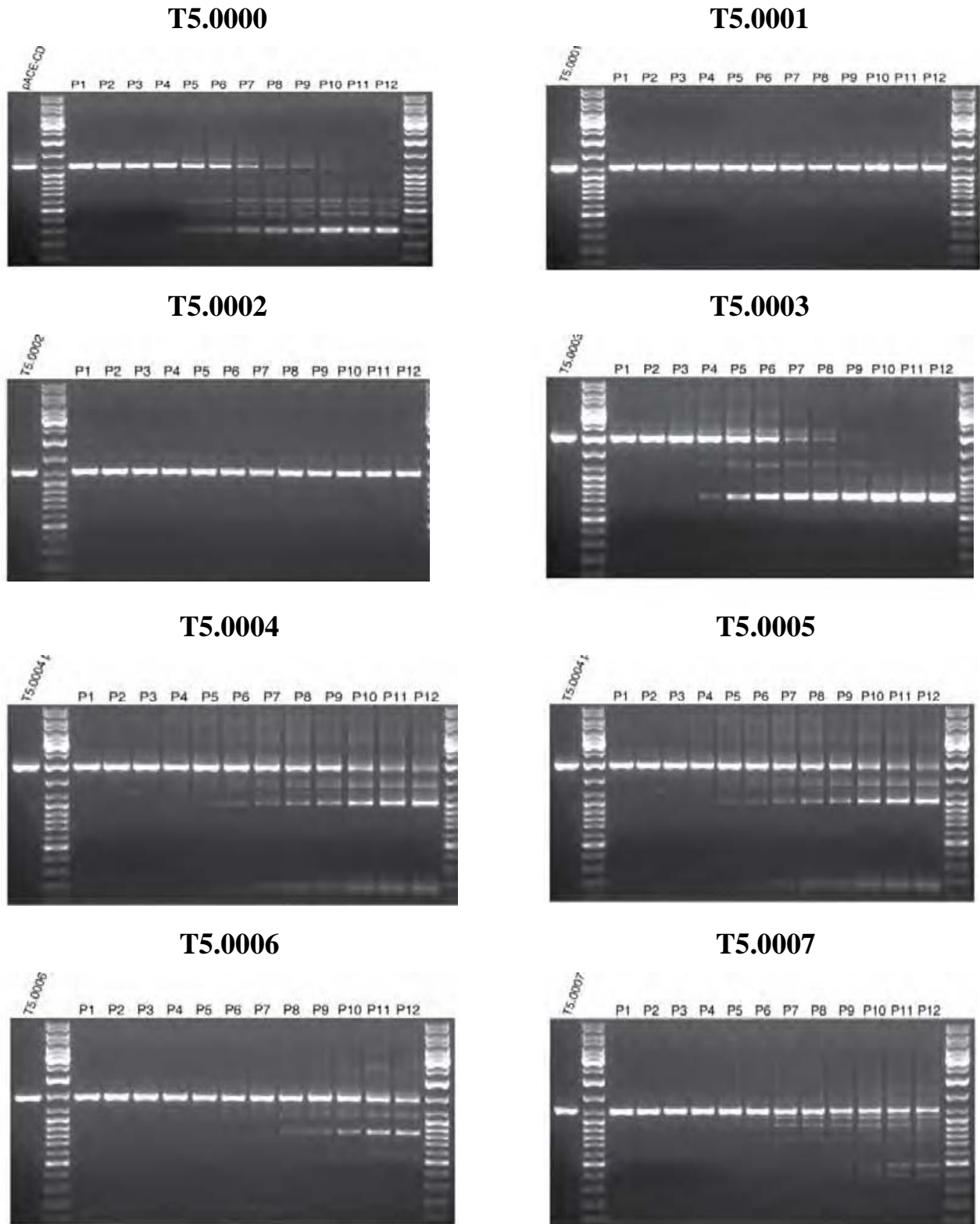
Enhanced potency of thermostabilized and human codon-optimized yCD suicide gene

We measured the specific activity of the cytosine deaminase in cell extracts of fully infected U87-MG glioblastoma cells (after 5 days of infection at a MOI of 0.1). The CD activity was measured, using a calibrated HPLC assay for 5-FU, in nanomoles of 5-FU generated /min at 37°C, per mg protein of the extract. The results are shown in **Fig. 11**, and demonstrate that T5.0002 infected cells have a specific activity of 74.3 nmoles 5-FU/min/mg protein, i.e., roughly two and a half times the activity of the original therapeutic vector, ACE-yCD (T5.0000). The advantage of the humanized codon optimization is reflected in the increased specific activity of T5.0001 vs. T5.0007 (48 nanomoles 5-FU/min/mg protein vs. 36.6 5-FU nanomoles/min/mg protein), which were both higher than the original vector with wild-type CD (30 5-FU nanomoles/min/mg protein). Therefore, the combination of vector backbone improvements, thermostabilizing point mutations and human codon optimization resulted in higher protein expression levels and enhanced specific enzymatic activity relative to wild-type yeast CD.

The resultant optimal pAC3-yCD2 (T5.0002) vector, retaining the wild type LTR, has now proceeded to first-in-man Phase I clinical trials for treatment of patients with recurrent glioblastoma multiforme. Furthermore, based on these genomic stability and potency results, we proceeded to re-clone the ARR2PB-MLV and PSES-MLV hybrid LTRs into the optimal pAC3-yCD2 (T5.0002) vector for use in subsequent therapeutic experiments employing prostate-targeted RCR vectors. These vectors were designated pAC3-At-yCD2 and pAC3-PSES-yCD2, respectively (**Fig. 12**).

Figure 10: Genomic stability comparison of RCR vectors with optimized suicide genes.

Each panel shows the relative stability of the integrated proviruses at 12 serial passages (P1 – P12) by displaying the PCR product amplified across the IRES + transgene sequence, using genomic DNA from infected cells at each passage. The positive control, amplified directly from each vector plasmid, is shown on the far left lane, and a size marker is in the next lane in each panel. Bands with mobility less than the positive control indicate the appearance of deletion mutants in the IRES-transgene region.



Unpublished Data

Figure 11: Enhanced potency of RCR vector with human codon-optimized, heat-stabilized yCD gene.

Specific enzyme activity at 37°C of wild type yCD (T5.0000, T5.0007), human codon-optimized yCD (T5.0001), and human codon-optimized yCD with 3 thermo-stabilizing point mutations (T5.0002). The specific enzyme activity was measured by a calibrated HPLC assay to detect 5FU, the conversion product of the 5FC prodrug, in protein extracts from infected cells harvested 5 days post-infection at MOI = 0.1, and is expressed as nmol 5FU produced per min per mg protein.

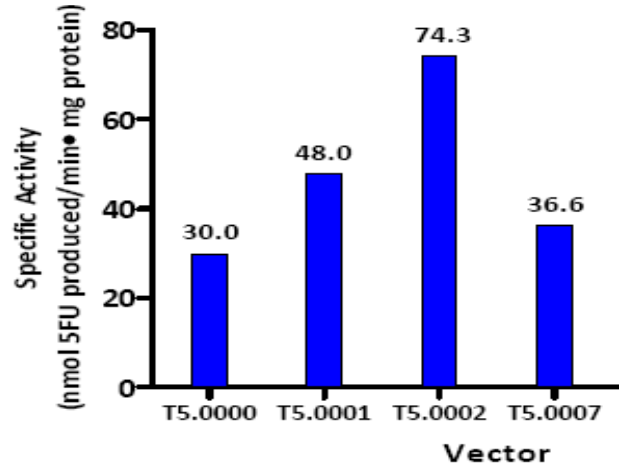


Figure 12: Structure of prostate-targeted vectors containing optimized yCD2 suicide gene.

Each vector contains the *gag*, *pol*, and amphotropic (4070A strain-derived) *env* structural genes of MLV, with improvements to the vector backbone as described in the text, as well as the human codon-optimized and thermo-stabilized IRES-yCD2 cassette inserted downstream of the *env* gene.

pAC3-yCD2 (human codon optimized, thermostable)



pAC3-At-yCD2 (ARR2PB promoter-targeted)



pAC3-PSES-yCD2 (PSES promoter-targeted)



Task 3. Testing replicative specificity of prostate-targeted RCR vectors in vivo (Months 8–18)

In Task 3, we have performed animal studies with prostate-targeted RCR vectors expressing GFP to determine the efficiency and specificity of replicative spread in prostate cancer models *in vivo*. Originally, we had proposed to employ the *Pten*-knockout model of murine prostate cancer to test these targeted vectors. However, as shown above, the results from *in vitro* studies in Task 2 indicated that the ARR2PB- and PSES-targeted RCR vectors do not replicate well in 2 out of 3 murine prostate cancer cell lines derived from this model. These findings necessitated modifications to our proposed research design for the *in vivo* studies related to Task 3.

In this context, in previous studies testing the use of RCR vectors in a murine colorectal cancer (CT26) model in immunocompetent syngeneic mice, we had found that replication of even the wild type RCR vector proved to be highly restricted to the tumor, without spread to normal tissues including bone marrow, spleen, and intestine [32,33]. In recent studies employing a murine glioma (TU2449) model in syngeneic mice, similar results were observed. In contrast, it has been shown that in immunodeficient mice, intravenously administered MLV can infect lymphohematopoietic tissues [34]. This suggests that an intact immune system may be sufficient to prevent spread of wild type RCR vector to normal tissues.

Accordingly, we focused initial animal studies for Task 3 on testing the replicative efficiency of untargeted wild type RCR vector in the *Pten*-knockout model of spontaneous prostate cancer, with the rationale that this would provide insight into the role of the immune system in controlling RCR vector spread in immunocompetent animals.

Furthermore, in order to pursue our original goal of testing the tumor-selectivity of ARR2PB- and PSES-targeted RCR vector replication *in vivo*, we also refocused our efforts toward employing the LNCaP human prostate cancer xenograft model in athymic nude mice to evaluate these targeted vectors. In fact, as noted above, since immunodeficient animals are permissive for MLV infection in normal tissues, this xenograft model represents a more stringent test of the effectiveness of transcriptional targeting.

RESULTS:

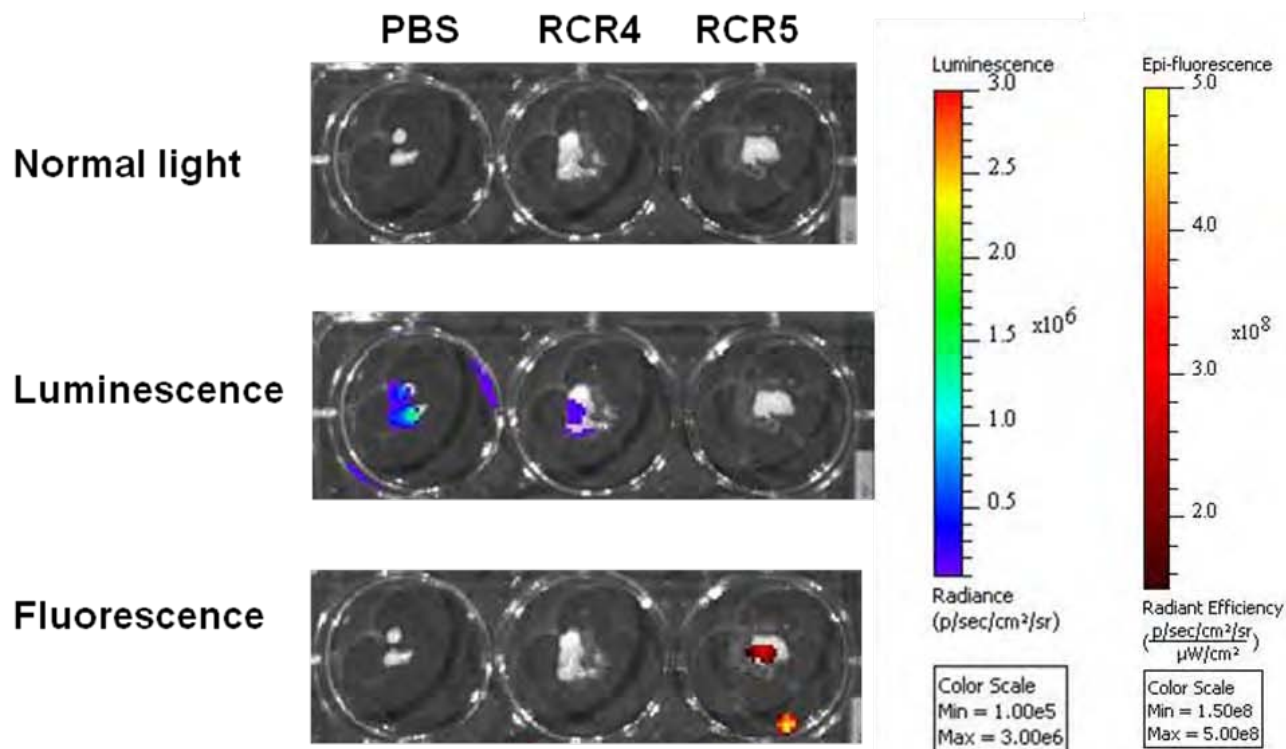
Wild type RCR vector replication in the CPPL *Pten*-knockout model of prostate cancer

In this bioluminescent variant of the *Pten* knockout prostate cancer model, the prostate-specific *Pten*-knockout mice were cross-bred with LucRep transgenic mice, in which the firefly luciferase (*Luc*) reporter gene is separated from a β -actin promoter by an intervening “floxed” polyadenylation sequence that inhibits its expression [35]. Probasin-driven Cre recombination excises both floxed *Pten* alleles and floxed polyA inhibitor, thereby resulting in a luciferase-marked prostate cancer model, designated as CPPL mice [36].

Orthotopic injection of RCR vector AC3-Stb, expressing the Strawberry red fluorescent protein in the context of the optimized vector backbone, was performed into areas of probable prostate tumor formation, as assessed by visual examination during laparotomy in 5- to 6-month-old CPPL mice. Mice were imaged at various time intervals post-vector injection, and tumors harvested for ex vivo imaging as well as molecular analysis by Q-PCR at these time points. **Figure 13** shows representative examples of imaging results from dissected tumor tissues.

Figure 13: Ex vivo imaging after intratumoral RCR vector injection in CPPL model.

Panels show dissected tumors from PBS-injected negative control, and two RCR vector-injected CPPL animals, examined under normal light, as well as for luminescence (tumor signal) and fluorescence (vector signal).



Unpublished Data

However, molecular analysis of CPPL mice injected with RCR vector and maintained for various time intervals ranging from 2 weeks to 23 weeks showed very low level transduction signals ranging between 3.3 - 564.4 vector copies per 300 ng genomic DNA, corresponding to 0.01 – 1.13 % levels of transduction (n=25). Unfortunately, there was no consistent temporal pattern of signals that might indicate progressive spread of RCR vector over time. This level of transduction is equivalent to what might be expected after injection of a replication-deficient vector.

It was noted that the tumors in CPPL animals at this age were still rather small (< 5mm) and often difficult to visualize and inject accurately, and instances of injection fluid backflow were not uncommon, which could significantly reduce the amount of initial virus inoculum reaching the tumors. Furthermore, these tumors still tended to grow very slowly, and uninjected tumor-bearing control animals in the same age group were observed to survive for more than a year afterward. MLV-based RCR vectors absolutely require active cell division to enter the nucleus and integrate into the host cell genome, and establish a productive infection. Therefore, given the low levels of transduction observed, whether adequate levels of virus injection were achieved, as well as whether the level of cell proliferation in these tumors was sufficient to support virus replication, are both open to question. Additionally, it is possible that anti-viral immune responses might have prevented virus replication in this immunocompetent model. These issues might be alleviated to some extent in older animals bearing larger tumors which could be injected more easily and accurately, which may be growing more aggressively and harboring a higher fraction of cells undergoing mitosis, and which may contain more extensive stroma that can form a more immunosuppressive microenvironment.

In studies performed in older animals, intratumoral injection of RCR vector (1 x10e3 TU) was performed during surgical laparotomy of *Pten*-knockout mice at 8 - 9 months of age, at which point the animals had already developed large tumors easily identifiable by visual inspection. Tumors and various normal tissues were harvested 3 weeks later and frozen tissue sections examined by fluorescence microscopy for GFP expression, with DAPI counterstain. Representative photomicrographs are shown in **Figure 14**.

Significant areas of GFP fluorescence were observed in cancerous areas from different lobes of the prostate (**Fig. 14, left panel**). GFP signals were also sometimes observed in regional lymph nodes, but no GFP expression could be observed in the lungs or liver (**Fig. 14, right panel**). It is likely that the GFP signals observed in the lymph nodes are due to the presence of metastatic prostate cancer cells that have been infected by the RCR vector and subsequently migrated to these ectopic sites, but we cannot rule out the possibility of direct viral spread to lymphoid cells.

Molecular confirmation of RCR vector transduction in the tumors was performed by PCR amplification of the GFP sequence from genomic DNA extracted from the anterior lobe of mice at 6 weeks post-vector injection, using methods as previously described [17,37]. To generate a standard curve, genomic DNA extracted from NIH3T3 cells pretransduced with RCR vector expressing GFP (confirmed to be 100% transduced by FACS analysis) was mixed with genomic DNA from untransduced naïve NIH3T3 cells at several different ratios, and amplified under the same conditions. The results show that the GFP sequence could be amplified only from RCR vector-injected prostate tissue, and not from PBS-injected control prostate tissue. The percentage of vector-positive cells was estimated to be approximately 20% (**Fig. 15**).

Thus it appears that, even with the use of untargeted wild type RCR vector, the level of transduction achieved in the *Pten*-knockout model of murine prostate cancer is limited by the small initial tumor size and slow growth rate, the limited volume of initial virus inoculum that can be delivered, and possibly innate and/or adaptive anti-viral immune responses. Also, as implicated by the *in vitro* studies, it is possible that endogenous murine retroviruses become activated in these spontaneously developing prostate cancer models. Again, prior activation of endogenous murine retroviruses appears to be associated with loss of permissivity for replication of MLV-based RCR vectors. Future studies in transgenic murine tumor models will need to assess the contribution of these various parameters individually to RCR vector spread and transduction efficiency. However, as many of these issues may represent technical problems arising specifically from the use of mouse models, it remains uncertain how relevant these parameters will be for the use of RCR vectors in human prostate cancer.

Figure 14: RCR vector transduction in PTEN-knockout prostate cancer model *in vivo*.

Fluorescence imaging of GFP (left column), DAPI (middle column), and GFP+DAPI overlay (right column) after intraprostatic injection of RCR vectors expressing GFP in Pten-knockout prostate cancer mice. Left panel: positive fluorescent signals from individual prostate lobes, as indicated. Right panel: GFP fluorescence detected in regional lymph nodes but not in distant site organs. Faint areas of background autofluorescence seen in lung tissue are due to elastin, and in liver are due to cytochromes.

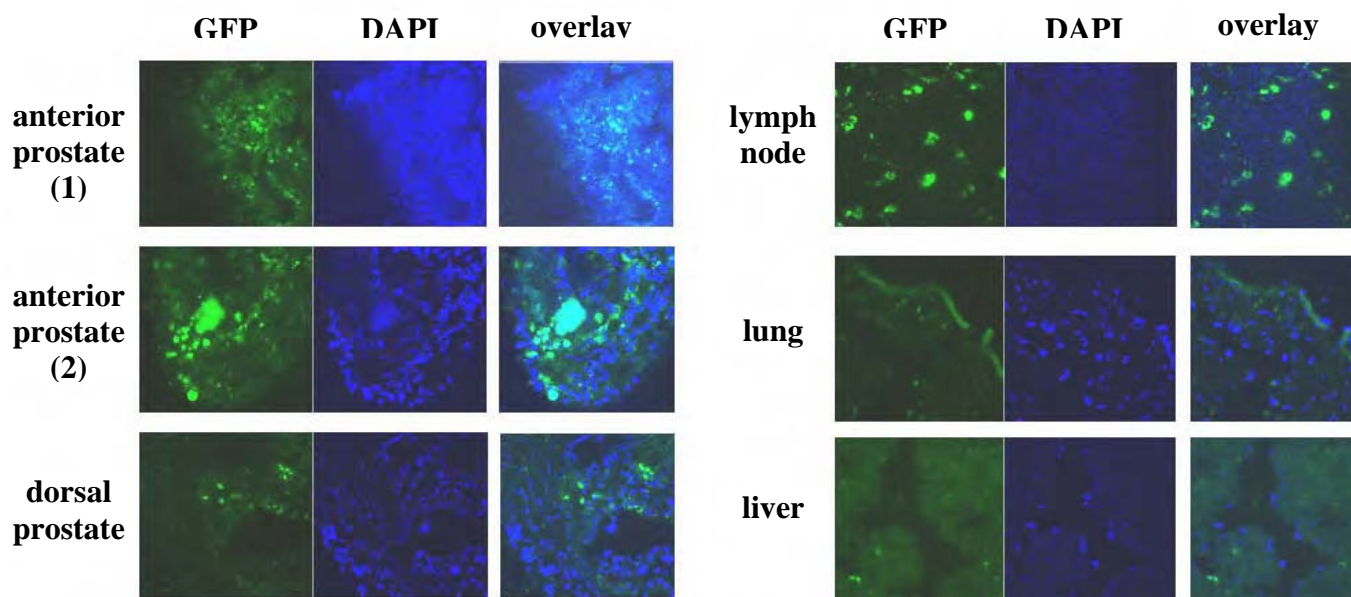
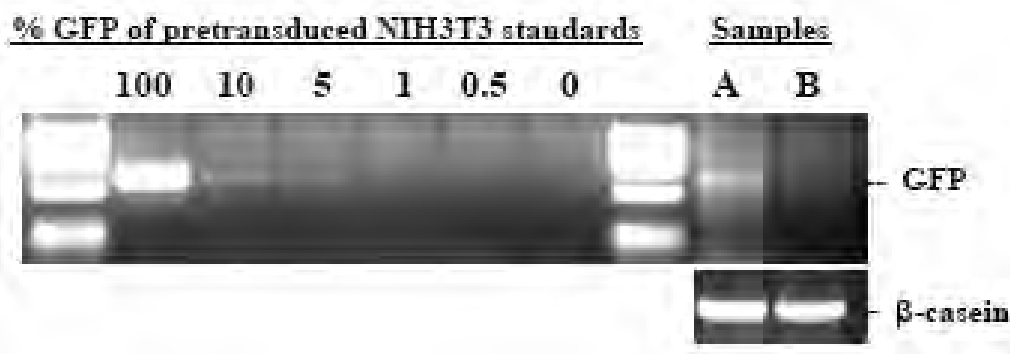


Figure 15: PCR analysis of RCR vector transduction in Pten-knockout mice.

500ng of genomic DNA was amplified by PCR using primers for GFP with an expected fragment size of 700bp. Standards using RCR vector-transduced and -untransduced NIH3T3 genomic DNA mixed at different ratios (0, 0.5, 1, 5, 10, and 100% transduced, as indicated) demonstrate that the detection limit of this assay is about 1%. Samples: (A) ACE-GFP injected prostate tissue, (B) PBS-injected control prostate tissue. Lower inset shows the endogenous beta-casein gene amplified as an internal control.



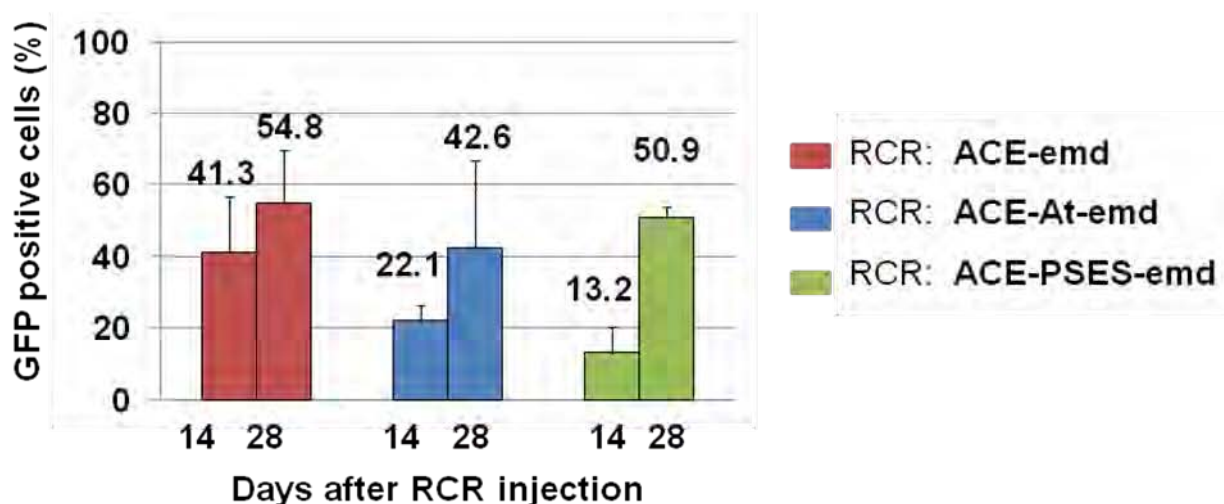
Wild type vs targeted RCR vector replication in LNCaP xenograft prostate cancer model

As noted above, we also re-focused our efforts to test the effectiveness of transcriptional targeting in the LNCaP model of human prostate cancer xenografted in athymic nude mice. Tumors were established by subcutaneous injection of 2×10^6 LNCaP cells into the anterior flanks of 8-week-old nude mice. Three to four weeks later, when the tumors had grown to 1-1.5 cm in diameter, intratumoral injections of untargeted or targeted RCR vectors (1×10^4 TU per 100 μ l), or PBS control were performed. Tumors were harvested 14 or 28 days later, treated with collagenase, and the resultant cell suspensions were analyzed by FACS for GFP expression (Fig. 16).

In this model, high levels of transduction were observed with untargeted as well as both ARR2PB- and PSES-targeted RCR vectors. Furthermore, transduction levels were observed to increase over time, indicating that efficient replication of untargeted and targeted RCR vector could be achieved in LNCaP prostate tumors *in vivo*.

Figure 16: Efficient replication of wild type and targeted RCR vectors in LNCaP model *in vivo*.

Bar graphs show levels of GFP expression, as measured by FACS analysis at each time point after harvest and collagenase digestion of tumors.



In collaboration with Dr. David Klatzmann (Hôpital Pitié-Salpêtrière, Paris) [34,38], we have established a real-time quantitative PCR (Q-PCR) assay using GFP-specific primers, as well as MLV-specific primers, which can detect the RCR vector even if the transgene is lost or mutated. The detection sensitivity of this qPCR assay is on the order of 20 copies/ 300ng genomic DNA (50,000 cell equivalents). Using this assay, in order to determine whether any extratumoral spread of RCR vector might have occurred, Q-PCR analysis was performed on various normal organs, including lungs, kidney, testis, liver, spleen, bone marrow, and upper and lower GI tracts, harvested at the 28-day time point. Notably, low level but distinctly positive signals could be detected from various extratumoral tissues in athymic mice bearing LNCaP tumors injected with untargeted RCR vector. In contrast, no positive signal could be detected from any sample in mice with LNCaP tumors injected with ARR2PB-targeted RCR vector except for the infected prostate tumors, indicating that the targeted vector had not disseminated to normal organs (Table 3).

Table 3: Biodistribution of untargeted and targeted RCR vectors in LNCaP models *in vivo*.

Results shown are copy number of vectors in 300ng of genomic DNA from each tissue, 3 independent experiments. Limit of detection: 20 copies / 300ng of genomic DNA (50,000 cell equivalents).

Vector	Liver	Spleen	BM	Lung	Kidney	Testis	UGI	LGI
ACE-GFP								
1	89.2	150.4	36.1	119.1	29.7	205.3	26.1	102.1
2	23.0	<20	73.1	133.4	22.7	22.2	<20	<20
3	<20	<20	43.1	44.6	<20	<20	<20	<20
ACE-At-GFP								
1	<20	<20	<20	<20	<20	<20	<20	<20
2	<20	<20	<20	<20	<20	<20	<20	<20
3	<20	<20	<20	<20	<20	<20	<20	<20

Untargeted vs targeted RCR vector biodistribution in immunologically immature hosts

Classically, leukemogenesis due to wild type MLV infection of bone marrow and spleen occurs only if the virus is inoculated into immunologically immature neonatal Balb/c mice. Therefore, to further assess the impact of transcriptional targeting on the potential for RCR vector dissemination in normal tissues, we examined biodistribution after intravenous injection of 2×10^4 TU/ 200 μ l of ACE-GFP (untargeted) or ACE-GFP-At (ARR2PB probasin-targeted) vectors, or 200 μ l of PBS as vehicle control, into immature 2-week-old vs. mature 8-week-old Balb/c mice. Various tissues were collected 3 months after viral injection, and the in vivo biodistribution and copy number of each vector was analyzed by real-time Q-PCR of genomic DNA from each tissue, as described above.

After injection at the age of 2 weeks, all mice injected with untargeted ACE-GFP vector showed high levels of integration 3 months later in spleen and bone marrow, and lower levels in liver, testis, and prostate. In contrast, the ARR2PB-targeted ACE-GFP-At vector could not be detected in any tissues analyzed, indicating that transcriptional targeting was effective in preventing potential genotoxicity to hematopoietic tissues even in immunologically immature Balb/c mice, the natural host for MLV leukemogenesis (Table 4). As expected, no signals were detected in any tissues harvested 3 months after injection of immunologically mature Balb/c mice either vector at 8 weeks of age (data not shown).

Table 4. Genomic Q-PCR analysis 3 months after systemic injection of immature Balb/c mice.

Vector	Liver	Spleen	BM	Testis	Prostate
ACE-GFP #1	142.4	985.7	395.9	81.0	105.4
ACE-GFP #2	198.1	2760.9	4511.2	131.6	89.4
ACE-GFP #3	318.9	1385.6	1465.3	109.9	121.7
ACE-GFP-At #1	< 20	< 20	< 20	< 20	< 20
ACE-GFP-At #2	< 20	< 20	< 20	< 20	< 20
ACE-GFP-At #3	< 20	< 20	< 20	< 20	< 20

Numbers show copy number of vectors in 300 ng of genomic DNA (equivalent to 5×10^4 genome) from each tissue.

To further assess viral dissemination and potential for insertional mutagenesis leading to malignancy, we employed a more sensitive bone marrow transplantation model. Lethally irradiated (9 Gy total body irradiation) 6-week-old Balb/c mice were transplanted with 1×10^6 pooled bone marrow cells from syngeneic mice that had been injected with the vectors at the age of 2 weeks. Physical examination on autopsy, histology, and molecular analysis of vector biodistribution by real-time Q-PCR of genomic DNA from various tissues, were performed 4 months later. Real-time qPCR analysis showed high copy numbers in spleen and bone marrow, and lower copy numbers in livers of recipient mice that had been transplanted with bone marrow from untargeted ACE-GFP-injected donors, whereas no signals were detected in recipient mice transplanted with prostate-targeted ACE-GFP-At-injected donors (Table 5).

Table 5. Genomic Q-PCR analysis of recipient mice 4 months after bone marrow transplant.

Vector	Copy number			Spleen weight (mg)	WBC (/ μ l)
	Liver	Spleen	BM		
ACE-GFP #1	297.6	3477.2	10381.2	72.0	7260
ACE-GFP #2	320.9	689.7	12463.2	44.0	7080
ACE-GFP #3	7933.4	25738.7	12332.6	81.4	5860
ACE-GFP-At #1	< 20	< 20	< 20	52.9	7540
ACE-GFP-At #2	< 20	< 20	< 20	64.2	4160
ACE-GFP-At #3	< 20	< 20	< 20	49.7	5180

Numbers show copy number of vectors in 300 ng of genomic DNA (equivalent to 5×10^4 genome) from each tissue.

Thus, in the LNCaP human xenograft model, ARR2PB-directed transcriptional targeting results in a high degree of tumor-specificity for RCR vector replication, as well as a substantial reduction in genotoxicity and oncogenic risk. Further studies are currently being pursued to determine whether similar results can be obtained with PSES-targeted RCR vectors.

Task 4. Testing therapeutic efficacy of prostate-targeted RCR vectors in vivo (Months 12–24)

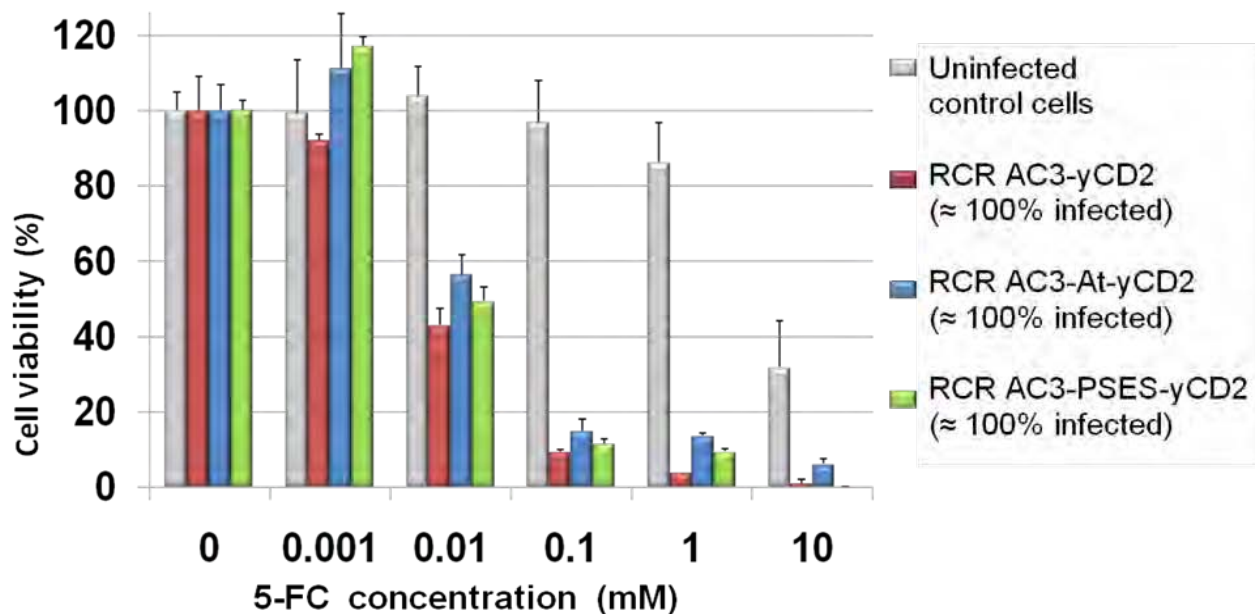
Prior to embarking on therapeutic studies *in vivo*, we have performed and completed *in vitro* studies to test the suicide gene activity and potency of ARR2PB- and PSES-targeted RCR vectors expressing the optimized version of yCD, as described below. On-going studies are currently being pursued to test the therapeutic efficacy of targeted RCR vectors expressing the optimized yCD2 suicide gene *in vivo*.

RESULTS:

Prodrug concentration-dependent cell killing by RCR vectors expressing optimized yCD gene LNCaP cells that had been fully transduced with untargeted RCR vector AC3-yCD2, ARR2PB-targeted RCR vector AC3-At-yCD2, or PSES-targeted RCR vector AC3-PSES-yCD2, were exposed to different concentrations of 5-FC prodrug, and cell viability was measured by a chromogenic assay 5 days later. The results showed that cell viability was maintained without significant non-specific toxicity to uninfected negative control cells at prodrug concentrations of 1 mM or less. In contrast, at 5-FC concentrations in the range of 0.01 – 1.0 mM, LNCaP cells infected with untargeted, ARR2PB-targeted, or PSES-targeted vectors all showed dose-dependent cytotoxicity with increasing concentrations of prodrug. Notably, at 0.1 mM 5-FC, there was virtually no toxicity to uninfected cells, while cells infected with any of the 3 RCR vectors showed reduction in cell viability down to 10-15% that of uninfected controls by Day 5 of incubation. These results indicate that untargeted and targeted vectors show equivalent potency of cell killing at the same prodrug concentration.

Figure 17: LNCaP cell viability after activation of yCD2 suicide gene function at various concentrations of prodrug.

Cell viability of LNCaP cells, seeded into 96-well plates (1x10e3 cells/well) was determined by MTS assay using the soluble tetrazolium salt, MTS (3-(4,5-dimethylthiazol-2-yl)-5-(3-carboxymethoxyphenyl)-2-(4-sulfophenyl)-2H-tetrazolium; CellTiter-96 Non-Radioactive Cell Proliferation Assay, Promega). Error bars indicate standard deviations.



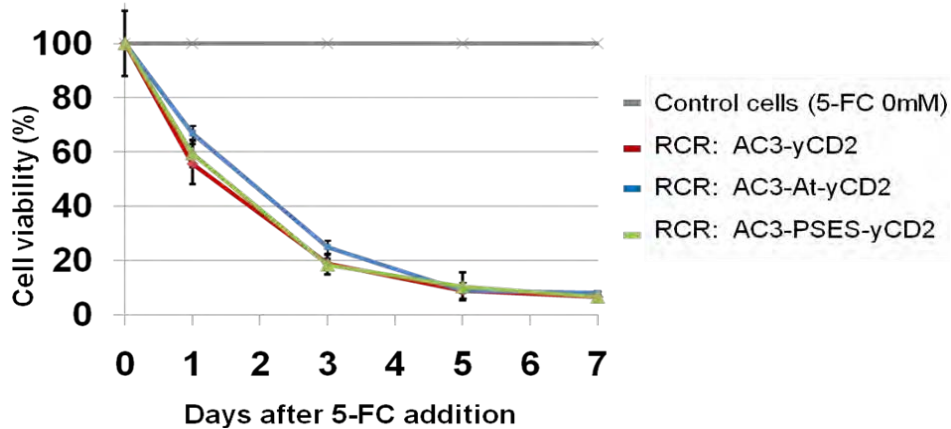
Unpublished Data

Time course of cell killing by RCR vectors expressing optimized yCD2 gene

Multiple replicates of LNCaP cells fully transduced with untargeted RCR vector AC3-yCD2, ARR2PB-targeted RCR vector AC3-At-yCD2, or PSES-targeted RCR vector AC3-PSES-yCD2, were simultaneously exposed to 5-FC at the optimal 0.1 mM prodrug concentration, and cell viability was measured by MTS assay at serial time points thereafter. The results showed progressive loss of cell viability over time, with the time course of cell killing observed to be virtually identical between LNCaP cells infected with untargeted, ARR2PB-targeted, or PSES-targeted RCR vectors expressing the yCD2 suicide gene, again indicating the equivalent potency of these vectors.

Figure 18: Time course of reduction in LNCaP cell viability after suicide gene activation.

Viability of LNCaP cells was determined at each time point by MTS assay as described above, and the results normalized to control cells without prodrug treatment, as indicated.

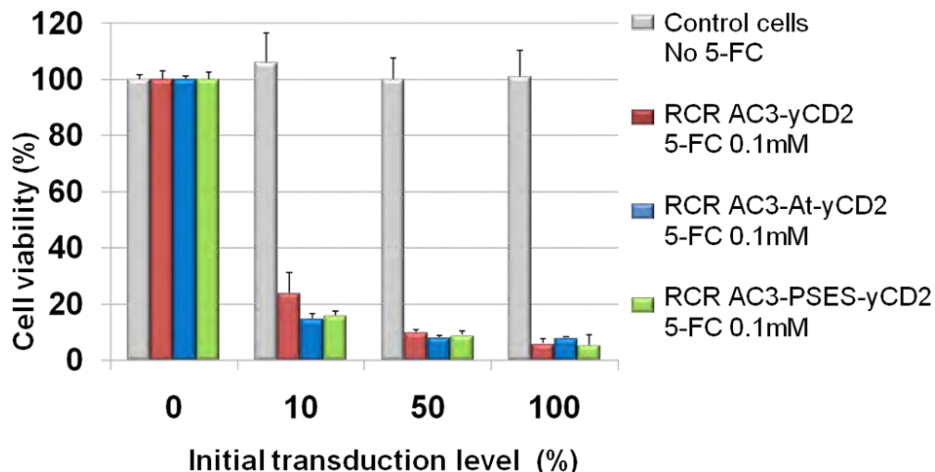


Virus replication potentiates cell killing by RCR vectors expressing optimized yCD2 gene

We then examined whether efficient cell killing could be maintained even at initial transduction levels as low as 10%, due to on-going RCR vector spread. The results indicated that the cell killing efficiency was comparable regardless of the initial transduction level, and are consistent with the time course of RCR vector replication observed in previous experiments, in which 40% to 80% transduction of LNCaP cells was achieved by untargeted and targeted RCR vectors starting at an MOI of 0.01. Hence, while it is also conceivable that a substantial bystander effect might have also contributed to enhanced killing at low transduction levels, it is more likely that on-going RCR vector replication during the prodrug treatment period was responsible for the potent killing effects despite low initial transduction efficiencies.

Figure 19: Effective killing by RCR vectors even at low initial transduction levels.

Infected and uninfected LNCaP cells were mixed at different ratios ranging from 10% to 100% as indicated, and treated with a fixed concentration (0.1 mM) of 5-FC prodrug for 5 days, after which cell viability was determined by MTS assay as described above.



Thus, we have confirmed that the optimized yCD2 suicide gene provides highly efficient killing activity *in vitro*, even in the context of the ARR2PB- and PSES-targeted RCR vectors. Accordingly, we are now pursuing experiments in LNCaP xenograft models to examine the therapeutic efficacy of these vectors *in vivo*. Unfortunately, the timeline for these experiments has been delayed, due both to unexpected turnover of personnel (the primary post-doctoral researcher on this project abruptly left the lab to assume a clinical faculty position in Japan, and it took several months to recruit another post-doctoral researcher to take over his role), and due to the unanticipated difficulties in achieving efficient RCR vector replication in the *Pten*-knockout model, which forced a re-evaluation of our research strategy, as reported above.

In view of the difficulties encountered in achieving efficient intratumoral RCR vector spread in *Pten*-knockout mice, we have also explored additional therapeutic strategies in this model. In particular, as this model represents a true adenocarcinoma that spontaneously arises from prostate epithelium and faithfully recapitulates many aspects of the human disease, it now provides an excellent opportunity for testing of immunotherapeutic strategies against prostate cancer, which has hitherto been impeded by the lack of relevant tumor models in immunocompetent animals. Therefore, we investigated the feasibility of using prostate cancer cell lines derived from this model to test tumor vaccination and adoptive immunotherapy strategies.

PTEN-CaP8 adenocarcinoma cells derived from the bi-allelic *Pten*-knockout prostate cancer model were used to vaccinate non-tumor-bearing littermates. Tumor-specific effector cells were generated from splenocytes of vaccinated mice by mixed lymphocyte-tumor cell reactions, and anti-proliferative effects and cytokine generation were first examined *in vitro*. The *in vivo* effect of vaccination or adoptive immunotherapy on luciferase-marked PTEN-CaP8 subcutaneous tumors was then monitored by tumor volumetric measurements and non-invasive bioluminescence imaging.

The results showed that vaccination of littermate mice with irradiated PTEN-CaP8 cells resulted in a significant prophylactic effect against subsequent tumor challenge. Tumor formation was significantly inhibited in the vaccinated group compared to the control group at 2 weeks after tumor challenge ($p < 0.01$). In fact, no tumor establishment was observed at all in 2 out of 5 of the vaccinated mice, while all of the control mice showed approximately 5-fold increased tumor growth compared to the average tumor size of the vaccinated group (**Fig. 20A**). Thus, PTEN-CaP8 can serve as an effective cell vaccine to prevent and/or retard tumor formation in immunocompetent syngeneic hosts.

Furthermore, effector cells harvested from vaccinated littermates showed significant activation of IFN- γ secretion upon co-incubation with PTEN-CaP8 target cells (**Fig. 20B**), and were capable of efficient target cell growth inhibition *in vitro* (**Fig. 20C**).

Intratumoral adoptive transfer of effector cells resulted in significant growth inhibition of pre-established prostate tumors *in vivo*. Adoptive transfer of activated effector cells to PTEN-CaP8/RL tumors resulted in significant tumor growth suppression compared to untreated control tumors which continued to show progressive growth; by Day 60, there was a significant difference in average tumor volume of 117 ± 53 mm³ in the treated group vs. 1168 ± 627 mm³ in the control group ($p < 0.01$) (**Fig. 21**).

Thus, *Pten*-knockout prostate cancer can serve as a highly useful model to investigate both tumor cell vaccination and adoptive immunotherapy strategies in the context of true adenocarcinoma of the prostate. We have reported these findings in a recent publication [39], and this model now enables further improvements in RCR vector-mediated suicide gene therapy, combined with immunotherapy.

For example, transcriptionally targeted RCR vectors can be combined with a new strategy to improve the efficiency and safety of RCR-mediated gene therapy for systemic metastases by engineering tumor-specific cytotoxic T lymphocytes (CTLs) to function also as vector producer cells or 'carriers' for RCR vectors. This strategy takes advantage of natural tumor homing mechanisms of tumor antigen-directed CTLs, and also affords protection from immunological degradation via shielding by heparan sulfate glycosaminoglycans after virus adsorption to the T cell surface [40]. After reaching the tumor, multi-focal propagation of RCR vectors can be initiated from individual CTL carriers as they migrate throughout the tumor mass, enhancing tumor penetration and accelerating the kinetics of viral spread. Finally, combining tumor-homing CTL-mediated systemic delivery with transcriptional targeting, which restricts subsequent RCR spread to rapidly dividing prostate cancer cells, should provide a combined approach that enhances overall selectivity and safety.

Figure 20: Tumor vaccine effect of PTEN-CaP8 cells in a syngeneic model.

(A.) Non-tumor-bearing littermates of *Pten*-knockout prostate cancer mice were subcutaneously vaccinated with 1×10^6 irradiated PTEN-CaP8 cells (total of 3 times over 2 weeks), followed 2 weeks later by challenge with 1×10^6 live PTEN-CaP8 cells into the contralateral flank. Contralateral flank tumors were measured at day 14 post-challenge in unvaccinated (Control) and vaccinated animals. (B.) Effector cell cultures were prepared from splenocytes harvested 2 weeks after vaccination as above. IFN- γ production by activated effector cells was examined upon co-culture with PTEN-P8 cells. Conditioned medium after overnight CTL culture in absence ('No PTEN-P8') or presence ('With PTEN-P8'; E/T ratio= 1:1) of target cells was assayed by ELISA. Results are expressed as fold-increase compared to negative control. (C.) PTEN-P8 target cell viability after culture in absence ('No Effectors') or presence ('With Effectors'; E/T ratio= 1:1) of effector cells from PTEN-CaP8-vaccinated littermates, evaluated by MTS assay and shown as percentage of cell viability compared to negative control. In each panel, error bars denote standard deviations, asterisks indicate statistical significance ($p < 0.01$).

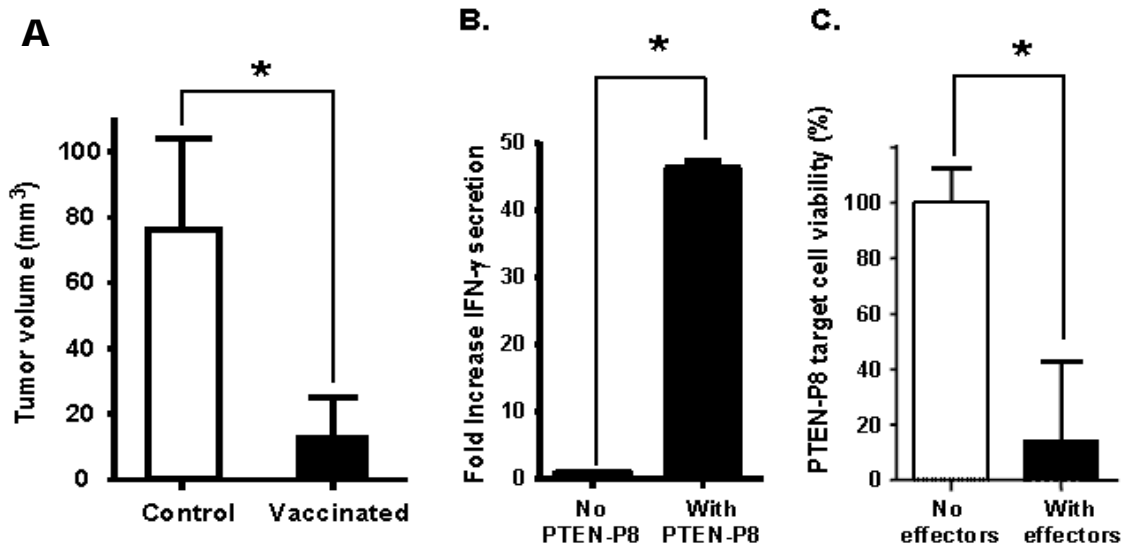
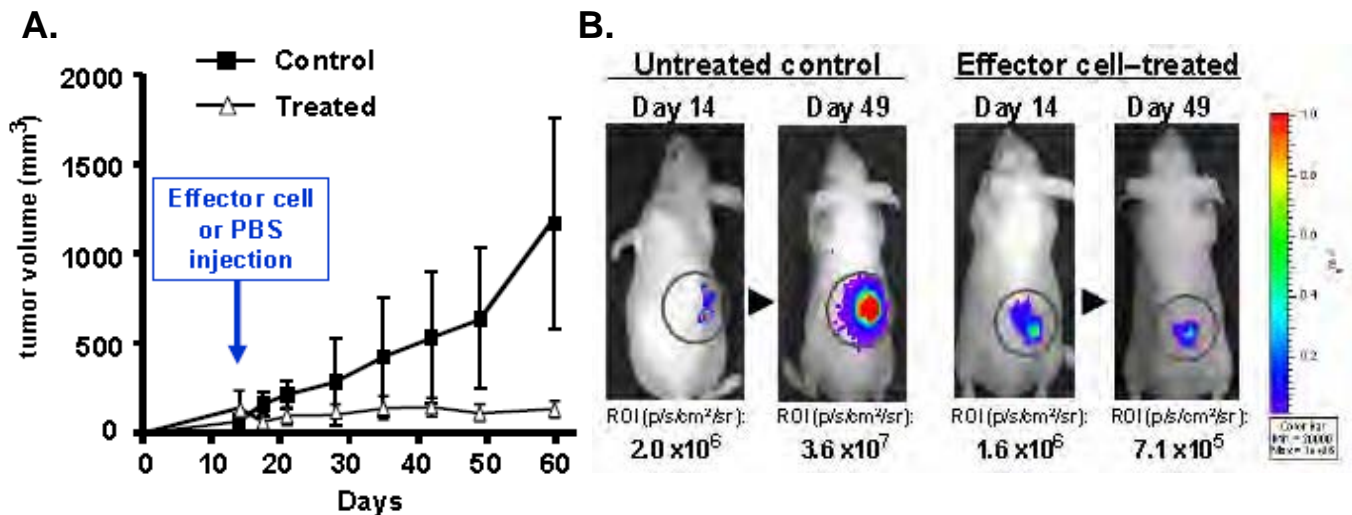


Figure 21: Adoptive immunotherapy in PTEN-CaP8 syngeneic model.

(A.) Growth of PTEN-CaP8/RL subcutaneous tumors in nude mice after treatment by intratumoral injection of effector cells harvested from PTEN-CaP8-vaccinated mice ('Treated') or PBS vehicle ('Control'). Error bars indicate standard deviations. Statistically significant differences in tumor size between the two groups was obtained on Day 60, $p < 0.01$. (C) Representative in vivo bioluminescence images of PTEN-CaP8/RL tumors on Day 14 (prior to treatment) and Day 49, i.e., 5 weeks after injection of saline ('Untreated control') or effector cells ('Effector cell-treated'). Numbers below each panel show the bioluminescence signal measured from the indicated ROI (circled areas) in p/s/cm²/sr.



III. KEY RESEARCH ACCOMPLISHMENTS

1. We have developed replication-competent retrovirus (RCR) vectors that are transcriptionally targeted to prostate cancer cells by introduction of prostate-specific regulatory elements into the retroviral LTR promoter:
 - RCR vectors regulated by the ARR2PB promoter for use in androgen-dependent prostate cancer cells, as well as RCR vectors regulated by the PSES element for use in androgen-independent PSA+/PSMA+ prostate cancer cells, have been constructed.
 - ARR2PB- and PSES-targeted RCR vectors containing the GFP marker gene, as well as those containing the yCD suicide gene, have been constructed.
2. We have developed improved RCR vectors containing an optimized yeast cytosine deaminase (yCD) suicide gene:
 - Optimization of the yCD sequence for human codon usage and incorporation of point mutations for enhanced thermostability at 37°C significantly improved prodrug converting enzyme activity and suicide gene function.
 - Vector backbone sequence as well as optimized yCD coding sequence modifications resulted in significantly improved genomic stability of the RCR vector over serial passage.
 - Notably, this improved RCR vector carrying the optimized yCD suicide gene was selected for further clinical development, and a first-in-man Phase I clinical trial using this vector for treatment of patients with recurrent glioblastoma has been initiated as of August 2010.
3. We have tested the efficiency and cell type-specificity of prostate-targeted RCR vector replication and transgene expression in cell culture:
 - ARR2PB-targeted RCR vector replication was efficient in human prostate cancer cells, and was confirmed to be androgen-dependent and correlated with functional androgen receptor status.
 - PSES-targeted RCR vector replication was also efficient in human prostate cancer cells, and was confirmed to be androgen-independent.
 - Expression of the optimized yCD suicide gene from both ARR2PB- and PSES-targeted RCR vectors achieved highly efficient pro-drug activation and killing of prostate cancer cells.
4. We have confirmed prostate cancer cell-specific replication of prostate-targeted RCR vectors *in vivo* in tumor xenograft models.
 - Efficiency and specificity of ARR2PB-targeted RCR vector replication in prostate cancer cells was confirmed *in vivo* by FACS analysis of disaggregated tumors, and Q-PCR analysis of vector biodistribution in normal tissues of primary recipients as well as secondary transplant recipients.
 - Studies to examine the efficiency and specificity of PSES-targeted RCR vector replication in animal models, as well as *in vivo* therapeutic efficacy studies, are on-going.
5. We have confirmed that Pten-knockout prostate cancer provides a unique immunocompetent model that can be used to test new strategies involving immunotherapy.
 - Both tumor vaccine and adoptive transfer strategies were tested in this model.
 - New strategies to combine tumor-specific T cell therapy with RCR suicide gene therapy are being developed.

IV. REPORTABLE OUTCOMES

Peer-reviewed publications:

1. Haga, K., Tomioka, A., Liao, C.-P., Kimura, T., Matsumoto, H., Ohno, I., Hermann, K., Logg, C. R., Jiao, J., Tanaka, M., Hirao, Y., Wu, H., Kruse, C. A., Roy-Burman, P., Kasahara, N.
PTEN-Knockout Prostate Cancer as a Model for Experimental Immunotherapy.
Journal of Urology, 181: 354-362. (2009)
2. Kimura, T., Hiraoka, K., Kasahara, N., Logg, C. R.
Optimization of enzyme-substrate pairing for bioluminescence imaging of gene transfer using Renilla and Gaussia luciferases.
Journal of Gene Medicine, 12 (6): 528-537. (2010)

Abstracts and Presentations

1. Haga, K., Tomioka, A., Liao, C.-P., Kimura, T., Logg, C. R., Matsumoto, H., Ohno, I., Hermann, K., Tanaka, M., Uemura, H., Hirao, Y., Roy-Burman, P., Kasahara, N.
Suicide gene therapy using replication-competent retrovirus (RCR) combined with tumor-specific cytotoxic T lymphocytes (CTLs) for PTEN knock-out spontaneous prostate cancer model.
(Abstract presented at the 2008 Annual Meeting of the American Urological Association (AUA); Orlando, Florida.)
2. Kasahara, N.
Engineering Multiple Mechanisms of Tumor Selectivity into Replication-Competent Retrovirus Vectors.
(Invited speaker, 2009 International Conference on Oncolytic Viruses as Cancer Therapeutics; Banff, Canada.)
3. Gruber, H., Perez, O., Ibanez, C., Pertschuk, D., Gessner, D., Robbins, J., Kasahara, N., Logg C. R., Jolly, D. J.
Improved Prodrug Activator Gene Therapy for Cancer.
(Abstract selected for oral presentation at the 2009 Annual Meeting of the Japan Society of Gene Therapy; Osaka, Japan.)
4. Kasahara, N.
RCR Vectors: Enhancing Transduction Efficiency and Tumor Selectivity.
(Invited speaker, International Symposium, 2009 Annual Meeting of the Japan Society of Gene Therapy; Osaka, Japan.)
5. Kasahara, N.
Replication-Competent Retrovirus Vectors for Cancer Gene Therapy: Enhancing intratumoral biodistribution, tumor selectivity, and therapeutic efficacy.
(Invited speaker, 2009 Cold Spring Harbor Laboratory biotechnology conference on "In Vivo Barriers to Gene Delivery"; Cold Spring Harbor, NY.)

6. Hiraoka, K., Logg, C. R., Inagaki, A., Matsumoto, H., Diago, O., Perez, O., Robbins, J., Gruber, H., Jolly, D., Kasahara, N.
Optimizing the genomic stability, transgene expression, and therapeutic efficacy of replication-competent retrovirus vectors for prodrug activator gene transfer.
(Abstract presented at the 2010 Annual Meeting of the American Society of Gene & Cell Therapy; Washington DC.)
7. Kamijima, S., Kimura, T., Haga, K., Hiraoka, K., Inagaki, A., Logg, C. R., Kao, C., Bochner, B. H., Kasahara, N.
Tumor-selectivity of replication-competent retrovirus (RCR) vectors regulated by prostate-specific promoters and cytotoxic effect of suicide gene therapy mediated by RCR vector in vitro.
(Abstract selected for oral presentation at the 2010 Annual Meeting of the American Society of Gene & Cell Therapy; Washington DC.)

Cell lines, tissue or serum repositories developed

Murine PTEN-CaP8, human LNCaP, and human PC-3 prostate cancer-derived cell lines expressing firefly, Gaussia, or Renilla luciferase.

V. CONCLUSION

The use of replication-competent viruses represents an emerging technology with the potential to achieve highly efficient gene transfer to tumors, as each transduced tumor cell itself becomes a virus-producing cell, sustaining further transduction events even after initial administration. Unique among replicating viruses being developed as oncolytic agents, murine leukemia virus (MLV)-based replication-competent retroviruses (RCR) replicate without immediate lysis of host cells and maintain viral persistence through stable integration. We and others have previously demonstrated that replicative retrovirus vectors can achieve highly efficient replicative spread and gene transfer in a wide variety of human and rodent tumor cells both in vitro and in vivo, achieving >99% transduction after direct injection of cell-free RCR vector supernatant at MOIs as low as 0.01 into pre-established tumors, representing a tremendous enhancement in efficiency over conventional replication-defective retroviral vectors, which exhibited gene transfer to $\leq 1\%$ of the tumor at the same dose. This enhanced gene transfer efficiency was found to translate into highly significant therapeutic benefit in both immunodeficient xenograft models [17,22] and immunocompetent syngeneic tumor models [32,33].

Until now, however, use of RCR vectors has rarely been contemplated due to potential risks associated with uncontrolled virus spread. Yet, due to MLV's intrinsic inability to infect quiescent normal cells, RCR vectors have proven to be highly selective for rapidly dividing cancer cells. In fact, this selectivity for tumor cells was precisely the rationale underlying the original clinical trials of retrovirus-mediated cancer gene therapy [41,42]. This approach ultimately failed in Phase III trials because conventional replication-defective retrovirus vectors could not achieve therapeutically adequate levels of transduction [43]. With the use of RCR vectors, however, the original promise of this strategy might be fulfilled.

In discussing the feasibility of pursuing human clinical trials of RCR vector-mediated cancer gene therapy, there were three main stipulations from staff at the FDA Center for Biologics Evaluation and Research (CBER). These stipulations were: 1) therapeutic efficacy in rodent models of cancer should be re-confirmed using clinical grade RCR vector preparations that are substantially similar to those proposed for testing in humans, 2) in view of prior literature documenting lack of pathological consequences after i.v. injection of wild type MLV in immunocompetent primates, large animal toxicology studies were not considered necessary, however, 3) *given the known potential for insertional genotoxicity leading to leukemogenesis, particularly in immunodeficient hosts, additional mechanisms for specific targeting to cancer cells are desirable and should be pursued.*

Now, we have shown that virus replication can be restricted through transcriptional control of the retroviral RNA genome with both androgen-dependent and androgen-independent promoters, thereby targeting RCR vector replication and transgene delivery to prostate cancer cells. By taking advantage of the amplification process inherent in virus replication, we can achieve significantly enhanced transduction efficiency and therapeutic efficacy in vivo, and with the ability to target these vectors specifically and exclusively to prostate cancer cells, we can now limit and control the replicative process and minimize risk to normal cells. Hence this represents a significant improvement in RCR vector design that should further enhance the risk:benefit ratio of these vectors and promote regulatory acceptance for future testing in clinical trials as a novel therapy for prostate cancer.

In clinical scenarios, we envision that the use of RCR vectors could be a useful adjunct to standard treatment procedures, before or after primary tumor resection; e.g., intratumoral injection of prostate specific RCR vectors transurethrally might allow neo-adjuvant suicide gene therapy to reduce tumor size prior to scheduled prostatectomy, or the stably transduced dormant suicide genes could provide a means to later eliminate locally recurrent disease, or to kill metastatic cells that might be "seeded" into the circulation during resection.

VI. REFERENCES

1. Greenberg NM, DeMayo FJ, Sheppard PC, Barrios R, Lebovitz R, Finegold M, Angelopoulou R, Dodd JG, Duckworth ML, Rosen JM, and et al. The rat probasin gene promoter directs hormonally and developmentally regulated expression of a heterologous gene specifically to the prostate in transgenic mice. *Mol Endocrinol*, 1994. 8(2): 230-239. **(PMID: 8170479)**
2. Rennie PS, Bruchofsky N, Leco KJ, Sheppard PC, McQueen SA, Cheng H, Snoek R, Hamel A, Bock ME, and MacDonald BS. Characterization of two cis-acting DNA elements involved in the androgen regulation of the probasin gene. *Mol Endocrinol*, 1993. 7(1): 23-36. **(PMID: 8446105)**
3. Greenberg NM, DeMayo F, Finegold MJ, Medina D, Tilley WD, Aspinall JO, Cunha GR, Donjacour AA, Matusik RJ, and Rosen JM. Prostate cancer in a transgenic mouse. *Proc Natl Acad Sci U S A*, 1995. 92(8): 3439-3443. **(PMID: 7724580)**
4. Wu X, Wu J, Huang J, Powell WC, Zhang J, Matusik RJ, Sangiorgi FO, Maxson RE, Sucov HM, and Roy-Burman P. Generation of a prostate epithelial cell-specific Cre transgenic mouse model for tissue-specific gene ablation. *Mech Dev*, 2001. 101(1-2): 61-69. **(PMID: 11231059)**
5. Zhang J, Thomas TZ, Kasper S, and Matusik RJ. A small composite probasin promoter confers high levels of prostate-specific gene expression through regulation by androgens and glucocorticoids in vitro and in vivo. *Endocrinology*, 2000. 141(12): 4698-4710. **(PMID: 11108285)**
6. Wen Y, Giri D, Yan DH, Spohn B, Zinner RG, Xia W, Thompson TC, Matusik RJ, and Hung MC. Prostate-specific antitumor activity by probasin promoter-directed p202 expression. *Mol Carcinog*, 2003. 37(3): 130-137. **(PMID: 12884364)**
7. Huang J, Powell WC, Khodavirdi AC, Wu J, Makita T, Cardiff RD, Cohen MB, Sucov HM, and Roy-Burman P. Prostatic intraepithelial neoplasia in mice with conditional disruption of the retinoid X receptor alpha allele in the prostate epithelium. *Cancer Res*, 2002. 62(16): 4812-4819. **(PMID: 12183441)**
8. Song Z, Wu X, Powell WC, Cardiff RD, Cohen MB, Tin RT, Matusik RJ, Miller GJ, and Roy-Burman P. Fibroblast growth factor 8 isoform B overexpression in prostate epithelium: a new mouse model for prostatic intraepithelial neoplasia. *Cancer Res*, 2002. 62(17): 5096-5105. **(PMID: 12208767)**
9. Jin C, McKeenan K, and Wang F. Transgenic mouse with high Cre recombinase activity in all prostate lobes, seminal vesicle, and ductus deferens. *Prostate*, 2003. 57(2): 160-164. **(PMID: 12949940)**
10. Rubinchik S, Wang D, Yu H, Fan F, Luo M, Norris JS, and Dong JY. A complex adenovirus vector that delivers FASL-GFP with combined prostate-specific and tetracycline-regulated expression. *Mol Ther*, 2001. 4(5): 416-426. **(PMID: 11708878)**
11. Lowe SL, Rubinchik S, Honda T, McDonnell TJ, Dong JY, and Norris JS. Prostate-specific expression of Bax delivered by an adenoviral vector induces apoptosis in LNCaP prostate cancer cells. *Gene Ther*, 2001. 8(18): 1363-1371. **(PMID: 11571575)**
12. Andriani F, Nan B, Yu J, Li X, Weigel NL, McPhaul MJ, Kasper S, Kagawa S, Fang B, Matusik RJ, Denner L, and Marcelli M. Use of the probasin promoter ARR2PB to express Bax in androgen receptor-positive prostate cancer cells. *J Natl Cancer Inst*, 2001. 93(17): 1314-1324. **(PMID: 11535706)**
13. Logg CR, Logg A, Matusik RJ, Bochner BH, and Kasahara N. Tissue-specific transcriptional targeting of a replication-competent retroviral vector. *J Virol*, 2002. 76(24): 12783-12791. **(PMID: 12438603)**
14. Lee SJ, Kim HS, Yu R, Lee K, Gardner TA, Jung C, Jeng MH, Yeung F, Cheng L, and Kao C. Novel prostate-specific promoter derived from PSA and PSMA enhancers. *Mol Ther*, 2002. 6(3): 415-421. **(PMID: 12231179)**

15. Li X, Zhang YP, Kim HS, Bae KH, Stantz KM, Lee SJ, Jung C, Jimenez JA, Gardner TA, Jeng MH, and Kao C. Gene therapy for prostate cancer by controlling adenovirus E1a and E4 gene expression with PSES enhancer. *Cancer Res*, 2005. 65(5): 1941-1951. **(PMID: 15753394)**
16. Korkegian A, Black ME, Baker D, and Stoddard BL. Computational thermostabilization of an enzyme. *Science*, 2005. 308(5723): 857-860. **(PMID: 15879217)**
17. Wang W, Tai CK, Kasahara N, and Chen TC. Highly efficient and tumor-restricted gene transfer to malignant gliomas by replication-competent retrovirus vectors. *Hum Gene Ther*, 2003. 14: 117-127. **(PMID: 12614563)**
18. Erbs P, Regulier E, Kintz J, Leroy P, Poitevin Y, Exinger F, Jund R, and Mehtali M. In vivo cancer gene therapy by adenovirus-mediated transfer of a bifunctional yeast cytosine deaminase/uracil phosphoribosyltransferase fusion gene. *Cancer Res*, 2000. 60(14): 3813-3822. **(PMID: 10919655)**
19. Bourbeau D, Lavoie G, Nalbantoglu J, and Massie B. Suicide gene therapy with an adenovirus expressing the fusion gene CD::UPRT in human glioblastomas: different sensitivities correlate with p53 status. *J Gene Med*, 2004. 6(12): 1320-1332. **(PMID: 15515126)**
20. Suttle DP, Bugg BY, Winkler JK, and Kanalas JJ. Molecular cloning and nucleotide sequence for the complete coding region of human UMP synthase. *Proc Natl Acad Sci U S A*, 1988. 85(6): 1754-1758. **(PMID: 3279416)**
21. Sakamoto E, Nagase H, Kobunai T, Oie S, Oka T, and Fukushima M. Orotate phosphoribosyltransferase expression level in tumors is a potential determinant of the efficacy of 5-fluorouracil. *Biochem Biophys Res Commun*, 2007. 363(1): 216-222. **(PMID: 17854773)**
22. Tai CK, Wang WJ, Chen TC, and Kasahara N. Single-shot, multicycle suicide gene therapy by replication-competent retrovirus vectors achieves long-term survival benefit in experimental glioma. *Mol Ther*, 2005. 12(5): 842-851. **(PMID: 16257382)**
23. Wu HC, Hsieh JT, Gleave ME, Brown NM, Pathak S, and Chung LW. Derivation of androgen-independent human LNCaP prostatic cancer cell sublines: role of bone stromal cells. *Int J Cancer*, 1994. 57(3): 406-412. **(PMID: 8169003)**
24. Gotoh A, Ko SC, Shirakawa T, Cheon J, Kao C, Miyamoto T, Gardner TA, Ho LJ, Cleutjens CB, Trapman J, Graham FL, and Chung LW. Development of prostate-specific antigen promoter-based gene therapy for androgen-independent human prostate cancer. *J Urol*, 1998. 160(1): 220-229. **(PMID: 9628654)**
25. Knouf EC, Metzger MJ, Mitchell PS, Arroyo JD, Chevillet JR, Tewari M, and Miller AD. Multiple integrated copies and high-level production of the human retrovirus XMRV (xenotropic murine leukemia virus-related virus) from 22Rv1 prostate carcinoma cells. *J Virol*, 2009. 83(14): 7353-7356. **(PMID: 19403664)**
26. Jiao J, Wang S, Qiao R, Vivanco I, Watson PA, Sawyers CL, and Wu H. Murine cell lines derived from Pten null prostate cancer show the critical role of PTEN in hormone refractory prostate cancer development. *Cancer Res*, 2007. 67(13): 6083-6091. **(PMID: 17616663)**
27. Wang S, Gao J, Lei Q, Rozengurt N, Pritchard C, Jiao J, Thomas GV, Li G, Roy-Burman P, Nelson PS, Liu X, and Wu H. Prostate-specific deletion of the murine Pten tumor suppressor gene leads to metastatic prostate cancer. *Cancer Cell*, 2003. 4(3): 209-221. **(PMID: 14522255)**
28. Stambolic V, Suzuki A, de la Pompa JL, Brothers GM, Mirtsos C, Sasaki T, Ruland J, Penninger JM, Siderovski DP, and Mak TW. Negative regulation of PKB/Akt-dependent cell survival by the tumor suppressor PTEN. *Cell*, 1998. 95(1): 29-39. **(PMID: 9778245)**
29. Cairns P, Okami K, Halachmi S, Halachmi N, Esteller M, Herman JG, Jen J, Isaacs WB, Bova GS, and Sidransky D. Frequent inactivation of PTEN/MMAC1 in primary prostate cancer. *Cancer Res*, 1997. 57(22): 4997-5000. **(PMID: 9371490)**

30. Liao CP, Liang M, Cohen MB, Flesken-Nikitin A, Jeong JH, Nikitin AY, and Roy-Burman P. Mouse prostate cancer cell lines established from primary and post-castration recurrent tumors. *Horm Cancer*. 1(1): 44-54. **(PMID: 20631921)**
31. Logg CR, Logg A, Tai CK, Cannon PM, and Kasahara N. Genomic stability of murine leukemia viruses containing insertions at the Env-3' untranslated region boundary. *J Virol*, 2001. 75(15): 6989-6998. **(PMID: 11435579)**
32. Hiraoka K, Kimura T, Logg CR, and Kasahara N. Tumor-selective gene expression in a hepatic metastasis model after locoregional delivery of a replication-competent retrovirus vector. *Clin Cancer Res*, 2006. 12(23): 7108-7116. **(PMID: 17145835)**
33. Hiraoka K, Kimura T, Logg CR, Tai CK, Haga K, Lawson GW, and Kasahara N. Therapeutic efficacy of replication-competent retrovirus vector-mediated suicide gene therapy in a multifocal colorectal cancer metastasis model. *Cancer Res*, 2007. 67(11): 5345-5353. **(PMID: 17545615)**
34. Solly SK, Trajcevski S, Frisen C, Holzer GW, Nelson E, Clerc B, Abordo-Adesida E, Castro M, Lowenstein P, and Klatzmann D. Replicative retroviral vectors for cancer gene therapy. *Cancer Gene Ther*, 2003. 10(1): 30-39. **(PMID: 12489026)**
35. Lyons SK, Meuwissen R, Krimpenfort P, and Berns A. The generation of a conditional reporter that enables bioluminescence imaging of Cre/loxP-dependent tumorigenesis in mice. *Cancer Res*, 2003. 63(21): 7042-7046. **(PMID: 14612492)**
36. Liao CP, Zhong C, Saribekyan G, Bading J, Park R, Conti PS, Moats R, Berns A, Shi W, Zhou Z, Nikitin AY, and Roy-Burman P. Mouse models of prostate adenocarcinoma with the capacity to monitor spontaneous carcinogenesis by bioluminescence or fluorescence. *Cancer Res*, 2007. 67(15): 7525-7533. **(PMID: 17671224)**
37. Logg CR, Tai CK, Logg A, Anderson WF, and Kasahara N. A uniquely stable replication-competent retrovirus vector achieves efficient gene delivery in vitro and in solid tumors. *Hum Gene Ther*, 2001. 12(8): 921-932. **(PMID: 11387057)**
38. Trajcevski S, Solly SK, Frisen C, Trenado A, Cosset FL, and Klatzmann D. Characterization of a semi-replicative gene delivery system allowing propagation of complementary defective retroviral vectors. *J Gene Med*, 2005. 7(3): 276-287. **(PMID: 15515136)**
39. Haga K, Tomioka A, Liao CP, Kimura T, Matsumoto H, Ohno I, Hermann K, Logg CR, Jiao J, Tanaka M, Hirao Y, Wu H, Kruse CA, Roy-Burman P, and Kasahara N. PTEN knockout prostate cancer as a model for experimental immunotherapy. *J Urol*, 2009. 181(1): 354-362. **(PMID: 19010487)**
40. Cole C, Qiao J, Kottke T, Diaz RM, Ahmed A, Sanchez-Perez L, Brunn G, Thompson J, Chester J, and Vile RG. Tumor-targeted, systemic delivery of therapeutic viral vectors using hitchhiking on antigen-specific T cells. *Nat Med*, 2005. 11(10): 1073-1081. **(PMID: 16170322)**
41. Short MP, Choi BC, Lee JK, Malick A, Breakefield XO, and Martuza RL. Gene delivery to glioma cells in rat brain by grafting of a retrovirus packaging cell line. *J Neurosci Res*, 1990. 27(3): 427-439. **(PMID: 2129047)**
42. Culver KW, Ram Z, Wallbridge S, Ishii H, Oldfield EH, and Blaese RM. In vivo gene transfer with retroviral vector-producer cells for treatment of experimental brain tumors. *Science*, 1992. 256(5063): 1550-1552. **(PMID: 1317968)**
43. Rainov NG. A phase III clinical evaluation of herpes simplex virus type 1 thymidine kinase and ganciclovir gene therapy as an adjuvant to surgical resection and radiation in adults with previously untreated glioblastoma multiforme. *Hum Gene Ther*, 2000. 11(17): 2389-2401. **(PMID: 11096443)**

VII. FINAL REPORT BIBLIOGRAPHY / PERSONNEL LIST
(see also Reportable Outcomes section above)**Peer-reviewed publications:**

1. Haga, K., Tomioka, A., Liao, C.-P., Kimura, T., Matsumoto, H., Ohno, I., Hermann, K., Logg, C. R., Jiao, J., Tanaka, M., Hirao, Y., Wu, H., Kruse, C. A., Roy-Burman, P., Kasahara, N.
PTEN-Knockout Prostate Cancer as a Model for Experimental Immunotherapy.
Journal of Urology, 181: 354-362. (2009)
2. Kimura, T., Hiraoka, K., Kasahara, N., Logg, C. R.
Optimization of enzyme-substrate pairing for bioluminescence imaging of gene transfer using Renilla and Gaussia luciferases.
Journal of Gene Medicine, 12 (6): 528-537. (2010)

Abstracts and Presentations

1. Haga, K., Tomioka, A., Liao, C.-P., Kimura, T., Logg, C. R., Matsumoto, H., Ohno, I., Hermann, K., Tanaka, M., Uemura, H., Hirao, Y., Roy-Burman, P., Kasahara, N.
Suicide gene therapy using replication-competent retrovirus (RCR) combined with tumor-specific cytotoxic T lymphocytes (CTLs) for PTEN knock-out spontaneous prostate cancer model.
(Abstract presented at the 2008 Annual Meeting of the American Urological Association (AUA); Orlando, Florida.)
2. Kasahara, N.
Engineering Multiple Mechanisms of Tumor Selectivity into Replication-Competent Retrovirus Vectors.
(Invited speaker, 2009 International Conference on Oncolytic Viruses as Cancer Therapeutics; Banff, Canada.)
3. Gruber, H., Perez, O., Ibanez, C., Pertschuk, D., Gessner, D., Robbins, J., Kasahara, N., Logg C. R., Jolly, D. J.
Improved Prodrug Activator Gene Therapy for Cancer.
(Abstract selected for oral presentation at the 2009 Annual Meeting of the Japan Society of Gene Therapy; Osaka, Japan.)
4. Kasahara, N.
RCR Vectors: Enhancing Transduction Efficiency and Tumor Selectivity.
(Invited speaker, International Symposium, 2009 Annual Meeting of the Japan Society of Gene Therapy; Osaka, Japan.)
5. Kasahara, N.
Replication-Competent Retrovirus Vectors for Cancer Gene Therapy: Enhancing intratumoral biodistribution, tumor selectivity, and therapeutic efficacy.
(Invited speaker, 2009 Cold Spring Harbor Laboratory biotechnology conference on "In Vivo Barriers to Gene Delivery"; Cold Spring Harbor, NY.)

6. Hiraoka, K., Logg, C. R., Inagaki, A., Matsumoto, H., Diago, O., Perez, O., Robbins, J., Gruber, H., Jolly, D., Kasahara, N.
Optimizing the genomic stability, transgene expression, and therapeutic efficacy of replication-competent retrovirus vectors for prodrug activator gene transfer.
(Abstract presented at the 2010 Annual Meeting of the American Society of Gene & Cell Therapy; Washington DC.)
7. Kamijima, S., Kimura, T., Haga, K., Hiraoka, K., Inagaki, A., Logg, C. R., Kao, C., Bochner, B. H., Kasahara, N.
Tumor-selectivity of replication-competent retrovirus (RCR) vectors regulated by prostate-specific promoters and cytotoxic effect of suicide gene therapy mediated by RCR vector in vitro.
(Abstract selected for oral presentation at the 2010 Annual Meeting of the American Society of Gene & Cell Therapy; Washington DC.)

Personnel:

UCLA

Noriyuki Kasahara, M.D. Ph.D. (Principal Investigator)
Christopher R. Logg, Ph.D. (Research Associate)
Emmanuelle Faure-Kumar, Ph.D. (Research Associate)
Kazunori Haga, M.D. Ph.D. (Research Associate)
Shuichi Kamijima, M.D. Ph.D.. (Research Associate)

USC

Pradip Roy-Burman, Ph.D. (Co-Investigator)
Gohar Saribekyan (Research Associate)

VIII. APPENDICES

Please see attached publications.

(also listed in Reportable Outcomes section and Final Report Bibliography section above).

1. Haga, K., Tomioka, A., Liao, C.-P., Kimura, T., Matsumoto, H., Ohno, I., Hermann, K., Logg, C. R., Jiao, J., Tanaka, M., Hirao, Y., Wu, H., Kruse, C. A., Roy-Burman, P., Kasahara, N.
PTEN-Knockout Prostate Cancer as a Model for Experimental Immunotherapy.
Journal of Urology, 181: 354-362. (2009)
2. Kimura, T., Hiraoka, K., Kasahara, N., Logg, C. R.
Optimization of enzyme-substrate pairing for bioluminescence imaging of gene transfer using Renilla and Gaussia luciferases.
Journal of Gene Medicine, 12 (6): 528-537. (2010)

PTEN Knockout Prostate Cancer as a Model for Experimental Immunotherapy

Kazunori Haga,* Atsushi Tomioka,* Chun-Peng Liao, Takahiro Kimura, Hiroshi Matsumoto, Izumi Ohno, Kip Hermann, Christopher R. Logg, Jing Jiao, Motoyoshi Tanaka, Yoshihiko Hirao, Hong Wu, Carol A. Kruse, Pradip Roy-Burman and Noriyuki Kasahara†

From the Departments of Medicine (KH, AT, TK, HM, IO, KH, CRL, HW, NK) and Molecular and Medical Pharmacology (JJ, HW, NK), University of California-Los Angeles and Departments of Pathology, and Biochemistry and Molecular Biology, University of Southern California (CPL, PRB), Los Angeles and Sidney Kimmel Cancer Center (CAK), San Diego, California, and Departments of Urology, Nara Medical University (AT, YH), Nara, Jikei Medical University (TK), Tokyo and Kinki University (MT), Osaka, Japan

Abbreviations and Acronyms

ADI-Ca = androgen depletion independent cancer

CTL = cytotoxic T lymphocyte

ELISA = enzyme-linked immunosorbent assay

E/T = effector-to-target

GFP = green fluorescent protein

IFN- γ = interferon- γ

MLTR = mixed lymphocyte-tumor reaction

MTS = (3-(4,5-dimethylthiazol-2-yl)-5-(3-carboxymethoxy-phenyl)-2-(4-sulfophenyl)-2H-tetrazolium

PBS = phosphate buffered saline

PTEN = phosphatase and tensin homologue deleted on chromosome 10

ROI = region of interest

RL = Renilla luciferase

Purpose: Testing immunotherapeutic strategies for prostate cancer has been impeded by the lack of relevant tumor models in immunocompetent animals. This opportunity is now provided by the recent development of prostate specific PTEN knockout mice, which show spontaneous development of true adenocarcinoma arising from prostate epithelium and more faithfully recapitulate the human disease than any previous model. We investigated the feasibility of using tumor cells derived from this model to test tumor vaccination and adoptive immunotherapeutic strategies for prostate cancer.

Materials and Methods: PTEN-CaP8 adenocarcinoma cells derived from the biallelic PTEN knockout prostate cancer model were used to vaccinate nontumor bearing litter mates. Tumor specific effector cells were generated from splenocytes of vaccinated mice by mixed lymphocyte-tumor reactions, and antiproliferative effects and cytokine generation were examined in vitro. The effect of vaccination or adoptive immunotherapy on luciferase marked PTEN-CaP8 subcutaneous tumors was monitored by tumor volumetric measurements and noninvasive bioluminescence imaging.

Results: Vaccination of litter mate mice with irradiated PTEN-CaP8 cells showed a significant prophylactic effect against the subsequent tumor challenge. Effector cells harvested from vaccinated litter mates showed significant interferon- γ secretion upon co-incubation with PTEN-CaP8 target cells and they were capable of efficient target cell growth inhibition in vitro. Intratumor adoptive transfer of effector cells resulted in significant growth inhibition of preestablished prostate tumors in vivo.

Conclusions: The PTEN knockout model serves as a highly useful model in which to investigate tumor cell vaccination and adoptive immunotherapeutic strategies in the context of true adenocarcinoma of the prostate. This model should accelerate efforts to develop effective immunotherapies for human prostate cancer.

Key Words: prostate; prostatic neoplasms; PLIP protein, mouse; cancer vaccines; immunotherapy, adoptive

PROSTATE cancer is currently the most commonly diagnosed cancer and the second leading cause of cancer death in men in the United States.¹ Gener-

ally patients with metastatic prostate cancer are initially responsive to androgen ablation therapy but most patients subsequently progress to

Submitted for publication April 2, 2008.

Study received approval from University of California-Los Angeles and University of Southern California (Project No. 2003-120-12).

Supported by National Institutes of Health Grants R01 CA121258 (NK), R01 CA059705 and R01 CA113392 (PRB), Idea Award PC074133 (NK and PRB) and Post-Doctoral Training Award PC073547 (KH) from the Department of Defense Prostate Cancer Research Program, and Developmental Research Program seed grant from the University of California-Los Angeles Specialized Program of Research Excellence in Prostate Cancer (NK).

* Equal study contribution.

† Correspondence and requests for reprints: Department of Medicine, University of California-Los Angeles, 675 Charles E. Young Dr. South, MRL-1551, Los Angeles, California 90095 (telephone: 310-825-7112; FAX: 310-825-5204; e-mail: nkasahara@mednet.ucla.edu).

ADI-Ca, for which treatment options are limited. The prognosis in patients with ADI-Ca is poor despite aggressive multimodal therapy and there is currently no standard of care. Hence, there is a need to pursue new and potentially more effective treatment strategies.

To improve the long-term outcome it is desirable to develop new therapeutic modalities capable of eliminating metastatic foci of cancer cells that have become resistant to previous therapies. Immunotherapeutic strategies show promise in this regard. The activation of humoral and cellular responses can mobilize antibodies and effector cells, which can circulate systemically and cause cytotoxicity to tumor cells, and immunological memory may be engendered to prevent recurrence. In fact, currently a number of immuno-activating agents are in advanced stages of clinical testing for prostate cancer, including an allogeneic prostate cancer cell vaccine product engineered to express granulocyte-macrophage colony-stimulating factor (GVAX®) and an autologous dendritic cell vaccine produced by ex vivo pulsing with the prostatic acid phosphatase/granulocyte-macrophage colony-stimulating factor fusion peptide sipuleucel-T.² However, there have been few studies of prostate cancer exploring the potential of adoptive immunotherapy with activated CTLs, which is a strategy that has shown promise for other malignancies, such as melanoma and glioma.³

A number of groups have developed strategies for activating CTLs against prostate cancer cells or for their genetic modification with artificial T-cell receptors.^{4–8} Many of these investigators have used adoptive transfer of human CTLs in the setting of human prostate cancer xenografts in immunodeficient rodents, a milieu in which interaction with the endogenous immune system and the immunosuppressive tumor environment cannot be adequately assessed.^{4–6} Other groups have pursued studies of adoptive immunotherapy using syngeneic cancer cells and immunocompetent hosts derived from the TRAMP (transgenic adenocarcinoma of mouse prostate) model of prostate cancer.^{7–9} However, this transgenic model was generated by prostate specific expression of the SV40 T antigen, which itself represents a foreign target antigen, and it is now known that the cancer arising in this model manifests extensive neuroendocrine differentiation, unlike human adenocarcinoma of the prostate.¹⁰

The Dunning model is also a syngeneic adenocarcinoma model of prostate cancer that has served as a highly useful model for the development of immunotherapy.¹¹ Nonetheless, based on the expression of nonprostatic proteins there has also been some controversy as to the true origin of the spontaneous Dunning tumor from which the R3227 subline system was derived.¹²

Thus, to date more comprehensive investigation of immunotherapeutic strategies for prostate cancer has been hampered by the relative dearth of syngeneic cell lines and immunocompetent animal models that represent genetically well-defined examples of true adenocarcinoma and faithfully recapitulate important biological and clinical aspects of the human disease. In this regard the recent development of a unique murine model of spontaneously occurring prostate adenocarcinoma, as generated by biallelic knockout of the PTEN tumor suppressor gene, shows considerable promise as a tool for developing and evaluating novel immunotherapies for this disease. This tumor suppressor gene encodes a phosphatase that antagonizes phosphatidylinositol-3-kinase/protein kinase B (Akt) signaling¹³ and is frequently disrupted in various tumors, including prostate cancer.¹⁴ Loss of PTEN leads to the up-regulation of pro-survival pathways and contributes to chemoresistance, which correlates with high grade and advanced stage disease, especially in ADI-Ca.¹⁵

In this recently developed transgenic knockout model biallelic deletion of loxP flanked sequences in the PTEN gene is achieved by prostate specific expression of Cre recombinase. The resultant animals show spontaneous development of hyperplasia and metaplasia of the prostatic epithelium, followed by PIN lesions, and progression to invasive adenocarcinoma and subsequent micrometastasis.¹⁶

Thus, the prostate specific PTEN knockout model is the first transgenic murine model of true prostate adenocarcinoma that arises reproducibly and spontaneously in vivo, is genetically well-defined and causally linked to a genetic deficiency commonly observed in human disease, and faithfully mimics the course of human prostate cancer. Therefore, this model seems highly suitable as a model in which to test immunotherapeutic strategies. Accordingly we have used syngeneic PTEN deleted, androgen receptor positive prostate adenocarcinoma cells derived from this unique model^{16,17} to test their potential usefulness for the development and evaluation of tumor vaccination and adoptive immunotherapeutic strategies.

MATERIALS AND METHODS

Cells and Vectors

The murine prostate cancer cell lines PTEN-P8 and PTEN-CaP8 were derived from the PTEN knockout model of prostate cancer, as reported previously,^{16,17} and maintained in Dulbecco's modified Eagle's medium supplemented with 10% fetal bovine serum (Omega Scientific, Tarzana, California), 25 µg/ml bovine pituitary extract (Invitrogen™), 5 µg/ml bovine insulin (Sigma-Aldrich), 6 ng/ml recombinant human epidermal growth factor

(Sigma-Aldrich®) and 1% penicillin in a humidified incubator at 37C in 5% CO₂.

To generate PTEN-CaP8 cells that stably expressed RL (PTEN-CaP8/RL) PTEN-CaP8 cells were transduced with lentiviral vector CCL-m4/hr1-IRES-GFP¹⁸ at a ratio of 1 µg p24/1 × 10⁶ cells. After expansion in culture cells were analyzed for GFP expression by fluorescence activated cell sorting analysis using an EPICS® XL™ flow cytometer.

MLTR to Generate Effector Cells

After irradiation with 20,000 Ci to prevent further cell division 5 × 10⁶ PTEN-CaP8 cells were injected subcutaneously into 6 to 8-week-old male C57BL/6 mice (Charles River Laboratories, Wilmington, Massachusetts) every 2 weeks for a total of 3 inoculations. Two weeks following the last vaccination splenocytes were harvested and washed after red blood cell removal with lysis buffer (Sigma-Aldrich).

Stimulator PTEN-CaP8 cell monolayers were treated with mitomycin C (Sigma-Aldrich) for 1 hour at 37C, washed and subsequently incubated with responder mouse splenocytes at a responder-to-stimulator ratio of 10:1. Cells were placed into RPMI-1640 medium containing 10% fetal bovine serum and 100 IU/ml recombinant mouse interleukin-2 (Sigma-Aldrich), and incubated at 37C in humidified air with 5% CO₂ for 6 to 7 days. Subsequently effector cells were characterized *in vitro* or used in adoptive transfer experiments.

Assessment of Antiproliferative Effects In Vitro

The viability of PTEN-P8 cells seeded into 96-well plates at 1 × 10³ cells per well with or without MLTR derived effector cells was determined by MTS assay using the soluble tetrazolium salt MTS and a CellTiter 96® nonradioactive cell proliferation assay. Washed effector cells were mixed with PTEN-P8 target cells at a ratio of 1:1 and incubated for 2 days. The medium was changed to remove the nonadherent effector cells and any detached PTEN-P8 target cells, and then adherent cell viability was analyzed by measuring optical density absorbance using an ELISA plate reader at 490 nm to detect formazan produced in the MTS assay after 2 hours of reaction at 37C. The surviving cell fraction was calculated as the ratio of the average absorbance achieved in effector cell treated test cultures to that of conditioned medium from untreated control samples. Results in pentaplicate wells are expressed as the mean percent of metabolically active cells compared to those in untreated wells.

IFN-γ Assay

MLTR derived effector cell cultures from vaccinated animals were co-cultured for 2 days with or without an equal number of PTEN-P8 cells. The levels of murine IFN-γ present in clarified supernatants of conditioned medium from these co-cultures was measured by ELISA using the Quantikine™ murine IFN-γ immunoassay. Recombinant mouse IFN-γ served as the positive control. Results were normalized as the rate of cytokine production, ie pg/10⁶ cells per 24 hours, and comparisons are expressed as the fold difference between effector cells incubated with and without relevant tumor target cells.

Animal Experiments

All animal experiments were performed according to institutional guidelines under approved protocols at UCLA and University of Southern California. Principles of the Helsinki Declaration were followed.

For immunization and prophylactic vaccination experiments 6 to 8-week-old male C57BL/6 mice were vaccinated by subcutaneous injection with irradiated PTEN-CaP8 cells (5 per vaccination group and 5 × 10⁶ cells per mouse with irradiation with 20,000 Ci delivered to 2 × 10⁷ cells per 3 ml culture) into the left flank for a total of 3 vaccinations every 2 weeks, as described. Five each of vaccinated mice and a paired number of control mice were subsequently challenged by subcutaneous injection into the right flank with 1 × 10⁶ naive PTEN-CaP8 cells. Observations to assess tumor growth were performed for 2 weeks.

For adoptive transfer experiments tumors were established in 6 to 8-week-old male athymic nude mice (Charles River Laboratories) by subcutaneous injection of 1 × 10⁶ PTEN-CaP8/RL cells. Tumor dimensions were measured on days 14, 18, 21, 28, 35, 42 and 60. Tumor volume was calculated using the formula, (length) × (width)²/2.¹⁹ Two weeks after tumor establishment each mouse was assigned randomly to a treatment arm of 12 per group, followed by a single intratumor injection of 1 × 10⁶ effector cells harvested from PTEN-CaP8 vaccinated mice, as described, or PBS vehicle control.

In Vitro and In Vivo Optical Imaging Analysis

For *in vitro* imaging studies RL expression in PTEN-CaP8/RL cells was confirmed by bioluminescence optical imaging using a cooled charge coupled device system (Xenogen®) 2 minutes after the addition of its imidazopyrazine substrate, coelenterazine with maximum emission read at 480 nm upon oxidation by RL.²⁰

For *in vivo* imaging studies mice bearing PTEN-CaP8/RL tumors were anesthetized with ketamine (100 mg/kg) and xylazine (10 mg/kg). After the administration of coelenterazine (1 mg/kg) intravenously the anesthetized mice were imaged using the Xenogen system with a 1 minute acquisition time at different time points after tumor implantation according to previously described techniques.¹⁸ Grayscale background photographic images of the tissues were overlaid with color images of bioluminescent signals using Living Image® 2.2 and IGOR Pro image analysis software (WaveMetrics, Lake Oswego, Oregon). The bioluminescence *in vivo* signal was calculated using the signal in the ROI as photons per second per cm²/sr.²¹

Statistical Analysis

All statistical analyses were done using GraphPad® Prism®, version 4 for Windows®. Results between different groups were compared using the Mann-Whitney or unpaired t test with p < 0.01 considered significant.

RESULTS

Immunization and Tumor Vaccine Prophylaxis

We examined whether the highly tumorigenic murine prostate adenocarcinoma cell line PTEN-CaP8,

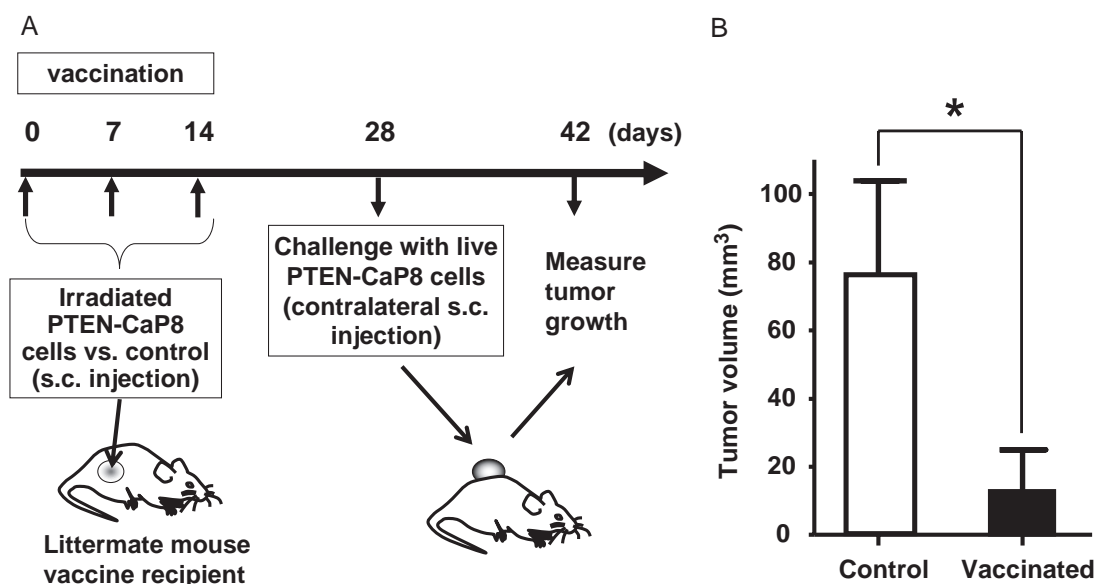


Figure 1. A, tumor vaccination protocol schedule. Nontumor bearing litter mates of PTEN knockout prostate cancer mice were vaccinated by subcutaneous (s.c.) injection of 1×10^6 irradiated PTEN-CaP8 cells total of 3 times in 2 weeks, followed 2 weeks later by challenge with 1×10^6 live PTEN-CaP8 cells into contralateral flank. B, tumor vaccine effect in subcutaneous models. Contralateral flank PTEN-CaP8 tumors were measured on day 14 after challenge in unvaccinated control and vaccinated animals. Error bars indicate SD. Asterisk indicates statistically significant ($p < 0.01$).

which was derived from the PTEN knockout model of prostate cancer, would be capable of eliciting a robust antitumor immune response in syngeneic hosts and, thereby, serve as a tumor vaccine. Adult male C57BL/6 background litter mate mice were vaccinated subcutaneously with injections of irradiated PTEN-CaP8 cells and 2 weeks later the animals were challenged with fresh nonirradiated PTEN-CaP8 cells injected subcutaneously into the contralateral flank (fig. 1, A). Control mice were also challenged in the same manner but they received injections of saline vehicle instead of irradiated tumor cells. Tumor formation was observed to be significantly inhibited in the vaccinated group compared to the control group 2 weeks after the tumor challenge ($p < 0.01$, fig. 1, B). In fact, no tumor establishment was observed in 2 of the 5 vaccinated mice, while all control mice showed approximately 5-fold increased tumor growth compared to the average tumor size in the vaccinated group (fig. 1, B). Thus, PTEN-CaP8 could serve as an effective cell vaccine to prevent and/or retard tumor formation in immunocompetent syngeneic hosts.

In Vitro Analysis of Cellular Immune Response

To determine whether this prophylactic vaccination effect was mediated by a cellular immune response and confirm that such responses could be elicited by endogenous tumor antigens litter mate mice were again immunized by subcutaneous injection of irradiated PTEN-CaP8 cells, as described, but this time

their splenocytes were harvested for explant culture in mixed lymphocyte tumor cell reactions with PTEN-P8 cells. Parental PTEN-P8 cells, which are the precursor to PTEN-CaP8 cells, were used as target cells in this case because, although they are less tumorigenic, the parental cells lack detectable Cre recombinase expression.^{16,17} Hence, this foreign enzyme protein would not serve as a target antigen. Cellular immune responses seen against PTEN-P8 cells in vitro likely represented reactivity to true endogenous tumor antigens.

Accordingly mixed lymphocyte tumor cell reactions were performed by co-culture of splenocytes from PTEN-CaP8 vaccinated mice in the absence and presence of PTEN-P8 target cells and 24-hour conditioned medium was analyzed by ELISA to measure the levels of secreted murine IFN- γ . Effector cells co-cultured with relevant PTEN-P8 target cells produced significantly increased levels of IFN- γ compared to those of effector cells cultured alone (fig. 2, A). This suggests that the activated effector cells were capable of a robust T-helper type 1-type cytokine response upon the recognition of endogenous tumor antigens.

We then examined whether effector cells isolated from vaccinated animals could exert antiproliferative effects on PTEN-P8 cells in a dose dependent manner. Activated effector cells from PTEN-CaP8 vaccinated mice were co-cultured with PTEN-P8 target cells at different E/T cell ratios. Subsequently nonadherent

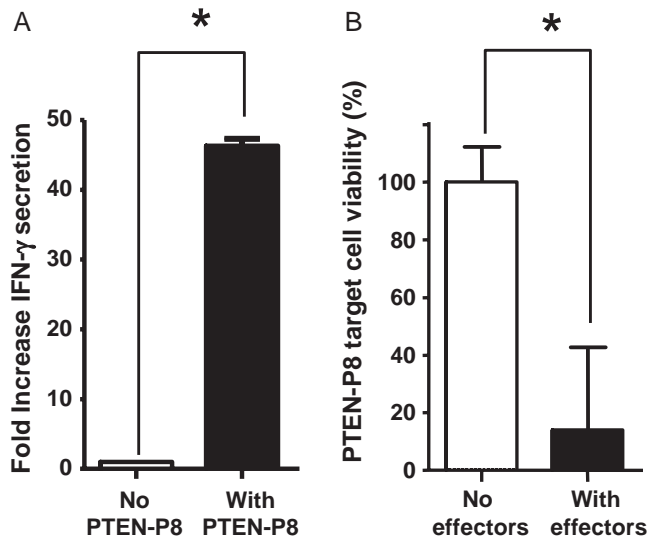


Figure 2. A, IFN- γ production by activated effector cells upon co-culture with PTEN-P8 prostate cancer cells. Conditioned medium after overnight culture of CTLs in absence (*No PTEN-P8*) or presence (*With PTEN-P8*) (E/T ratio 1:1) of target cells was assayed by ELISA. Results are expressed as fold increase compared to negative control. B, PTEN-P8 target cell viability after culture in absence (*No effectors*) or presence (*With Effectors*) (E/T ratio 1:1) of effector cells isolated from PTEN-CaP8 vaccinated litter mates was evaluated by MTS assay for metabolic activity. Results are expressed as percent of cell viability compared to negative control. Error bars indicate SD. Asterisk indicates statistically significant ($p < 0.01$).

effector cells as well as any nonviable target cells were removed by washing and metabolic activity was measured by MTS assay as an indicator of the viability of any remaining adherent target cells. At a low E/T ratio of 1:10 there was no significant cytotoxicity to PTEN-P8 target cells (data not shown). However, activated CTLs incubated with PTEN-P8 target cells at higher E/T ratios of 1:1 and 10:1 showed significant antiproliferative effects. As measured by MTS assay, at an E/T ratio of 10:1 metabolic activity of the prostate cancer cells was completely suppressed (data not shown). Even at an E/T ratio of 1:1 activated effector cells achieved greater than 80% suppression of PTEN-P8 target cell growth during the 2 day co-culture period, as measured by metabolic activity (fig. 2, B). These results further suggest that vaccination results in the generation of activated effector cells, which can exert antiproliferative effects against PTEN knockout prostate cancer cells.

Generation of PTEN Knockout Prostate Cancer Cells Expressing RL

Bioluminescence optical imaging is a noninvasive method for serially monitoring tumor progression and the response to treatment in living animals with time. The availability of PTEN knockout prostate adenocarcinoma cell lines provides an opportunity to

take advantage of this imaging technology because genetically engineering these cells to express a luciferase enzyme enables detection by bioluminescence upon the addition of the appropriate substrate. Accordingly the lentiviral vector CCL-m4/hrl-IRES-GFP, which encodes RL and Aequorea GFP, was used to stably transduce the PTEN-CaP8 cell line. The resultant population of transduced cells, designated PTEN-CaP8/RL, showed high levels of GFP expression on fluorescence microscopy (fig. 3, A). Fluorescence activated cell sorting analysis confirmed that highly efficient gene delivery to 99.5% of the cell population had been achieved (fig. 3, B).

We further confirmed RL expression in the PTEN-CaP8/RL cells by the detection of biolumines-

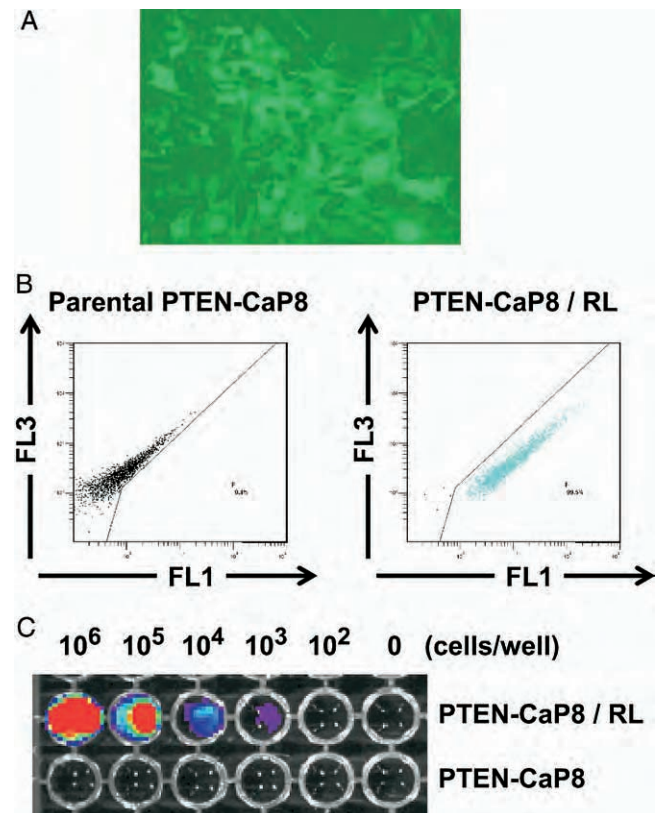


Figure 3. Characterization of PTEN-CaP8/RL cells. Parental PTEN-CaP8 cells were transduced with a recombinant lentiviral vector expressing RL and GFP, as described. A, fluorescence microscopy 72 hours after lentiviral transduction shows high GFP expression. B, after expansion in culture viral transduction was quantified by flow cytometry. Compared to parental PTEN-CaP8 cells fluorescence profile of PTEN-CaP8/RL cells showed that entire population was completely shifted along FL1 (green) fluorescence axis but not along FL3 (red) fluorescence axis, indicating complete transduction with GFP marker gene. C, PTEN-CaP8/RL cells were examined by bioluminescence optical imaging in vitro. Bioluminescence signals from PTEN-CaP8/RL cells increased in correlation with number of cells per well, while no bioluminescence was detected from parental PTEN-CaP8 cells regardless of number of cells plated.

cence signals using a charge coupled device imaging system upon incubation with the substrate coelenterazine *in vitro*. Bioluminescence emission was confirmed to be cell dose dependent by measuring the signals obtained from 10-fold serial dilutions of the cells (range 10^2 to 10^6) (fig. 3, C).

Adoptive Transfer of Effector Cells Generated by MLTR From the Splenocytes of Vaccinated Animals

Luciferase marked PTEN-CaP8/RL prostate adenocarcinoma cells were used in experiments to monitor the efficacy of immunotherapy by the adoptive transfer of effector cells *in vivo*. To assess therapeutic efficacy in the absence of potential additional effects from endogenous immune responses athymic nude mice served as hosts for the establishment of subcutaneous PTEN-CaP8/RL tumors. Two weeks later activated effector cells generated as described by vaccination of nontumor bearing litter mates with irradiated PTEN-CaP8 cells were administered by direct intratumor injection. Tumor growth was then examined by bioluminescence imaging as well as by confirmatory direct measurement of tumor size at serial time points.

Adoptive transfer of activated effector cells to PTEN-CaP8/RL tumors resulted in significant tumor growth suppression compared to that of untreated control tumors, which continued to show progressive growth. By day 60 there was a significant difference in the average \pm SD tumor volume of 117 ± 53 mm³ in the treated group vs $1,168 \pm 627$ mm³ in the control group ($p < 0.01$, fig. 4, A).

These findings were corroborated by the bioluminescence imaging results, which were obtained by

recording sequential images of the PTEN-CaP8/RL tumors in individual animals at serial time points after intravenous injection of coelenterazine. Figure 4, B shows representative images of control and treated mice. The bioluminescent signal within the ROI, ie the tumor area, in the control mouse was measured as 2.0×10^6 photons per second per cm²/sr on day 14, ie just before treatment, which then increased to 3.6×10^7 photons per second per cm²/sr on day 49. However, the ROI signal in the treated mouse remained at 1.6×10^6 and 7.1×10^5 photons per second per cm²/sr on days 14 and 49, respectively (fig. 4, B). As demonstrated *in vitro*, bioluminescence signal intensity can be used as a semiquantitative measure that correlates in a cell dose dependent manner with the number of viable tumor cells. Hence, the results indicate that the number of cells in the control tumor had increased approximately 15-fold between days 14 and 49, while the tumor treated with effector cells remained static.

DISCUSSION

We report the feasibility of using syngeneic cell lines, derived from the PTEN knockout model of prostate cancer, as tumor vaccines to elicit prophylactic effects against tumor establishment and progression. We further confirmed that vaccination and tumor inhibition were associated with a cellular immune response resulting in the generation of effector cells capable of exerting highly potent antiproliferative effects against these prostate cancer cells. Finally, we also noted that effective growth suppression could be achieved upon the adoptive transfer of these effector cells to preestablished tumors.

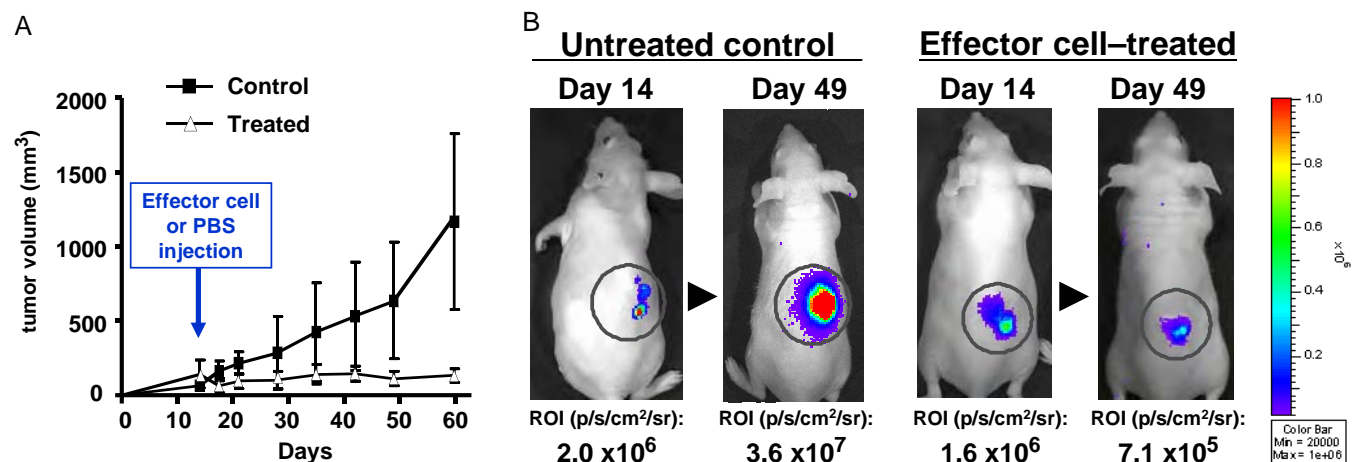


Figure 4. A, growth of PTEN-CaP8/RL subcutaneous tumors in nude mice after adoptive immunotherapy by intratumor injection of effector cells harvested from PTEN-CaP8 vaccinated mice (*Treated*) or injection of PBS vehicle (*Control*). Tumor volume was measured as described. Error bars indicate SD. Statistically significant differences in tumor size between 2 groups was noted on day 60 ($p < 0.01$). B, representative *in vivo* bioluminescence images show PTEN-CaP8/RL tumors on day 14 before treatment and on day 49, 5 weeks after injection of saline (*Controls*) or effector cells (*CTL treated*). Values below images indicate bioluminescence signal measured from indicated ROI (circled areas) in photons per second per cm²/sr.

The PTEN-P8 cell line was isolated directly from true prostate adenocarcinoma arising spontaneously in this model, as generated by mating mice with biallelic floxed PTEN loci with mice expressing Cre recombinase under the control of a prostate specific promoter.¹⁶ Notably PTEN-P8 cells are deleted in only 1 PTEN allele, they are only weakly tumorigenic in vivo and they no longer express the recombinase.¹⁷ Subsequently PTEN-CaP8 cells were derived from PTEN-P8 by the introduction of a retroviral vector constitutively expressing Cre, resulting in deletions in the 2 PTEN alleles and showing much more robust tumorigenicity in vivo.¹⁷

Therefore, in these experiments we used the PTEN-CaP8 prostate cancer cell line for immunization and tumor establishment in vivo, and its parental cell line PTEN-P8 for confirmatory in vitro studies to characterize the cellular immune response. Effector cells were generated by MLTR after vaccinating nontumor bearing litter mates of PTEN deleted mice, which were of an identical genetic background except for the lack of prostate specific Cre. Hence, vaccination with PTEN-CaP8 best mimics the situation in the mice in which PTEN deleted prostate cancer developed, whose tumors initially expressed Cre. However, in vitro assays demonstrated that effector cells generated through vaccination and resensitization with PTEN-CaP8 showed robust reactivity against PTEN-P8 cells, which no longer expressed detectable levels of Cre. This indicated that the cellular immune response was not exclusively directed against Cre as a foreign antigen, but rather likely recognized endogenous tumor antigens.

Hence, it is possible that the expression of Cre as a foreign protein may have served an adjuvant function to stimulate an initial immune response against PTEN-CaP8 cells during vaccination, which then further resulted in epitope spreading to natural endogenous tumor antigens. However, notably no conventional immune adjuvants were used in the vaccination protocol. It is certainly possible that initial irradiation of the cells used in vaccination might also have somehow resulted in the exposure of epitopes that facilitated the immune response but the subsequent in vitro MLTR restimulation procedures used PTEN-CaP8 cells that had been treated with mitomycin C, rather than irradiated. Thus, a significant contribution of irradiation as an adjuvant seems less likely. In this context using radiation in situ is likely to have limited efficacy as an immuno-activating strategy due to intrinsic local mechanisms of tumor immunoresistance, including the expression of immunosuppressive cytokines, such as transforming growth factor- β , and the presence of inhibitory dendritic cells expressing anergizing co-regulators, such as B7-H1, as well as immu-

notolerizing T-regulatory cells in the tumor and draining lymph nodes. In fact, the ex vivo pre-activation of cytolytic T cells away from the immunosuppressive tumor environment and their removal from these inhibitory influences may indeed represent a critical factor in the effectiveness of adoptive transfer strategies for immunotherapy.

In these experiments we used bioluminescence imaging to detect the presence and quantity of luciferase marked PTEN-CaP8/RL cells in vitro and in vivo. Bioluminescence signal intensity showed good correlation with the cell number in vitro and tumor size in vivo, and it confirmed the usefulness of this methodology for monitoring tumor growth and the response to adoptive immunotherapy in living animals with time. In these studies unmarked parental PTEN-CaP8 cells were used for vaccination in nontumor bearing litter mates. Hence, the effector cells that mediated effective tumor growth inhibition upon adoptive transfer were not reacting to luciferase as a foreign antigen. Further studies using this methodology should be greatly facilitated by the recent generation of a new version of the prostate specific PTEN knockout model, which is also transgenic for prostate specific luciferase and, hence, spontaneously arising orthotopic prostate tumors are already marked.²²

The antiproliferative effects in vitro and tumor growth suppression in vivo achieved by effector cells derived from PTEN-CaP8 vaccinated hosts were found to be highly potent, particularly considering that the responses were not likely to be directed against xenogenic antigens, such as Cre or RL. Based on the MLTR culture conditions it was expected that in the presence of target antigens on the sensitizing tumor cells the effector cell preparation would be enriched for CTLs. However, it is certainly possible that the effector cell culture also may have contained subpopulations of natural killer or lymphokine activated killer cells, which contributed to the potent antiproliferative responses in vitro and in vivo. In this context it should also be noted that the MTS assay measures only the metabolic activity of viable adherent target cells, and so it is difficult to distinguish between decreased target cell proliferation, eg in response to immunocytokine signals released from effector cells, and actual target cell death due to effector cell mediated cytotoxicity.

Therefore, future studies will focus on the further characterization of effector cells generated by vaccination with the syngeneic prostate cancer cell lines derived from the PTEN knockout model as well as the identification of relevant endogenous tumor antigens that are expressed by these cancer cells and may be specifically recognized by CTLs. Additionally, this model is also likely to be highly informative and useful for testing various augmentation strate-

gies, such as lymphodepleting chemotherapy, which has shown promise as a preconditioning regimen to augment adoptive immunotherapy in experimental models dating back 25 years^{23–25} as well as in recent clinical trials.^{26,27}

In addition to adoptive transfer strategies, the reliable and reproducible nature of spontaneous prostate cancer arising in this model is well suited for assessing vaccination strategies administered before carcinogenesis or at an early (PIN) stage. To date cancer vaccine strategies have been considerably more effective in a prophylactic setting or against minimal residual disease. In fact, they have proved rather ineffective against established bulky disease. As noted, it is increasingly recognized that solid tumors create a highly immunosuppressive environment through a wide variety of mechanisms, and so preventive vaccination may prove to be the most effective approach.

In this context it is also interesting to note a recent report showing that targeted deletion of PTEN in T cells regulated the peripheral homeostasis of Tregs in vivo and allowed their expansion in response to interleukin-2. Because prostate specific expression of Cre recombinase results in biallelic deletion of PTEN only in prostate cells in our cur-

rent model, we are not currently able to directly observe the effects of PTEN deletion on T-cell function. However, in the human disease setting it is certainly conceivable that PTEN loss may represent a more generalized genetic predisposition in each cell compartment, which may conspire to simultaneously promote carcinogenesis and tolerize the immune system to the developing malignancy. Therefore, in future studies it may be valuable to evaluate the consequences of PTEN loss in prostate epithelium and T cells in a dual compartment knockout model.

CONCLUSIONS

We propose that this unique PTEN knockout model of prostate cancer can serve as a highly useful experimental system in which to assess immunotherapy strategies against true prostate adenocarcinoma in a fully immunocompetent rodent model that mimics the human disease with high fidelity. In particular we propose that this model would be especially useful in future studies for investigating the therapeutic potential of adoptive immunotherapy in ADI-Ca, which develops spontaneously in this model after castration.^{16,22}

REFERENCES

- Jemal A, Murray T, Ward E, Samuels A, Tiwari RC, Ghafoor A et al: Cancer statistics, 2005. *CA Cancer J Clin* 2005; **55**: 10.
- McNeel DG: Prostate cancer immunotherapy. *Curr Opin Urol* 2007; **17**: 175.
- Kruse CA and Rubinstein D: Cytotoxic T lymphocytes reactive to patient major histocompatibility proteins for therapy of recurrent primary brain tumors. In: *Brain Tumor Immunotherapy*. Edited by LM Liau, DP Becker, TF Cloughsey and DD Bigner. New York: Humana Press 2001; pp 149–170.
- Buhler P, Wolf P, Gierschner D, Schaber I, Katzenwadel A, Schultze-Seemann W et al: A bispecific diabody directed against prostate-specific membrane antigen and CD3 induces T-cell mediated lysis of prostate cancer cells. *Cancer Immunol Immunother* 2008; **57**: 43.
- Gade TP, Hassen W, Santos E, Gunset G, Sautemont A, Gong MC et al: Targeted elimination of prostate cancer by genetically directed human T lymphocytes. *Cancer Res* 2005; **65**: 9080.
- Pinthus JH, Waks T, Kaufman-Francis K, Schindler DG, Harmelin A, Kanety H et al: Immuno-gene therapy of established prostate tumors using chimeric receptor-redirected human lymphocytes. *Cancer Res* 2003; **63**: 2470.
- Young JG, Green NK, Mautner V, Searle PF, Young LS and James ND: Combining gene and immunotherapy for prostate cancer. *Prostate Cancer Prostatic Dis* 2007.
- Zhang Q, Yang X, Pins M, Javonovic B, Kuzel T, Kim SJ et al: Adoptive transfer of tumor-reactive transforming growth factor-beta-insensitive CD8+ T cells: eradication of autologous mouse prostate cancer. *Cancer Res* 2005; **65**: 1761.
- Anderson MJ, Shafer-Weaver K, Greenberg NM and Hurwitz AA: Tolerization of tumor-specific T cells despite efficient initial priming in a primary murine model of prostate cancer. *J Immunol* 2007; **178**: 1268.
- Roy-Burman P, Wu H, Powell WC, Hagenkord J and Cohen MB: Genetically defined mouse models that mimic natural aspects of human prostate cancer development. *Endocr Relat Cancer* 2004; **11**: 225.
- Tennant TR, Kim H, Sokoloff M and Rinker-Schaeffer CW: The Dunning model. *Prostate* 2000; **43**: 295.
- Goebel HW, Rausch U, Steinhoff M, Seitz J, Bacher M, Papotti M et al: Arguments against the prostatic origin of the R-3327 Dunning H tumor. *Virchows Arch B Cell Pathol Incl Mol Pathol* 1992; **62**: 9.
- Stambolic V, Suzuki A, de la Pompa JL, Brothers GM, Mirtsos C, Sasaki T et al: Negative regulation of PKB/Akt-dependent cell survival by the tumor suppressor PTEN. *Cell* 1998; **95**: 29.
- Cairns P, Okami K, Halachmi S, Halachmi N, Esteller M, Herman JG et al: Frequent inactivation of PTEN/MMAC1 in primary prostate cancer. *Cancer Res* 1997; **57**: 4997.
- Mulholland DJ, Dedhar S, Wu H and Nelson CC: PTEN and GSK3beta: key regulators of progression to androgen-independent prostate cancer. *Oncogene* 2006; **25**: 329.
- Wang S, Gao J, Lei Q, Rozengurt N, Pritchard C, Jiao J et al: Prostate-specific deletion of the murine Pten tumor suppressor gene leads to metastatic prostate cancer. *Cancer Cell* 2003; **4**: 209.
- Jiao J, Wang S, Qiao R, Vivanco I, Watson PA, Sawyers CL et al: Murine cell lines derived from Pten null prostate cancer show the critical role of PTEN in hormone refractory prostate cancer development. *Cancer Res* 2007; **67**: 6083.
- Bhaumik S and Gambhir SS: Optical imaging of Renilla luciferase reporter gene expression in living mice. *Proc Natl Acad Sci U S A* 2002; **99**: 377.
- Tomayko MM and Reynolds CP: Determination of subcutaneous tumor size in athymic (nude) mice. *Cancer Chemother Pharmacol* 1989; **24**: 148.
- Hiraoka K, Kimura T, Logg CR and Kasahara N: Tumor-selective gene expression in a hepatic metastasis model after locoregional delivery of a replication-competent retrovirus vector. *Clin Cancer Res* 2006; **12**: 7108.

21. Brakenhielm E, Burton JB, Johnson M, Chavarria N, Morizono K, Chen I et al: Modulating metastasis by a lymphangiogenic switch in prostate cancer. *Int J Cancer* 2007; **121**: 2153.
22. Liao CP, Zhong C, Saribekyan G, Bading J, Park R, Conti PS et al: Mouse models of prostate adenocarcinoma with the capacity to monitor spontaneous carcinogenesis by bioluminescence or fluorescence. *Cancer Res* 2007; **67**: 7525.
23. North RJ: Cyclophosphamide-facilitated adoptive immunotherapy of an established tumor depends on elimination of tumor-induced suppressor T cells. *J Exp Med* 1982; **155**: 1063.
24. Gomez GG, Hutchison RB and Kruse CA: Chemotherapy and chemo-adoptive immunotherapy of cancer. *Cancer Treat Rev* 2001; **27**: 375.
25. Kruse CA, Mitchell DH, Kleinschmidt-DeMasters BK, Bellgrau D, Eule JM, Parra JR et al: Systemic chemotherapy combined with local adoptive immunotherapy cures rats bearing 9L gliosarcoma. *J Neurooncol* 1993; **15**: 97.
26. Dudley ME, Wunderlich JR, Yang JC, Sherry RM, Topalian SL, Restifo NP et al: Adoptive cell transfer therapy following non-myeloablative but lymphodepleting chemotherapy for the treatment of patients with refractory metastatic melanoma. *J Clin Oncol* 2005; **23**: 2346.
27. Rosenberg SA, Yang JC, Robbins PF, Wunderlich JR, Hwu P, Sherry RM et al: Cell transfer therapy for cancer: lessons from sequential treatments of a patient with metastatic melanoma. *J Immunother* 2003; **26**: 385.

Optimization of enzyme–substrate pairing for bioluminescence imaging of gene transfer using *Renilla* and *Gaussia* luciferases

Takahiro Kimura^{1,2}
Kei Hiraoka¹
Noriyuki Kasahara^{1,3}
Christopher R. Logg^{1*}

¹Department of Medicine, University of California, Los Angeles, CA, USA

²Department of Urology, Jikei University School of Medicine, Tokyo, Japan

³Department of Molecular and Medical Pharmacology, University of California, Los Angeles, CA, USA

*Correspondence to: Christopher R. Logg, Department of Medicine, University of California, Los Angeles, 675 Charles E. Young Drive South, MacDonal Research Laboratories, Room 1541, Los Angeles, CA 90095, USA. E-mail: logg@ucla.edu

Abstract

Background Bioluminescence imaging (BLI) permits the non-invasive quantification and localization of transduction and expression by gene transfer vectors. The tendency of tissue to attenuate light in the optical region, however, limits the sensitivity of BLI. Improvements in light output from bioluminescent reporter systems would allow the detection of lower levels of expression, smaller numbers of cells and expression from deeper and more attenuating tissues within an animal.

Methods With the goal of identifying substrates that allow improved sensitivity with *Renilla* luciferase (RLuc) and *Gaussia* luciferase (GLuc) reporter genes, we evaluated native coelenterazine and three of its most promising derivatives in BLI of cultured cells transduced with retroviral vectors encoding these reporters. Of the eight enzyme–substrate pairs tested, the two that performed best were further evaluated in mice to compare their effectiveness for imaging vector-modified cells in live animals.

Results In cell culture, we observed striking differences in luminescence levels from the various enzyme–substrate combinations and found that the two luciferases exhibited markedly distinct abilities to generate light with the substrates. The most effective pairs were RLuc with the synthetic coelenterazine derivative ViviRen, and GLuc with native coelenterazine. In animals, these two pairs allowed similar detection sensitivities, which were eight- to 15-fold higher than that of the prototypical RLuc-native coelenterazine combination.

Conclusions Substrate selection can dramatically influence the detection sensitivity of RLuc and GLuc and appropriate choice of substrate can greatly improve the performance of reporter genes encoding these enzymes for monitoring gene transfer by BLI. Copyright © 2010 John Wiley & Sons, Ltd.

Keywords bioluminescence; coelenterazine; imaging; luciferase; reporter gene; retrovirus

Introduction

The development of more effective gene transfer techniques remains a fundamental goal in gene therapy research. Improvements in methods for non-invasively tracking and quantitating gene delivery and expression could greatly facilitate the development of better vectors and delivery strategies.

Received: 30 September 2009

Revised: 12 February 2010

Accepted: 15 April 2010

For this purpose, non-invasive bioluminescence imaging (BLI) stands out as particularly attractive as a result of its relatively high sensitivity, speed, ease of employment, and low cost [1,2]. In BLI, a cooled charge-coupled device camera is used to detect the emission of light from cells or tissues expressing a luciferase reporter protein. This light is generated when the luciferase catalyses oxidation of its substrate using molecular oxygen.

The most widely used luciferases are those of the firefly *Photinus pyralis*, and the sea pansy *Renilla reniformis*. Whereas firefly luciferase (FLuc) uses D-luciferin as substrate, the luciferases of *Renilla* (RLuc) and other bioluminescent marine organisms use coelenterazine. The cDNA for the marine copepod *Gaussia princeps* [3] was found to be capable, after codon optimization, of mediating levels of luminescence in combination with coelenterazine much higher than those of a humanized RLuc gene and comparable to those of a humanized FLuc gene in combination with D-luciferin [4]. Similar to RLuc, *Gaussia* luciferase (GLuc) catalyses the oxidation of coelenterazine to produce a broad spectrum of light with a peak at around 480 nm [5,6]. Although GLuc is secreted and released into the circulation in animals [7], it is nevertheless effective for imaging tissues expressing the enzyme [4].

RLuc and GLuc offer unique advantages over FLuc for imaging gene transfer and expression. One is the relatively small size of the marine luciferases. Compared to the coding sequence of FLuc, which is 1653 bp, those of RLuc and GLuc are compact, at 936 and 558 bp, respectively. The marine luciferases are therefore well suited for applications in which short transgene sequences are required. Another advantage is that, unlike FLuc, the marine enzymes do not require ATP as a cofactor and may thus be used for imaging transduced cells and tissues independently of their metabolic state and are less likely to perturb the cells in which they are expressed [2,8]. Because coelenterazine-utilizing luciferases do not catalyse D-luciferin oxidation and FLuc does not catalyse coelenterazine oxidation, these reporters may also be combined with FLuc for dual labeling [8].

A disadvantage of RLuc and GLuc relative to FLuc for BLI is that a greater proportion of the light produced by the marine luciferases is absorbed by tissue. Tissue chromophores, such as hemoglobin, most efficiently absorb wavelengths below 600 nm [9]. Because more of the FLuc emission spectrum, which peaks at 562 nm, is above 600 nm, more of its signal can reach the animal's surface. The utility of RLuc and GLuc as reporters for *in vivo* BLI could therefore particularly benefit from improvements in signal intensity. An overall increase in light output by RLuc and GLuc would be beneficial primarily by raising the level of light in the longer-wavelength regions of their spectra. Previous efforts at enhancing the performance of RLuc for BLI include the engineering of mutants that are more stable and produce brighter and red-shifted light [10,11].

A large number of analogs of native coelenterazine (clzn-*n*) have been synthesized and tested for their capacity to generate light *in vitro* with RLuc [12,13]. Zhao

et al. [14] evaluated several of these analogs with cells expressing RLuc and found that coelenterazine-f (clzn-f) and coelenterazine-h (clzn-h) produced stronger luminescence than clzn-*n*, while exhibiting autoluminescence levels similar to that of the native substrate. A variant of clzn-h called ViviRen, which bears protected oxidation sites, is sold by Promega Corporation (Madison, WI, USA) [15]. The ester protecting groups are cleaved intracellularly by endogenous esterases, thereby rendering the substrate available for catalysis by a luciferase. ViviRen has been reported to yield higher luminescence levels with RLuc *in vitro* and *in vivo* than clzn-*n* [16].

Because of the minimal homology between RLuc and GLuc [6], we suspected that their abilities to generate light with different coelenterazine-based substrates would be distinct and that optimization of pairing between enzyme and substrate could readily improve the effectiveness of reporter genes encoding these proteins for BLI of gene transfer. In the present study, we evaluated clzn-*n*, clzn-f, clzn-h, and ViviRen with respect to their autoluminescence properties and their ability to generate light from live cells transduced with replication-competent retroviral (RCR) vectors expressing RLuc or GLuc. We then evaluated the two most promising pairs from this group, RLuc/ViviRen and GLuc/clzn-*n*, in BLI of mice.

Materials and methods

Plasmids

Plasmids pAZ3-RLuc and pAZ3-GLuc, which contain full-length, amphotropic murine leukemia virus (MLV) proviruses bearing internal ribosome entry site (IRES)-luciferase cassettes inserted immediately after the *env* stop codon, were derived from plasmid pAZ3-GFP. pAZ3-GFP is a modified version of plasmid pAZE-GFP [17]. Details of the modifications will be provided upon request and consist, briefly, of removal of MLV 5' UTR sequence present downstream of the 3' long-terminal repeat, addition of a unique *Mlu*I site at the 5' end of the IRES and the replacement of a short region of ecotropic sequence at the 3' end of the *env* gene to render the entire *env* sequence of amphotropic 4070A MLV origin. The luciferase sequences were polymerase chain reaction (PCR) amplified from plasmids pCMV-GLuc-1 (Nanolight Technologies, Pinetop, AZ, USA) and phRL-CMV (Promega), respectively. The forward and reverse primers for RLuc were: 5'-TAATATGGCTTCCAAGGTGTACGA-3' and 5'-GGGCCGGCGCCGCTTACTGCTCGTTCTTCAGC-3', respectively, and those for GLuc were 5'-TAATATGGGC GTCAAAGTTCTGTTTGCCTG-3' and 5'-TAACCTGCGGC CGCTCAGTCGCTCCGGCCCCCTTGATCTTG-3'. The PCR products were digested with *Not*I and ligated into the *Psi*I and *Not*I sites of pAZ3-GFP, replacing the green fluorescent protein (GFP) gene.

Cell culture and transfections

293T and PC-3 cells were obtained from the American Type Culture Collection and grown in Dulbecco's modified Eagle's medium and RPMI 1640, respectively, supplemented with 10% fetal bovine serum and antibiotics. For transient transfection of PC-3 cells with pAZ3-RLuc or pAZ3-GLuc for luciferase assays, FuGENE 6 (Roche, Mannheim, Germany) was used according to the manufacturer's recommendations and GFP expression plasmid pGFP_{cmv}-R-control was cotransfected for normalization for transfection efficiency. Forty-eight hours post-transfection, the cultures were imaged as described below and transfection efficiency was determined by flow cytometry for GFP with an EPICS XL flow cytometer (Beckman Coulter, Fullerton, CA, USA).

Virus production, titration and infections

Virus was produced as described previously [18] by transfection of 293T cells with vector plasmid using Lipofectamine 2000 (Invitrogen, Carlsbad, CA, USA). Virus titers were determined by measurement of the reverse transcriptase (RT) activity of the 293T transfection supernatants with a Quan-T-RT kit (GE Healthcare, Milwaukee, WI, USA) as previously described [19] and by comparison of the activities with those of AZ3-GFP transfection supernatants of known GFP-transducing titer. Infections were performed at a multiplicity of infection (MOI) of 1 and when the cells were at approximately 25% confluence. The infections were allowed to proceed for 10 days and complete transduction was confirmed at that point by failure (as a result of superinfection resistance) of AZ3-GFP added to an MOI of 2 to transduce any cells as determined by flow cytometry for GFP, 3 days later.

Virus copy number analysis

To determine the numbers of integrated virus copies in the fully transduced PC-3 cells, we used a real-time quantitative PCR assay to detect the MLV *pol* gene in genomic DNA. The primer and probe sequences used were: forward primer, 5'-AACAAAGCGGGTGGGAAGACATC-3'; reverse primer, 5'-CAAAGGCGAAGAGAGGCTGAC-3'; and probe, 5'-FAM (6-carboxyfluorescein)-CCCACCGTGCC CAACCCTTACAACC-TAMRA (6-carboxytetramethylrhodamine). A PureLink Genomic DNA Mini Kit (Invitrogen) was used to isolate DNA from infected and naive PC-3 cells and the concentration of the resulting samples was determined spectrophotometrically. Three independently isolated genomic DNA preparations from each cell line was analyzed and all samples were analyzed in triplicate. Each 40- μ l PCR reaction contained 50 ng of genomic DNA, 600 nM of each primer, 200 nM of probe and 1 \times TaqMan Gene Expression Master Mix (Applied Biosystems, Foster City, CA, USA). The reactions were carried

out in a 7900HT Real-Time PCR System (Applied Biosystems) and the cycling conditions were 10 min at 95 °C followed by 40 cycles of 15 s at 95 °C and 1 min at 60 °C. Plasmid encoding the corresponding vectors was used to generate a standard curve for absolute quantification of copy number. Ten-fold serial dilutions of plasmid, containing between 1500 000 and 15 copies, plus 50 ng of genomic DNA from untransduced cells, were amplified in parallel with the unknown samples. The number of virus copies present in each sample was determined using the standard curve.

Coelenterazine analogs

Clzn-*n* was obtained from Nanolight Technologies, and clzn-f, clzn-h and ViviRen were obtained from Promega. Stock solutions of clzn, clzn-f and clzn-h were prepared by dissolving the substrates in methanol to a final concentration of 5 mM. ViviRen stock solution was prepared by dissolving the substrate in dimethylsulfoxide to a final concentration of 50 mM. All stock solutions were stored at -80 °C until use and aliquots were used only once.

Imaging

Imaging was performed with an IVIS optical imaging system (Xenogen, Alameda, CA, USA) and the data were processed using Igor Pro (WaveMetrics Inc., Portland, OR, USA) and Living Image (Xenogen) image analysis software. Acquisition times were in the range 1–60 s, depending on the light intensity of the source. For analysis of live cell cultures or culture supernatant alone, imaging was performed immediately upon addition of substrate to the supernatant. Regions of interest (ROI) were drawn around wells to determine photon flux. For mouse imaging, substrates were administered to the mice either by tail vein (1.7 and 7 nmol/kg doses) or intracardiac (17 nmol/kg doses) injection immediately prior to imaging. For measurement of luminescence from cell implants, ROIs were drawn around the implant region, and for *in vivo* autoluminescence measurements, ROIs were drawn around the entire mouse. Immediately prior to substrate injections for autoluminescence measurements, background light levels occurring independently of any substrate were determined and the values obtained were subtracted from luminescence readings taken after substrate injection. Signal-to-background ratios in the present study are defined as the ratio of luminescence measured from cells transduced with luciferase-encoding vector to that measured from nontransduced cells.

GLuc secretion kinetics determination

To determine the rate of accumulation of GLuc in the media of cultures transduced with AZ3-GLuc, 30 000 cells were plated in the wells of 24-well plates. At 12-h intervals

during the subsequent 72 h, culture supernatants were harvested from a subset of the wells and stored at -80°C . The cells in these wells were then trypsinized and counted using a hemocytometer for normalization of luminescence readings. After the final harvest, the GLuc activities in the samples were determined by imaging as described above after the addition of clzn-*n* to $15\ \mu\text{M}$.

Mice

Six- to 8-week-old male athymic nude mice (Charles River Laboratories, Wilmington, MA, USA) were used. The animals were maintained and handled in accordance with institutional guidelines, and all studies were conducted under protocols approved by the UCLA Animal Research Committee. To generate mice bearing luciferase-expressing implants, one million PC-3 cells, transduced with AZ3-RLuc or AZ3-GLuc, were injected subcutaneously into each dorsal flank in a volume of $200\ \mu\text{l}$ containing 50% Matrigel matrix (BD Biosciences, Franklin Lakes, NJ, USA). Imaging was performed 3 days after implantation. Prior to injection of substrate for imaging, mice were anaesthetized by intraperitoneal injection of ketamine ($100\ \text{mg/kg}$) and xylazine ($10\ \text{mg/kg}$).

Results

Construction and testing of RCR vectors expressing RLuc and GLuc

As a model gene delivery system with which to evaluate RLuc and GLuc, we constructed amphotropic

murine leukemia virus-based RCR vectors [17,20] expressing codon-optimized genes encoding RLuc and GLuc (Figure 1A). We generated cell lines stably transduced with the vectors by infecting, at equal MOI, PC-3 human prostate carcinoma cells and allowing the cells to become fully transduced. To determine the numbers of integrated provirus in the two cell lines, we performed quantitative PCR on genomic DNA from these cells using primers specific for the MLV *pol* gene. The mean copy numbers of vector per ng of DNA was 693 for the cells infected with AZ3-RLuc-infected and 673 for those infected with AZ3-GLuc (Figure 1B). For normal diploid cells, this corresponds to 4.85 or 4.71 integrations per cell, respectively. This difference was not statistically significant (unpaired *t*-test, $p = 0.259$). Addition of clzn-*n* directly to cultures of these cells or PC-3 cells transiently transfected with the corresponding plasmids produced approximately equivalent relative levels of expression for the two reporters using the two delivery methods (Figure 1C), further indicating that the stably-transduced cells could be used for reliable comparison of the two reporter genes.

Luminescence from intracellular versus secreted enzyme

Because GLuc is secreted [6], we wished to determine the kinetics of secretion from cells stably expressing the enzyme. The transduced cells were plated in fresh media and samples of the culture supernatant were taken at 12-h intervals thereafter and their luciferase activities were measured and normalized for the cell number at the

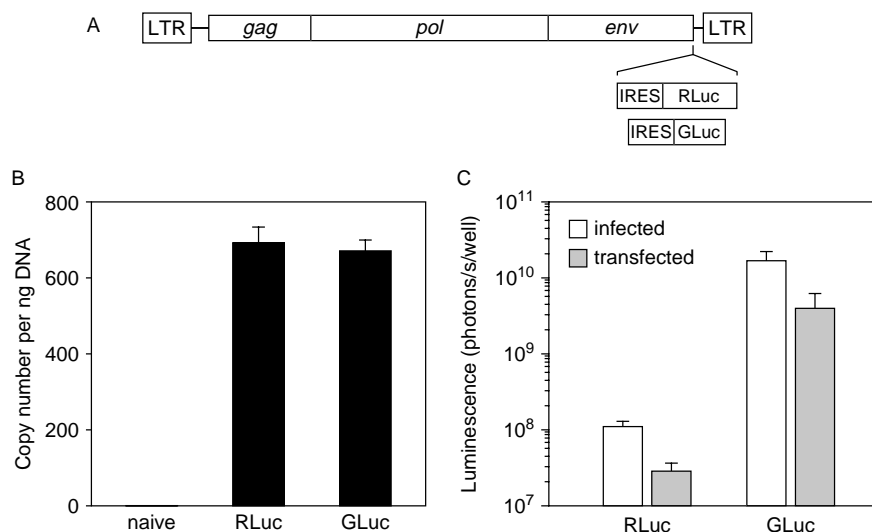
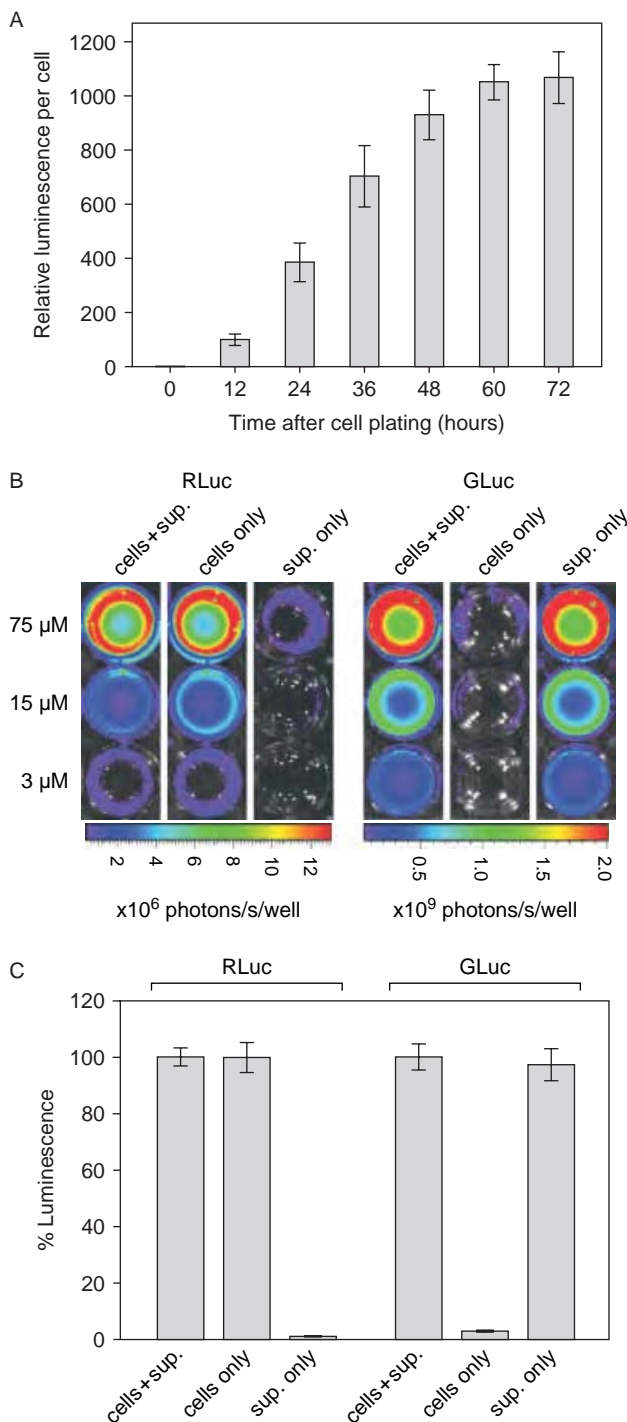


Figure 1. Delivery of RLuc and GLuc genes by a replication-competent retroviral vector. (A) Schematic of RCR vectors AZ3-RLuc and AZ3-GLuc. (B) Determination of vector copy number in cells fully transduced with the vectors after infection at an MOI of 1. A primer-probe set specific for the *pol* gene was used to measure copy number by real-time PCR. Shown are the mean \pm SD obtained from three independently prepared samples of genomic DNA from each cell population. (C) Peak light output attained after the addition of clzn-*n* to a concentration of $15\ \mu\text{M}$ directly to the supernatant of live cultures either stably infected with the vectors or transiently transfected with the corresponding plasmids. Background luminescence measured after exposure of naïve cultures to the same dose of coelenterazine was subtracted from the readings from the infected or transfected cultures to obtain the luminescence values shown

time of harvest (Figure 2A). Maximal GLuc activity in the supernatant was reached after approximately 60 h.

We quantified the contribution of cell-associated versus secreted luciferase to the production of light from the transduced cells. The cells were plated and grown for 3 days to allow for conditioning of the medium, after which time the cells alone, the supernatant alone, or intact cultures containing both cells and supernatant were assayed for luciferase activity. Figure 2B shows representative imaged plates. RLuc luminescence originated almost entirely (>99%)



intracellularly, whereas approximately 3% of the GLuc signal was from cell-associated enzyme (Figure 2C) and the remainder from secreted enzyme.

Evaluation of nonspecific and specific light generated with the coelenterazine analogs

To determine the autoluminescence background generated by the substrates, we measured the light produced upon addition of each substrate directly to the medium of naive cultures to three different concentrations (Figure 3). Although *clzn-n*, *clzn-f* and *clzn-h* produced similar levels of autoluminescence, those of *ViviRen* were considerably lower, at only 5–10% of the levels of the other three substrates. The relative intensities of autoluminescence from *clzn-n*, *clzn-f* and *clzn-h* are consistent with those previously reported for these substrates in serum-containing cell culture media [14].

We next determined the kinetics and peak intensity of luciferase-mediated luminescence after the addition of the substrates to cultures of vector-transduced cells. We found that the levels of light generated by each enzyme with the substrates differed greatly, and that the kinetic pattern of luminescence was characteristic of the enzyme (Figure 4A). With all substrates, luminescence from RLuc peaked at approximately 5 min and decayed slowly thereafter, whereas luminescence from GLuc peaked within the first 30 s and decayed very rapidly. The two enzymes exhibited opposite rank-order peak light output levels with the different substrates, demonstrating the importance of substrate selection with the two reporters. With RLuc, *ViviRen* produced the strongest signal and, with GLuc, *clzn-n* produced the strongest signal. Of particular note is that the most commonly used combination among the eight tested, RLuc/*clzn-n*, generated the least light. Addition of the substrates to three different concentrations, in the range 3–75 μM, revealed an approximately proportional relationship

Figure 2. Localization of luciferase activity in live cultures expressing RLuc or GLuc. (A) The secretion kinetics of GLuc were determined by plating PC-3 cells transduced with AZ3-GLuc and measuring luciferase activity in the culture supernatant at 12-h intervals thereafter. At each time point, cell numbers were also determined to normalize luminescence readings. The 0-h time point represents luminescence from fresh, unconditioned media and this value was arbitrarily set to 1. (B) Quantification of cell-associated versus secreted RLuc and GLuc activity. Transduced cells were plated and grown for three days and the following were then imaged to determine luciferase activities upon addition 3, 15 or 75 μM *clzn-n*: intact cultures containing cells and conditioned supernatant (left columns), cultures whose medium was replaced with medium from untransduced cultures (middle columns), or conditioned medium alone (right columns). Cultures whose medium was replaced were first washed twice with RPMI 1640 to eliminate any residual extracellular luciferase. (C) Luciferase activities from the 15 μM *clzn-n* doses described in (B) expressed as a percentage of light output from intact cultures. Data are the mean ± SD

between concentration and peak luminescence for all eight enzyme–substrate pairs (Figure 4B).

Using the obtained peak autoluminescence (Figure 3) and enzyme-mediated luminescence (Figure 4B) values, the signal-to-background ratio for each enzyme–substrate combination at each of the three concentrations tested were determined (Figure 5). The RLuc/ViviRen and GLuc/clzn-*n* pairs exhibited by far the most favourable ratios. Again, of all combinations tested, the most commonly used, RLuc/clzn-*n*, produced the poorest results. Additionally, despite the GLuc/clzn-*n* pair having generated much higher light output than RLuc/ViviRen, the two pairs possessed similar signal-to-background ratios as a result of the very low autoluminescence of ViviRen. Because these two pairs exhibited the best results in cell culture, we selected them for further characterization in *in vivo* BLI.

Comparison of RLuc and GLuc with ViviRen and clzn-*n* in live animal imaging

To assess the autoluminescence generated by clzn-*n* and ViviRen in live animals, we injected naïve mice with two different doses of the substrates and imaged the animals dorsally and ventrally. Surprisingly, the substrates produced similar overall levels of autoluminescence (Figure 6A), in contrast to the large difference in autoluminescence we observed in cell culture with these compounds. At both doses and at both mouse surfaces, the difference between total autoluminescence was in no case more than two-fold. We also found that the two substrates produced distinctive patterns of nonspecific light in the mice. Clzn-*n* generated a slight focus of autoluminescence in the abdominal region, whereas ViviRen generated more pronounced signals in the thoracic region (Figures 6B and 6C). The thoracic signals, which accounted for almost half of the total autoluminescence at the 1-min time point and were only seen dorsally, completely disappeared after four minutes.

To evaluate the light output from the RLuc/ViviRen and GLuc/clzn-*n* combinations in live animals, we generated nude mice transiently implanted with the vector-transduced cells. One million of the transduced PC-3 cells were introduced into the subcutaneous flanks of mice, with GLuc-expressing cells on the left and RLuc-expressing cells on the right. The animals were imaged 3 days later to allow time for accumulation of secreted GLuc. Substrate doses of either 1.7 or 17 nmol/kg were injected. It should be noted that the 17 nmol/kg dose is well above that normally required for imaging of subcutaneous tissues expressing RLuc or GLuc. We found that, as a result of the relatively small number of cells injected, lower doses of substrate produced only weak signals with this model (Figure 7C and data not shown).

The kinetics of luminescence from each of the four enzyme–substrate pairs in these animals (Figure 7A) was similar to that observed in cell culture. We

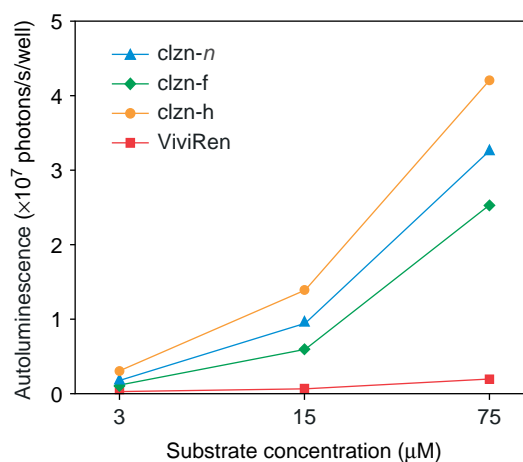


Figure 3. Comparison of the autoluminescence generated by the four substrates in live cultures. Each substrate was added directly to the media of naïve PC-3 cultures not expressing any luciferase and the resulting light emission was measured. Light output was determined from the plates every minute for 10 min after the addition of substrate to the indicated concentration. Each value is the mean peak luminescence level reached in four wells

noted, however, that the GLuc/clzn-*n* pair generated substantially lower light levels, relative to all three of the other pairs, in the mice compared to cell culture. In culture, the relative peak signal intensities for RLuc/clzn-*n*, RLuc/ViviRen, GLuc/clzn-*n* and GLuc/ViviRen were approximately 1, 8, 170 and 2 (Figure 4B), whereas, in the implant-containing mice, they were approximately 1, 8, 15 and 0.7 (17 nmol/kg doses; Figure 7C). Thus the GLuc/clzn-*n* pair, although producing very bright luminescence in mice, generated notably stronger relative signals from the cells in culture than in the animals. Possible explanations for this finding are discussed below.

Discussion

Improvements in techniques for localizing and quantitating gene transfer and expression will aid in the development of better vectors for gene therapy [2,21]. Optical imaging techniques such as BLI have particular promise for this purpose in that they permit the relatively inexpensive, technically straightforward and non-invasive analysis of animals at serial time points [1]. We therefore evaluated four of the most promising coelenterazine-based substrates with cells transduced by vectors expressing RLuc and GLuc to determine which substrates perform best in BLI with these two reporters.

Testing of the eight enzyme–substrate combinations in cell culture revealed striking differences in the ability of the two luciferases to generate light with the substrates. RLuc performed best with ViviRen, whereas GLuc performed best with the native substrate. Both *in vitro* and *in vivo*, these two enzyme–substrate pairs exhibited similar signal-to-background ratios, despite considerable differences in the levels of specific and nonspecific

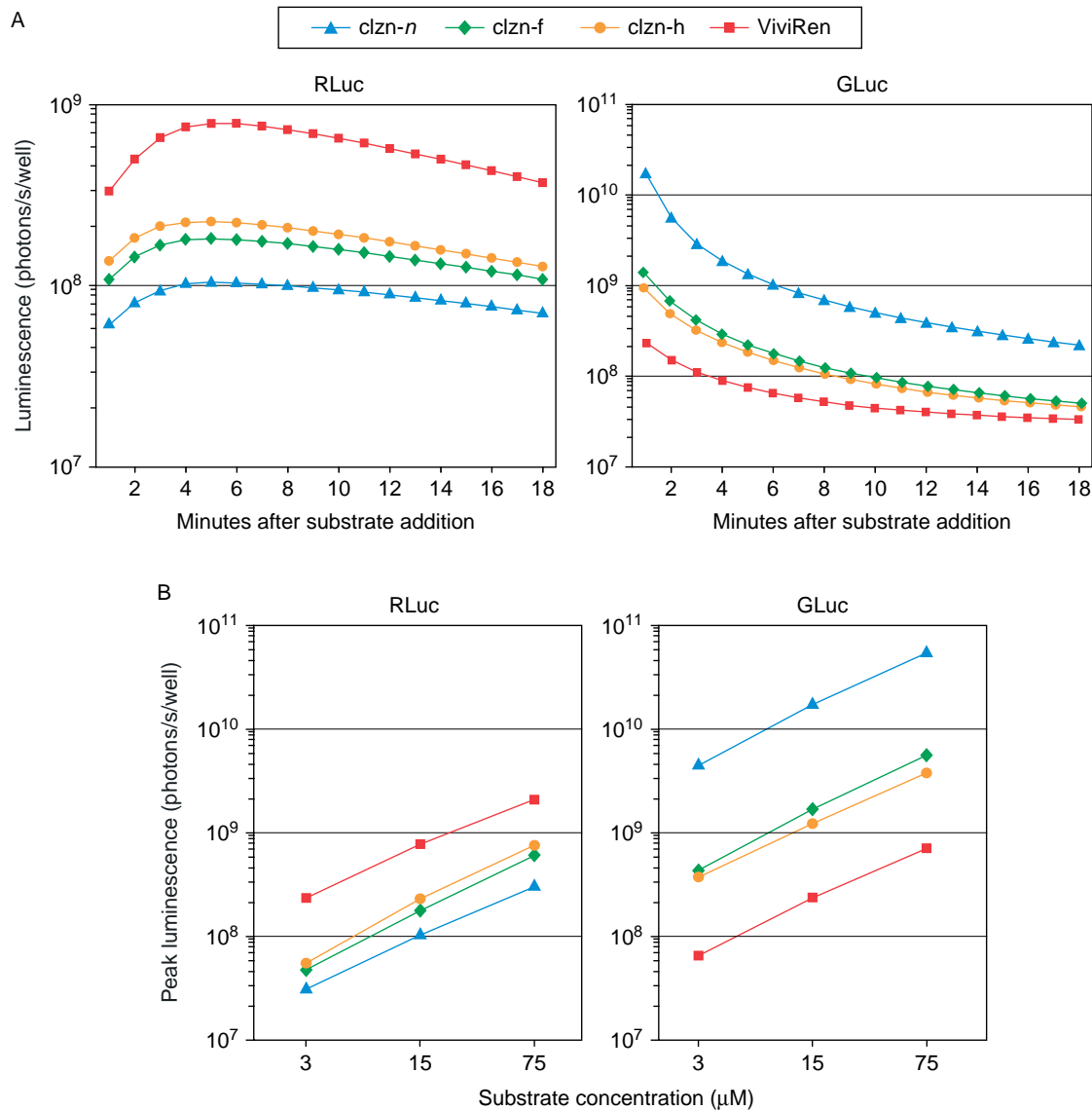


Figure 4. Kinetics and dose-responsiveness of luminescence from live cultures transduced with AZ3-RLuc or AZ3-GLuc and treated with clzn-*n*, clzn-*h*, clzn-*f* or ViviRen. (A) Time course of light output following addition of substrate to 15 μM . (B) Peak luminescence achieved upon addition of the substrates to three different concentrations. In both (A) and (B), substrate was added directly to the media and luminescence was measured immediately thereafter using the IVIS system. Each point represents the mean signal of three determinations following subtraction of autoluminescence measured from cultures treated with substrate but not expressing any luciferase

luminescence in cell culture and in mice. In cell culture, ViviRen produced much lower autoluminescence than clzn-*n*, but, *in vivo*, the difference in autoluminescence from the two substrates was small. The relative intensity of light from GLuc catalysis of clzn-*n*, however, was also lower in mice than in cell culture, resulting in similar overall detection sensitivities for the RLuc/ViviRen and GLuc/clzn-*n* pairs in culture and in mice.

Although ViviRen proved to be an excellent substrate for RLuc, it generated relatively weak signals with GLuc. This was presumably due to two factors. First, ViviRen must enter the cell in order to undergo deprotection. Because the vast majority of GLuc is extracellular, the deprotected substrate must then exit the cell to reach the major pool of enzyme. Second, the deprotected form of ViviRen is clzn-*h*, which itself performed relatively poorly

with GLuc. The findings obtained thus suggest that the development of a nonsecreted form of GLuc could permit improved light output with protected substrates such as ViviRen. Efforts to date, however, to create variants of GLuc that are maintained within the cell by removal of the predicted signal peptide sequence have resulted in steep reductions in luciferase activity within cells and in conditioned supernatant [4; present study, data not shown).

We found that of the four enzyme-substrate pairs tested in mice, those with GLuc generated markedly lower luminescence *in vivo* than *in vitro* relative to those with RLuc. Although the relative luminescence of RLuc/clzn-*n* and RLuc/ViviRen was similar in cell culture and in mice (approximately 1:7 in cell culture and 1:8 in mice), that of GLuc/clzn-*n* and GLuc/ViviRen were substantially

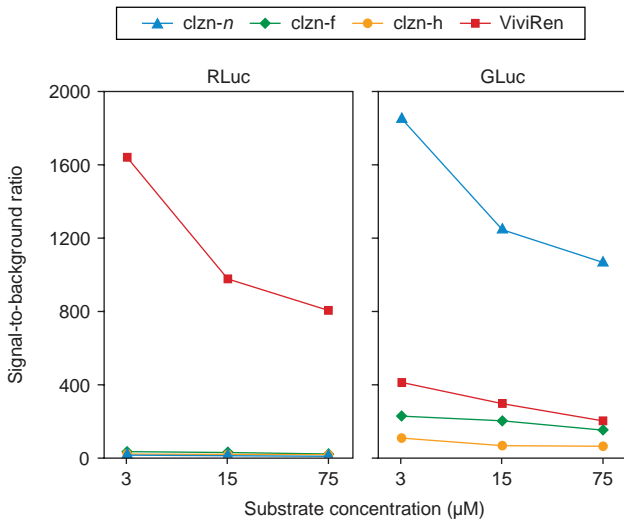


Figure 5. Signal-to-background ratios of the eight enzyme-substrate combinations in live cell cultures. Ratios were calculated by dividing the luminescence measured from transduced cultures by the luminescence measured from nontransduced cultures

reduced in the animals. Relative to the RLuc/clzn-*n* and RLuc/ViviRen pairs, they were approximately 12-fold and four-fold lower, respectively, in mice than in cell culture. These differences with GLuc in cell culture versus *in vivo* are likely in large part because, in cell culture, secreted GLuc is retained within the culture vessel, whereas, in animals, enzyme released from the expressing tissue enters into the bloodstream and undergoes clearance by the kidneys [7]. A recent study showed that maintenance of the association between GLuc and the cells from which it is expressed can be an effective approach to improving the detectability of GLuc by BLI [22].

In summary, the results obtained in the present study demonstrate that pairing of GLuc with clzn-*n* and RLuc with ViviRen allow similar and very high sensitivities for BLI of live cell cultures and mice. Compared to the prototypical RLuc/clzn-*n* pair, these combinations allow approximately 100–150-fold higher signal-to-background ratios in culture and eight- to 15-fold higher sensitivity in mice. Our findings should also be of interest to investigators using *in vitro* reporter gene assays in studies of gene transfer and expression. For such applications

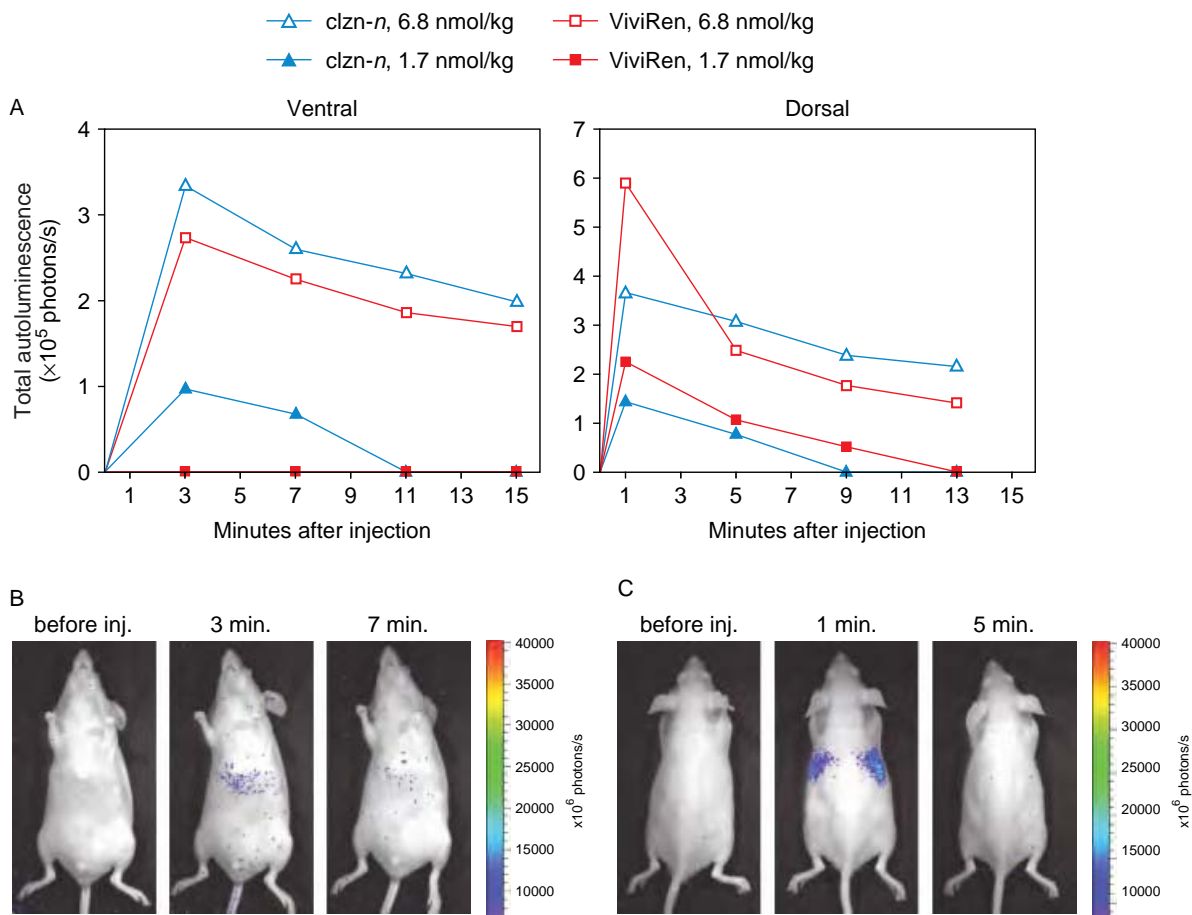


Figure 6. Autoluminescence from clzn-*n* and ViviRen *in vivo*. Mice were injected intravenously with the indicated doses of clzn-*n* or ViviRen and imaged ventrally or dorsally every 2 min for the subsequent 15 min. Dorsal and ventral measurements were obtained from the same injections, with either aspect of the mice being imaged at alternating time intervals. (A) Time course of autoluminescence from the entire dorsal or ventral aspect of the mice. Background light levels measured prior to substrate injection were subtracted from the readings taken after injection. Each data point is the average obtained from three injections. (B) Ventral images of a mouse injected with 6.8 nmol/kg of clzn-*n*, showing characteristic signal from the abdominal region. (C) Dorsal images of a mouse injected with 6.8 nmol/kg of ViviRen showing characteristic thoracic signal at 1 min

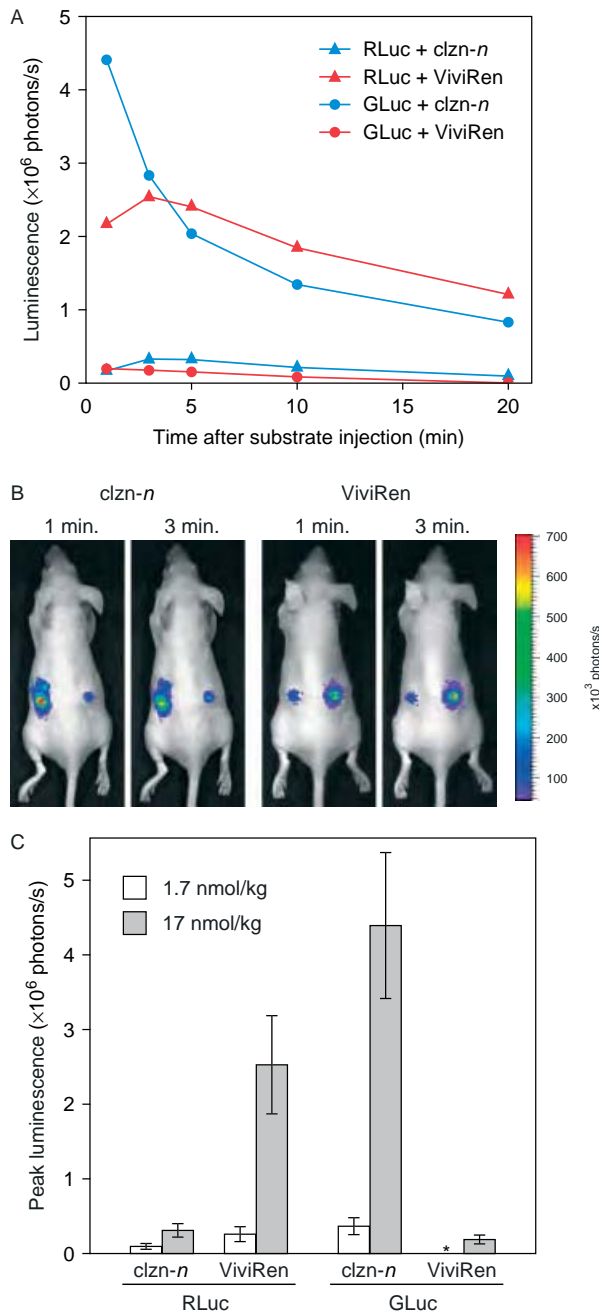


Figure 7. Light production from RLuc- or GLuc-expressing cells after implantation into nude mice. PC-3 cells, transduced with AZ3-GLuc (left side of mice) or AZ3-RLuc (right side), were injected subcutaneously into the flanks of the mice and imaged 3 days later immediately upon tail vein administration of clzn-n or ViviRen at doses of 1.7 or 17 nmol per kg of body weight. (A) Kinetics of luminescence from the implanted cells after injection of 17 nmol/kg substrate. (B) Representative images obtained at 1 and 3 min after injection of mice with 17 nmol/kg substrate. (C) Average peak luminescence levels from the implants at both doses. The asterisk denotes the absence of luminescence over background from GLuc with 1.7 nmol ViviRen. Error bars, SD

requiring very high signal-to-background, the GLuc/clzn-n and RLuc/ViviRen pairs both permit excellent detection sensitivity and have the advantage of being assayable directly from intact cultures.

Acknowledgements

We thank Lily Wu for helpful suggestions and David Stout for assistance with imaging. This work was supported by NCI grants R01 CA105171 and R01 CA121258 to N.K. C.L. was a UCLA Scholars in Molecular Oncologic Imaging Fellow (NCI grant R25 CA098010). Imaging was performed at the UCLA Crump Institute for Molecular Imaging, which is supported by NCI grants P50 CA086306, 2U24 CA092865 and P30 CA016042. The authors declare that they have no competing interests that might bias the content of this article.

References

- Iyer M, Sato M, Johnson M, Gambhir SS, Wu L. Applications of molecular imaging in cancer gene therapy. *Curr Gene Ther* 2005; **5**: 607–618.
- Raty JK, Liimatainen T, Unelma Kaikkonen M, Grohn O, Airene KJ, Yla-Herttua S. Non-invasive imaging in gene therapy. *Mol Ther* 2007; **15**: 1579–1586.
- Barnes AT, Case JF. Bioluminescence in the mesopelagic copepod, *Gaussia princeps* (T. Scott). *J Exp Mar Biol Ecol* 1972; **8**: 53–71.
- Tannous BA, Kim DE, Fernandez JL, Weissleder R, Breakefield XO. Codon-optimized *Gaussia luciferase* cDNA for mammalian gene expression in culture and in vivo. *Mol Ther* 2005; **11**: 435–443.
- Lorenz WW, Cormier MJ, O’Kane DJ, Hua D, Escher AA, Szalay AA. Expression of the *Renilla reniformis luciferase* gene in mammalian cells. *J Biolumin Chemilumin* 1996; **11**: 31–37.
- Szent-Gyorgyi C, Ballou BT, Dagnal E, Bryan B. Cloning and characterization of new bioluminescent proteins. *Proc SPIE* 2003; **3600**: 4–11.
- Wurdinger T, Badr C, Pike L, et al. A secreted luciferase for ex vivo monitoring of in vivo processes. *Nat Methods* 2008; **5**: 171–173.
- Bhaumik S, Gambhir SS. Optical imaging of *Renilla luciferase* reporter gene expression in living mice. *Proc Natl Acad Sci USA* 2002; **99**: 377–382.
- Zhao H, Doyle TC, Coquoz O, Kalish F, Rice BW, Contag CH. Emission spectra of bioluminescent reporters and interaction with mammalian tissue determine the sensitivity of detection in vivo. *J Biomed Opt* 2005; **10**: 41210.
- Loening AM, Fenn TD, Wu AM, Gambhir SS. Consensus guided mutagenesis of *Renilla luciferase* yields enhanced stability and light output. *Protein Eng Des Sel* 2006; **19**: 391–400.
- Loening AM, Wu AM, Gambhir SS. Red-shifted *Renilla reniformis luciferase* variants for imaging in living subjects. *Nat Methods* 2007; **4**: 641–643.
- Hart RC, Matthews JC, Hori K, Cormier MJ. *Renilla reniformis* bioluminescence: luciferase-catalyzed production of nonradiating excited states from luciferin analogues and elucidation of the excited state species involved in energy transfer to *Renilla* green fluorescent protein. *Biochemistry* 1979; **18**: 2204–2210.
- Inouye S, Shimomura O. The use of *Renilla luciferase*, *Oplophorus luciferase*, and apoaquorin as bioluminescent reporter protein in the presence of coelenterazine analogues as substrate. *Biochem Biophys Res Commun* 1997; **233**: 349–353.
- Zhao H, Doyle TC, Wong RJ, et al. Characterization of coelenterazine analogs for measurements of *Renilla luciferase* activity in live cells and living animals. *Mol Imaging* 2004; **3**: 43–54.
- Hawkins E, Unch J, Murphy N, et al. Measuring *Renilla luciferase* luminescence in living cells. *Promega Notes* 2005; **90**: 10–14.
- Otto-Duessel M, Khankaldyyan V, Gonzalez-Gomez I, Jensen MC, Laug WE, Rosol M. In vivo testing of *Renilla luciferase* substrate analogs in an orthotopic murine model of human glioblastoma. *Mol Imaging* 2006; **5**: 57–64.
- Logg CR, Logg A, Tai CK, Cannon PM, Kasahara N. Genomic stability of murine leukemia viruses containing insertions at the Env-3' untranslated region boundary. *J Virol* 2001; **75**: 6989–6998.
- Logg CR, Kasahara N. Retrovirus-mediated gene transfer to tumors: utilizing the replicative power of viruses to achieve

- highly efficient tumor transduction in vivo. *Methods Mol Biol* 2004; **246**: 499–525.
19. Baranick BT, Lemp NA, Nagashima J, Hiraoka K, Kasahara N, Logg CR. Splicing mediates the activity of four putative cellular internal ribosome entry sites. *Proc Natl Acad Sci USA* 2008; **105**: 4733–4738.
 20. Logg CR, Tai CK, Logg A, Anderson WF, Kasahara N. A uniquely stable replication-competent retrovirus vector achieves efficient gene delivery in vitro and in solid tumors. *Hum Gene Ther* 2001; **12**: 921–932.
 21. Waehler R, Russell SJ, Curiel DT. Engineering targeted viral vectors for gene therapy. *Nat Rev Genet* 2007; **8**: 573–587.
 22. Santos EB, Yeh R, Lee J, et al. Sensitive in vivo imaging of T cells using a membrane-bound *Gaussia princeps* luciferase. *Nat Med* 2009; **15**: 338–344.